2009-01-01

Design of 120cc Single Cylinder Experimental Engine for Analysis of Intake Swirl and Multiple Ignition Sites.

Patrick Seemann
University of Miami, p.s.seemann@gmail.com

UNIVERSITY OF MIAMI

DESIGN OF 120CC SINGLE CYLINDER EXPERIMENTAL ENGINE FOR ANALYSIS OF INTAKE SWIRL AND MULTIPLE IGNITION SITES

By

Patrick Seemann

A THESIS

Submitted to the Faculty
of the University of Miami
in partial fulfillment of the requirements for
the degree of Master of Science

Coral Gables, Florida

August 2009

UNIVERSITY OF MIAMI

A thesis submitted in partial fulfillment of
the requirements for the degree of
Master of Science

DESIGN OF 120CC SINGLE CYLINDER EXPERIMENTAL ENGINE FOR ANALYSIS OF INTAKE SWIRL AND MULTIPLE IGNITION SITES

Patrick Seemann

Approved:

_____ Michael R, Swain, Ph.D. Associate Professor of Mechanical & Aerospace Engineering	_____ Terri A. Scandura, Ph.D. Dean of the Graduate School
_____ Roberta D. Goode Adjunct Professor of Biomedical Engineering	_____ Matthew N. Swain, Ph.D. Research, Associate Professor Mechanical & Aerospace Engineering
_____ Singiresu S. Rao, Ph.D. Professor and Chairman of Mechanical & Aerospace Engineering	

SEEMANN, PATRICK (M.S., Mechanical Engineering)

Design of 120cc Single Cylinder Experimental Engine for Analysis of Intake Swirl and Multiple Ignition Sites. (August 2009)

Abstract of a thesis at the University of Miami.

Thesis supervised by Professor Michael Swain.
No. of pages in text. (90)

The intent of this thesis is to design, build, and test a cylinder head with variable swirl and ignition sites. The design aspect used Solid Works Floworks to model airflow within the head and cylinder. Swirl rate and volumetric flow rate were calculated from the results. Many design iterations took place before a suitable design was accomplished.

Once the suitable design was reached, it was built using the rapid prototyping method known as 3-D printing (Fused Deposition Modeling). Valve guides and seats were installed in the head. Then valves, springs, and retainers were installed to allow for testing. The inlet was created using stereo-lithography due to its smooth surface finish and thin walls. A pin wheel swirl measuring device was built to measure tangential rotation rate of gasses in the cylinder. The experimental head was tested on the University of Miami flow bench in the Internal Combustion Engines Laboratory.

The results of the experimental work and theoretical modeling were compared. The results matched closely. The difference between experimental and theoretical values for high swirl flow rates were less than 3% error and the swirl ratio was less than 10%. For the low swirl scenario, error was less than 30%. The measured flow rate for the high swirl scenario was 28.87 CFM and the swirl ratio was measured as 2.87. SolidWorks

Floworks created accurate results for the high swirl scenario and further experimentation should be conducted for different geometries.

Acknowledgment

I would like to thank my advisor, Dr. Michael Swain. Without his help, this would have never been possible.

I would like to thank my parents, who have loved me from the day I was born and encouraged me to do my best in school and life.

I would also like to thank my friend Markku Biedermann, who has helped me immensely during the building of the prototype and swirl meter.

I would also like to thank my friend, Dave Oblak, for his outstanding help.

TABLE OF CONTENTS

List of Figures

List of Tables

Definitions

3-D printing: Rapid prototyping method otherwise known as fused deposition modeling.

Combustion Chamber: Cavity in the cylinder head that contains valves and spark plugs where combustion takes place.

Flowbench: Device used to measure flow rate of gasses through a cylinder head or manifold using the pressure difference of a calibrated orifice.

Helical Port: Port with a helical cut in the roof that spirals air around the intake valve.

Intake Port: Portion of the intake runner inside the head from the intake manifold to the combustion chamber.

Intake Runner: Passage way in which gasses enter the combustion chamber.

Pin Wheel: Device used to measure swirl based on the axial rotation of gasses inside the cylinder. Consists of a small piece of sheet metal mounted on an axle allowed to rotate on a bearing. Rate of rotation can be measured using a stroboscope.

Quench: Cooling of gasses on the engine surface far enough so that combustion is extinguished.

Retainers: Device used to attach springs to the valves.

Shrouded Intake Valve: Intake valve that is close enough to the edge of combustion chamber to restrict flow. Valves may be designed to direct flow.

SLA: Stereo lithography a rapid prototyping method involving a laser to harden a UV curing polymer.

Squish: Gas motion caused when the piston is reaching TDC.A narrowing area between the piston and head causes flow into the main area of the combustion chamber.

Swirl: Bulk rotation of gasses about the axis of the cylinder.

Swirl Streamline angle: Angle that swirl streamlines propagate down into the cylinder.

Tangential Port: Port that's axis is offset from the valve in order to cause rotation of gasses in the cylinder.

Tumble: Bulk rotation of gasses perpendicular to the axis of the cylinder.

Valve Guide: Bushing allowing valve to open and close.

Valve Pocket: portion of cylinder head at the end of the intake port but before combustion chamber. Usually the area around the valve stem inside of the port.

Valve Seats: Sealing surface on head so that valves do not deform aluminum.

Valve Springs: Helical spring used to shut valves when the cam is not holding them open.

Volumetric Efficiency: Measure of ability of engine to induct air. (mass of air trapped in cylinder when intake valve closes/mass of air equal to the cylinder volume at inlet manifold temperature and pressure)

Chapter 1

Introduction:

The purpose of this project was to design a cylinder head with variable swirl and variable ignition sites. The test engine is a Honda GX120 single cylinder spark ignited internal combustion engine. It is 120cc and air cooled. This experiment used the CFD modeling tool Floworks; it is embedded in Solid Works. Floworks was used to optimize the experimental cylinder for swirl and flow rate. The Solid Works Flow Simulation software uses the K-E turbulence model. The software is capable of analyzing internal, external, compressible, incompressible, turbulent, and laminar flow. The software is also capable of heat transfer analysis. It was developed by Mentor Graphics Corporation and can be embedded in most major 3-D modeling programs.

As defined by Stone in Introduction to Internal Combustion Engines, swirl is the "ordered rotation of air about the cylinder axis". He mentions that there are two ways to create swirl. The first method is to use a shrouded intake valve so that the direction of the air can be controlled. This is difficult since the valve cannot rotate and often causes wear problems at the valve rocker arm contact point. There is also a large decrease in volumetric efficiency because of the small flow area. The second method is to design the inlet passage to create swirl. There are two port geometries commonly used helical and tangential. This is the concentration of this paper. There are many ways to define swirl. In this paper we will define swirl as the ratio between tangential velocity and vertical velocity of air traveling down the cylinder. This ratio should be directly proportional to angle of inclination of the streamlines. Based on the computer modeled data, the average tangential velocity will be found in the cylinder and compared with the average axial

velocity to give the swirl ratio. In order to verify these results, an experimental cylinder head was built and tested on a flow bench. A pin wheel was used to calculate the tangential velocity. In addition to comparing swirl, the flow bench was also used to compare the experimental and the computer model flow rate data.

There are three common types of swirl measuring techniques. The pin wheel is employed in this experiment. To construct a pin wheel swirl meter, a small piece of flat material (paddle) is attached to a bearing and allowed to rotate about the axis of the cylinder. The pin wheel is considered to move freely and not impede the flow of gasses. The rotational velocity of the pin wheel is used to calculate the velocity of the rotating gasses. Typically, measurements are take at 1 to 1.5 bore diameters down the cylinder. Another similar technique is to remove the paddle and place a honeycomb air straightener in its place. This is usually called an impulse swirl meter (Heywood). The torque exerted on the air straightener is used to determine the angular momentum of the rotating gasses. The third technique utilizes a laser anemometer to measure velocity and angle of flow. This technique is the most costly and requires averaging of data which can produce errors.

The advantage of swirl is that it increases burning rate, which decreases knock and increases homogeneity of mixtures. This is especially important at low operating speeds. Swirl and other gas motions create small scale turbulence during compression and combustion. This small scale turbulence is directly related to flame speed (Pozniak, 1985). As stated by Pozniak, “turbulence intensity should be proportional to the square root of dissipated swirl energy”. Squish is an additional method to create turbulence during the combustion process. Swirl is generally considered to create more turbulence

than squish. Squish is caused by creating a narrow area between the piston and head when at top dead center (TDC) that pushes gasses into the main combustion area. Squish causes increased un-burnt hydrocarbons. The amount of squish area in this design was determined by the restrictions imposed by swirl generation.

Chapter 2

Simulation:

As discussed earlier, the computer modeling for this thesis used Solid Works Floworks. Mesh generation was accomplished utilizing the methods provided by the software. The remainder of this chapter will discuss different iterations that eventually determined the final design of the cylinder head. The static pressure difference between the inlet and the outlet used in all iterations was 28 inches of water(6.97 kPa). These pressures were considered to be static and all walls were modeled as real walls in the solver. The valve lift was .200" (5.08mm).

The original design intent was to use two intake ports. One intake port would create swirl while the other would reduce the swirl. It was decided to begin the design process with the swirl port. The intake port in the original cylinder head was round, entering horizontally smoothly turning downward into the cylinder. The initial swirl port results can be seen in figure 1. A close up of the valve can be seen in figure 2. In figure 3 there is a bottom view of the cylinder. It is possible to see from this view that there is virtually no swirl developed. The bottom view shows the streamlines exiting around the valve and no noticeable swirl occurs. The flow rate through the head in the first iteration is 25.1 CFM and the swirl ratio was measured at .31.

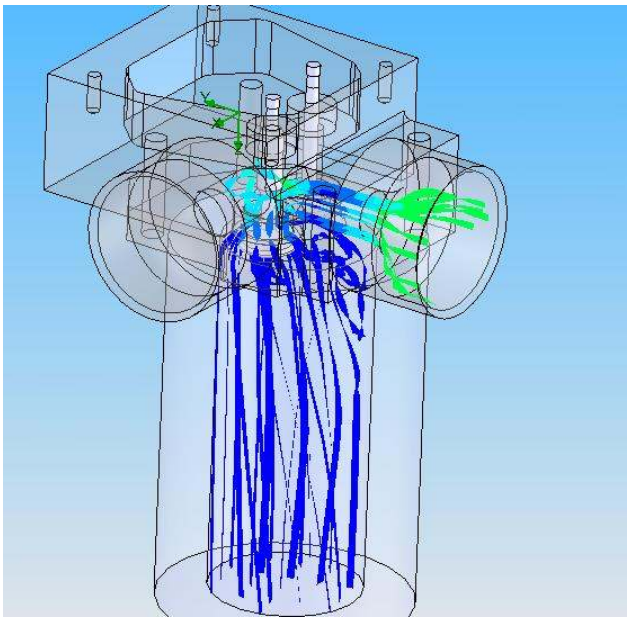

Figure 1- Iteration 1 - Isometric View

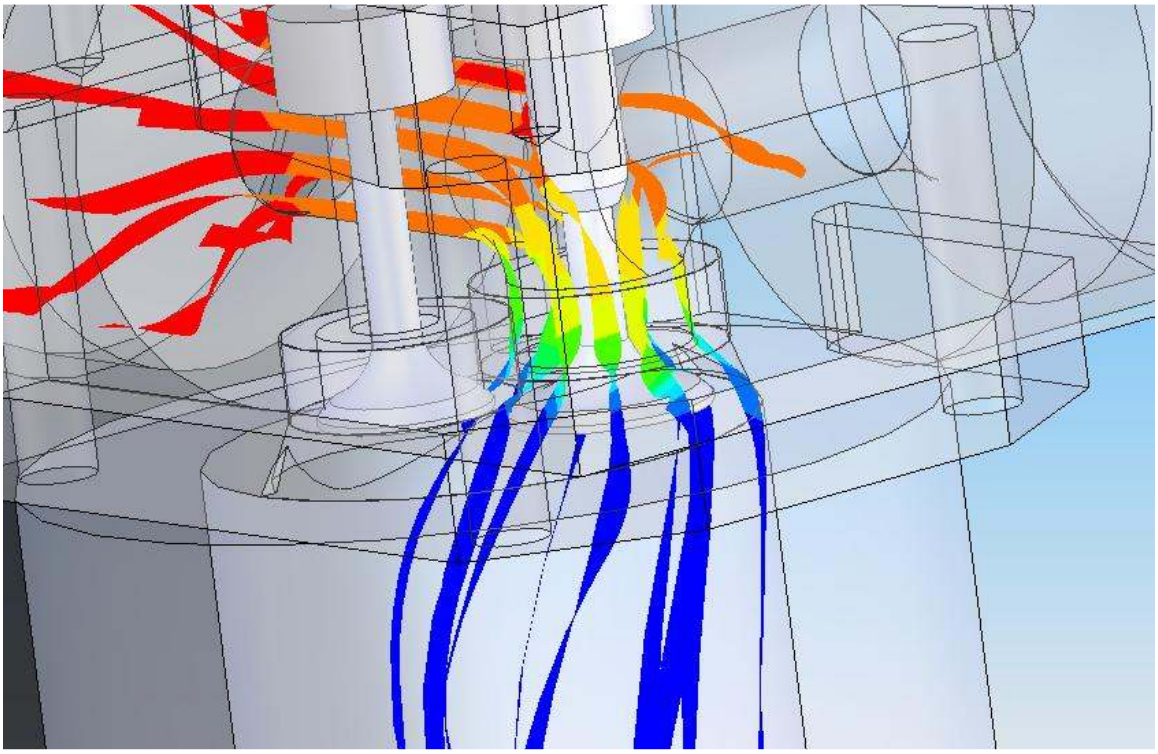

Figure 2 Iteration 1 - Valve View

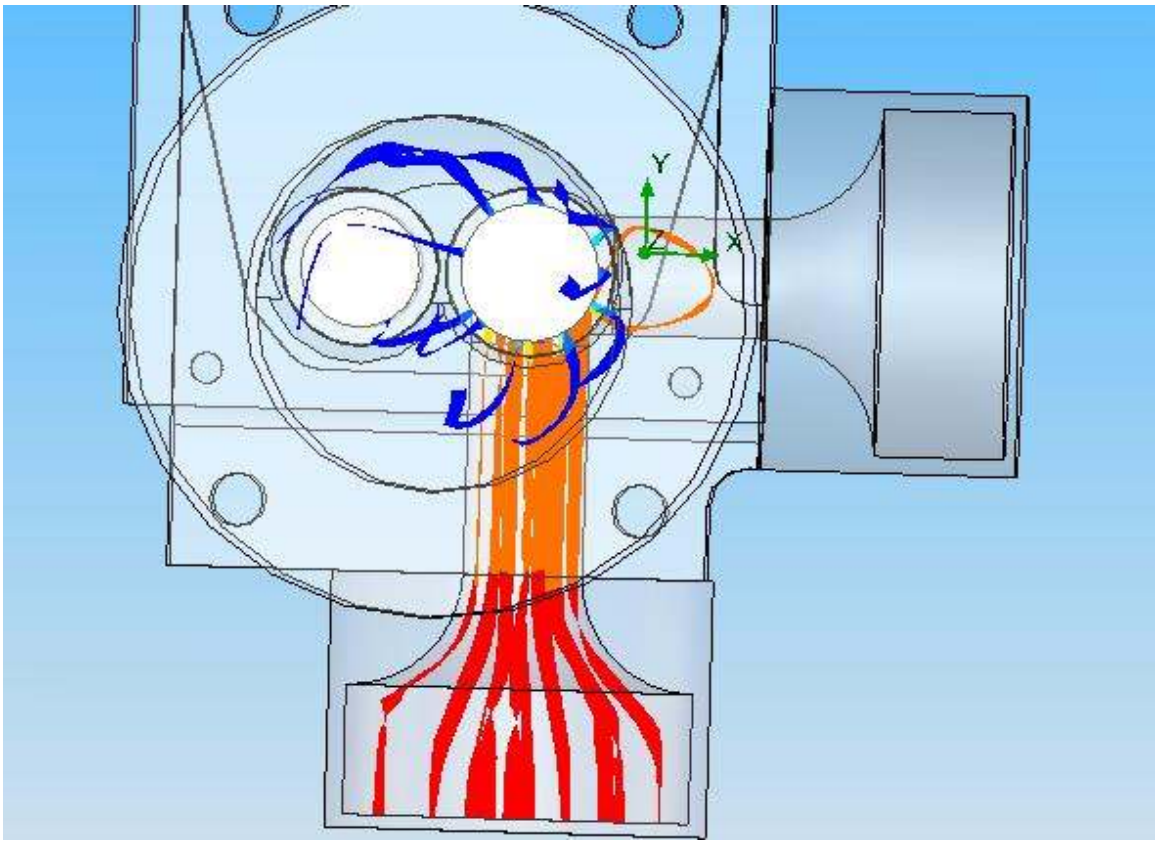

Figure 3 Iteration 1 - Bottom View

For the second iteration, a design from a production engine was copied. As a basis for this design, the cylinder head from the 4.6L Ford 4-valve modular V-8 was used. When one of the intake valves is deactivated during low RPM operation swirl is produced. When both intake valves are activated during high RPM, operation swirl is dramatically reduced. The use of both intake valves at high RPM is to increase volumetric efficiency and therefore, power. For this study, the original Honda 120cc engine utilized two valves, not four valves. This removed the option of deactivating one intake valve to produce swirl. The use of two intake valves increases engine cost substantially. In the Ford engine, the swirl port is elevated around 35 degree. The design of the swirl generating Ford port was used and the results can be seen in figure 4. The flow rate of the second iteration was measured at 23.2 CFM and the swirl ratio was .57.

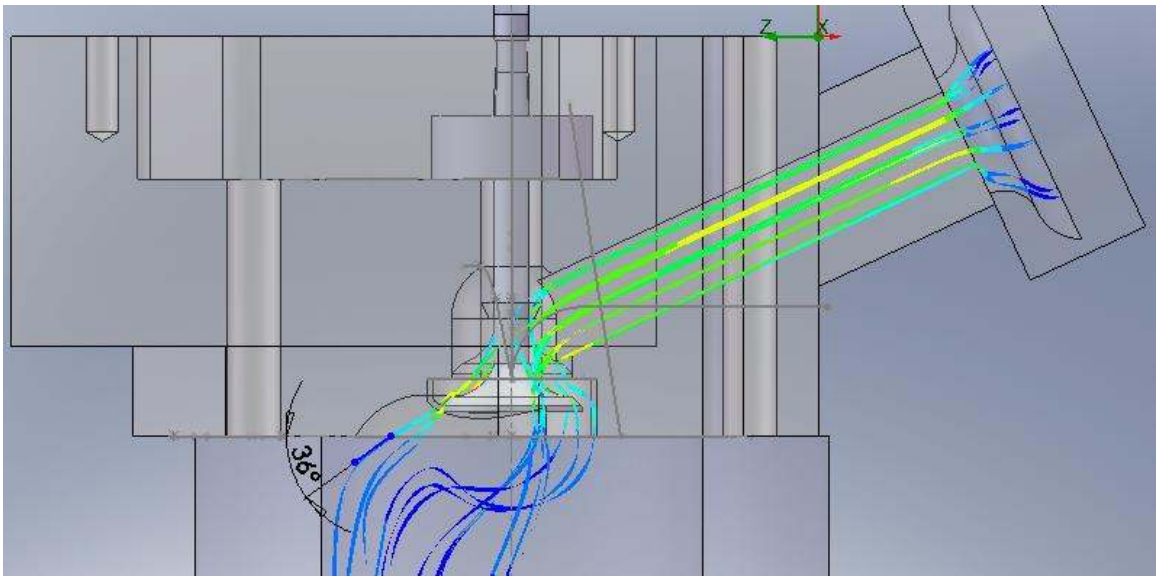

Figure 4 Iteration 2 - Side View

The steepest swirl streamline is about 36 degrees, but most are less than 45 degrees. The results from the front view can be seen in figure 5. An overall view can be seen in figure 6. This figure shows little overall swirl motion. Some of the streamlines rotate, but the bulk movement of the gasses is closer to a tumble.

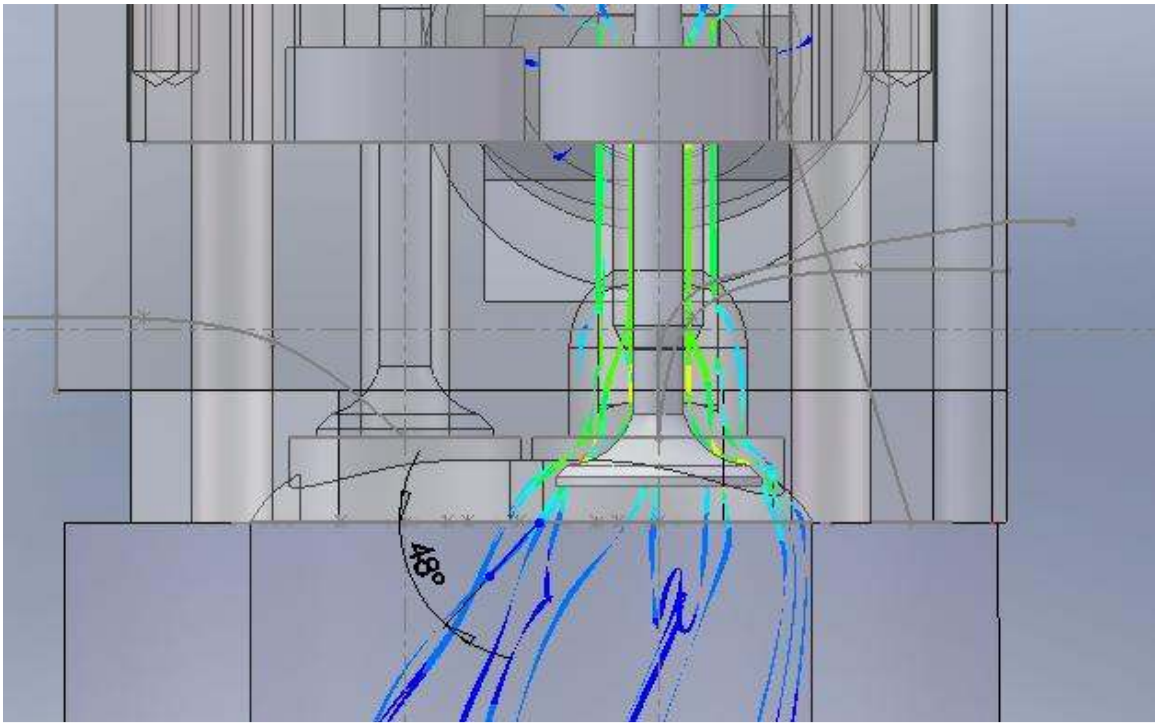

Figure 5 – Iteration 2- Back View

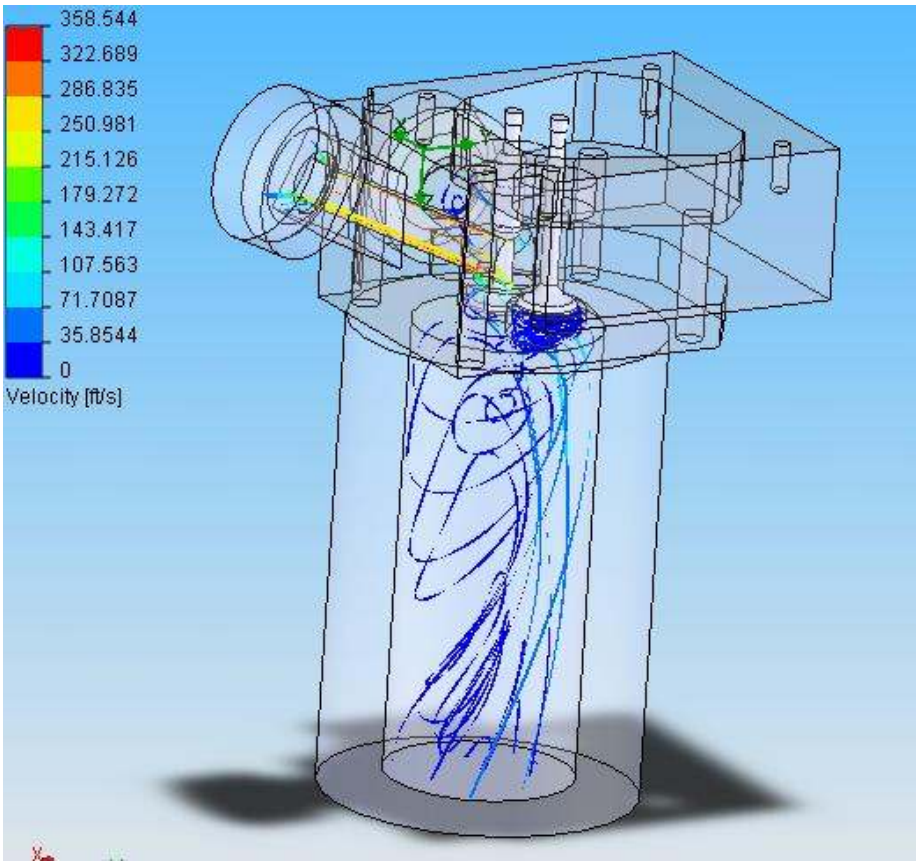

Figure 6 - Iteration 2- Isometric View

The previous design did not create sufficient swirl. The third iteration would be similar, but the port would be half as tall. The results from this experiment can be seen in figure 7. With this design there is more rotational flow, but the rotation is still not about the axis of the cylinder. The swirl pattern can be seen closer in figure 8. Even though the port that would be used to reduce swirl was closed off, its geometry could interfere with the generation of swirl. The flow rate for the third iteration was calculated as 10.5 CFM and the swirl ratio increased to .88. In the fourth iteration, the swirl reducing port was removed so that it would not interfere with the generation of swirl. These results can be seen in figures 9 and 10. The swirl that is generated is better defined. It appears that the swirl reducing port, though closed at its entrance, was interfering with the generation of swirl. The flow was 9.7 CFM and the swirl ratio measured as .98.

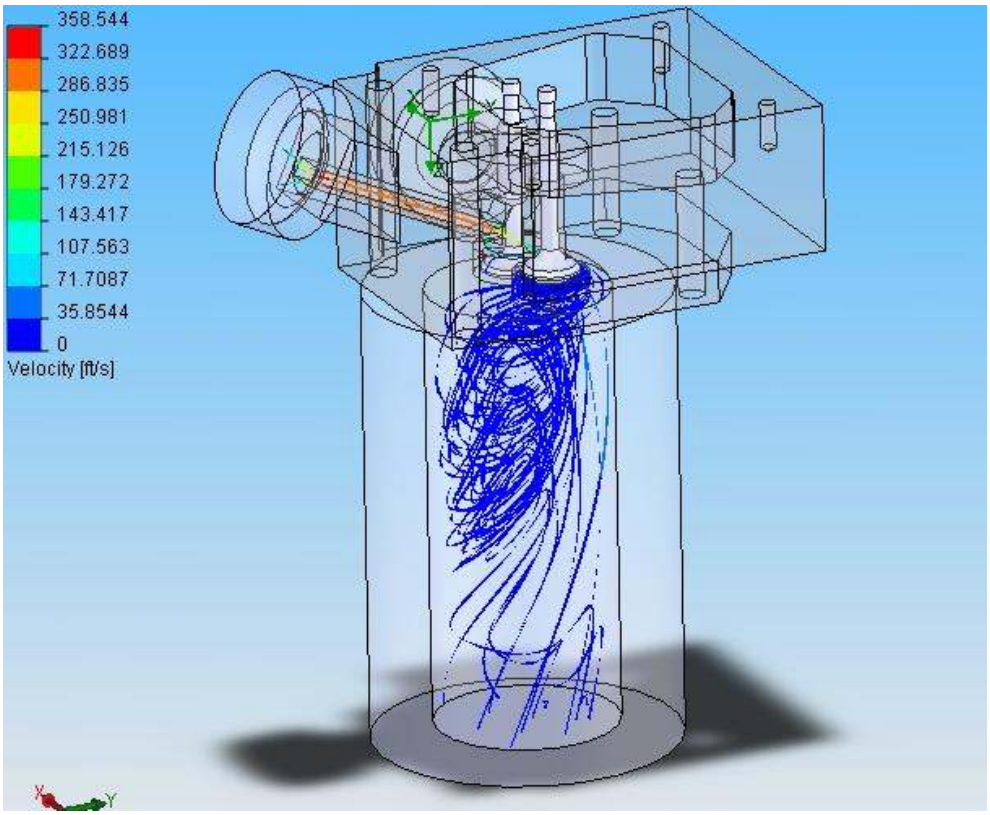

Figure 7 - Iteration 3- Isometric View

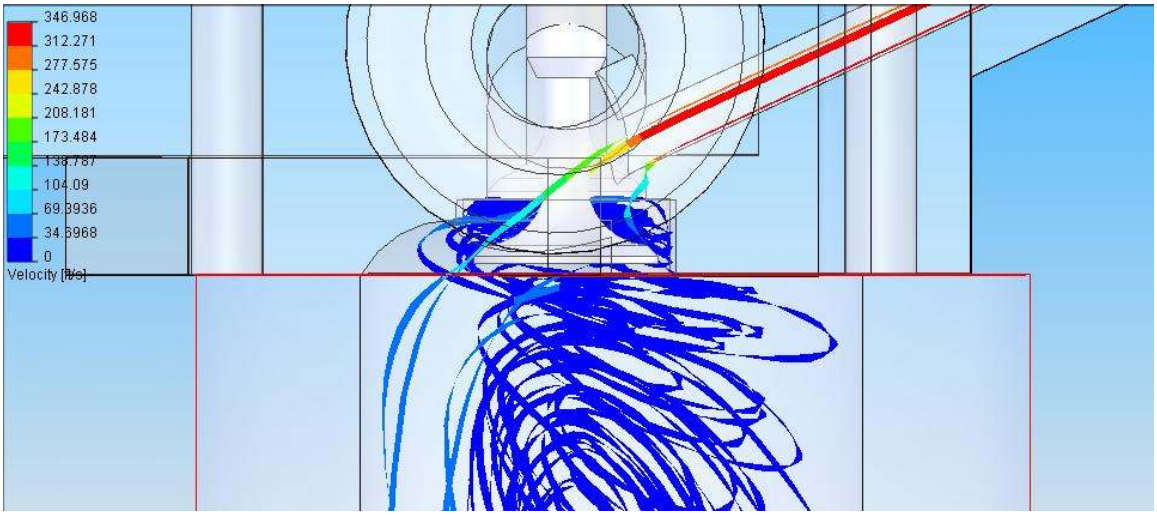

Figure 8- Iteration 3- Side View

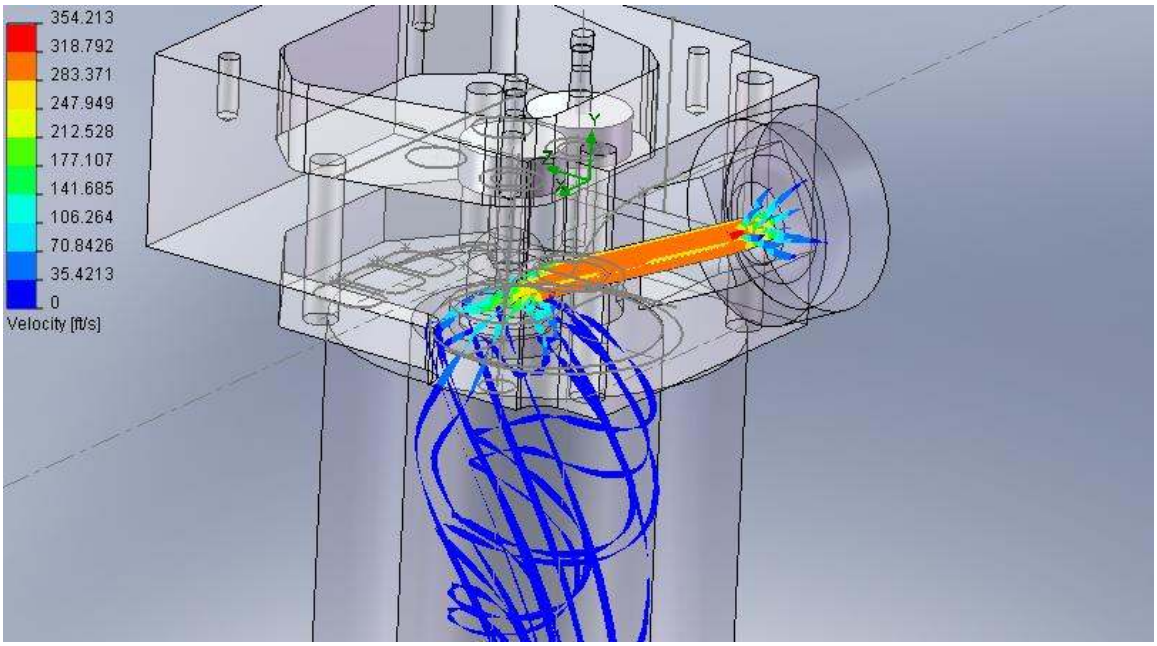

Figure 9- Iteration 4- Isometric View

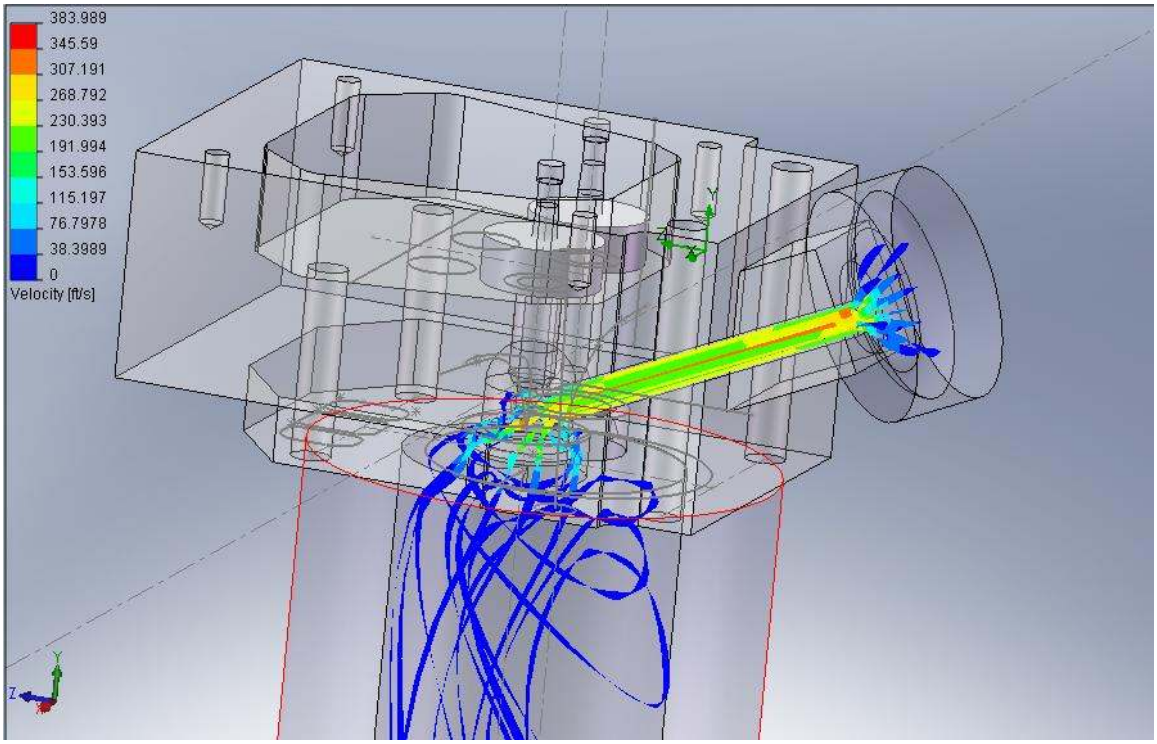

Figure 10- Iteration 4- Isometric View 2

Since swirl was being developed, combustion chamber size and shape needed to be addressed. To produce the original compression ratio a volume of 10cc was required. The iteration 4 volume was 15cc. In figure 11, the redesigned combustion chamber can be

seen. The chamber has a significantly larger squish region. The bowl is not as steep near the edges and does not protrude as far into the cylinder wall. The swirl pattern for this combustion chamber design can be seen in figure 12. The swirl pattern for this design becomes much more pronounced farther down in the cylinder, than up near the cylinder head. One of the streamlines from the outside of the runner exits the valve and travels nearly horizontally around the axis of the cylinder head. The fifth iteration flowed 9.6 CFM and the swirl ratio was 1.10.

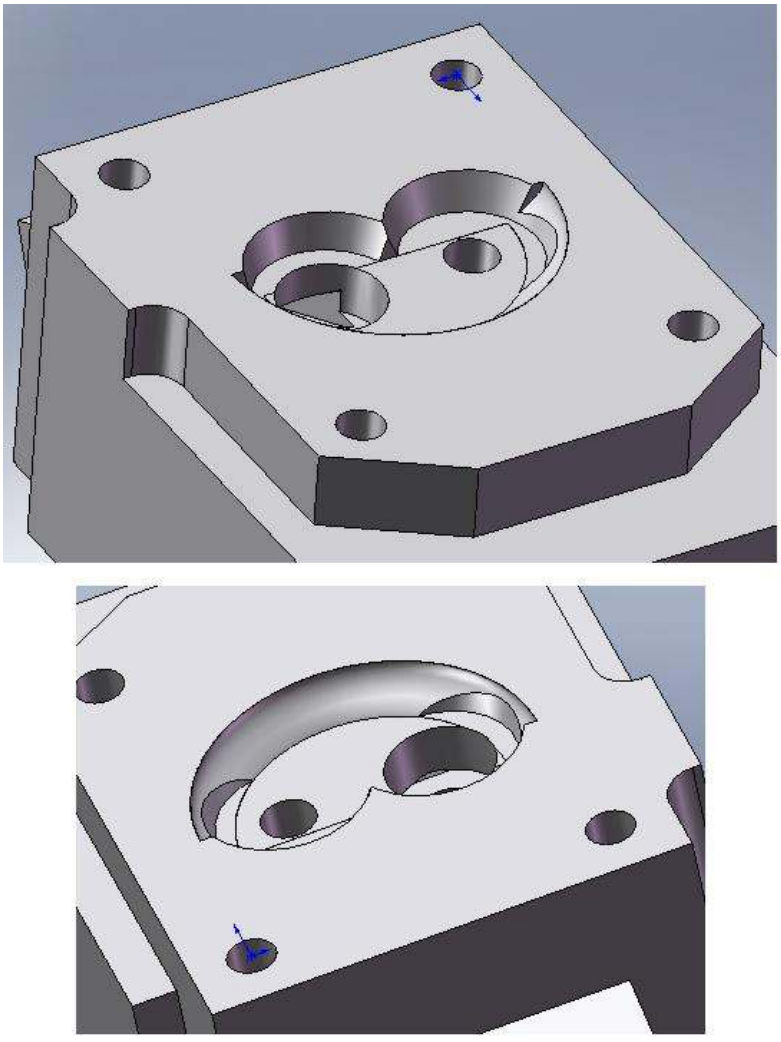

Figure 11 – Iteration 5 – Combustion Chamber

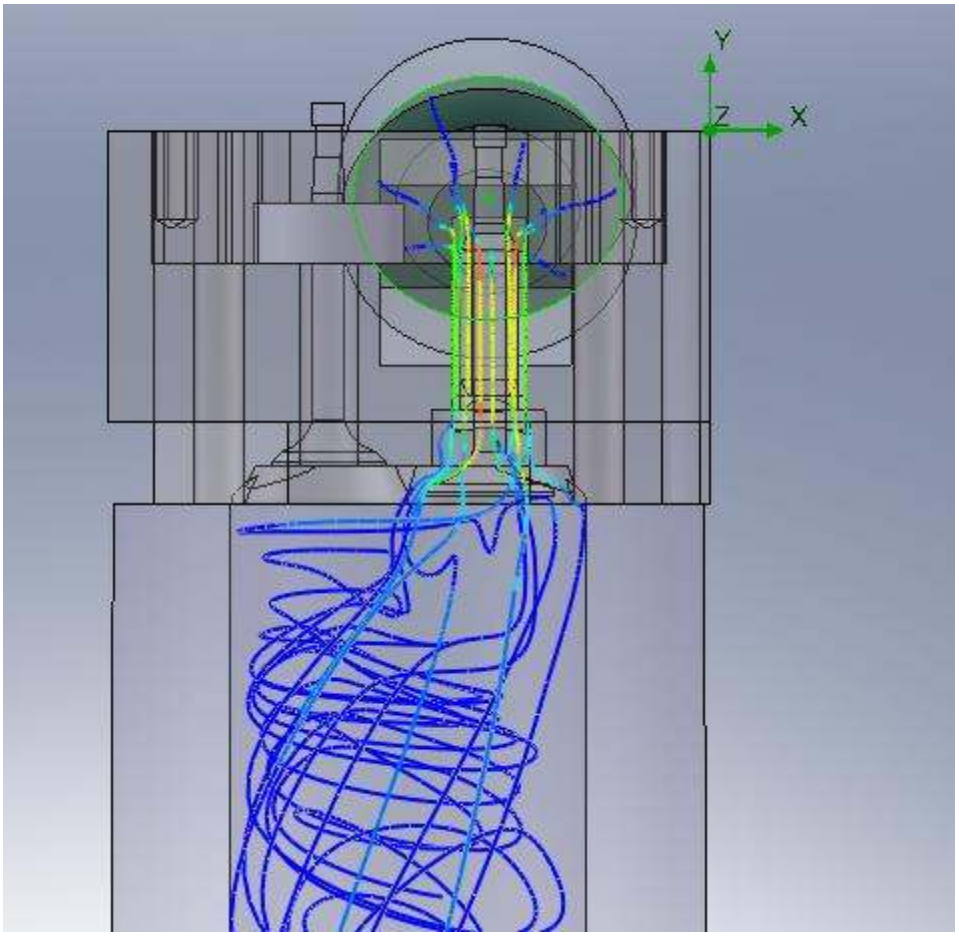

Figure 12 – Iteration 5 – Rear View

After viewing the last set of results, it was apparent that the shape of the combustion chamber could lead to significant changes in swirl. The next step would be to finalize the combustion chamber as much as possible. The volume was 10cc, but the shape needed to change significantly so that two spark plugs could be fitted with no exposed threads. The use of two spark plugs allows changed in the rate of combustion to be made by deactivating one of the spark plugs. The changes to the combustion chamber can be seen in figures 13 and 14. From these pictures, it can be seen that the protrusion in the squish side of the combustion chamber was removed. The opposite side of the chamber was moved closer to the center of the chamber and its wall was made steeper. This allowed

the spark plug to be placed in the wall without protruding past the head gasket plane. The flow rate in the sixth iteration was 9.9 CFM and the swirl ratio was .58.

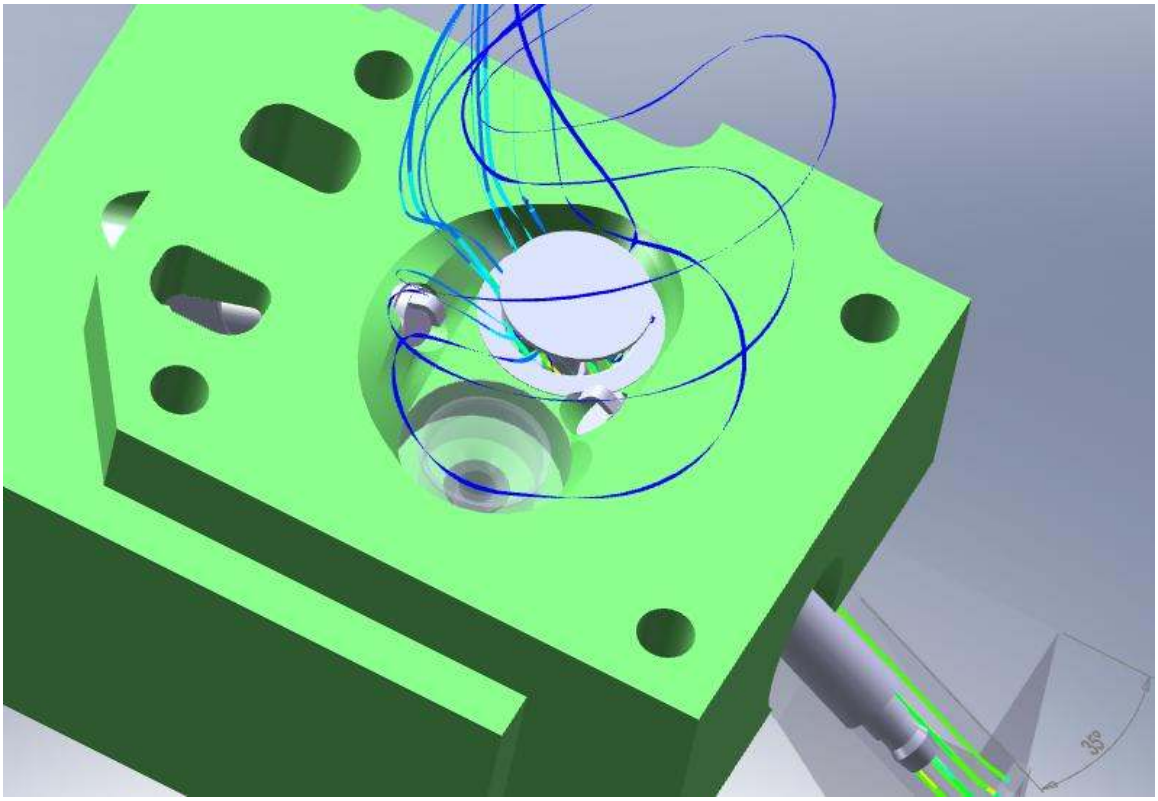

Figure 13 – Iteration 6 – Bottom View, Streamlines

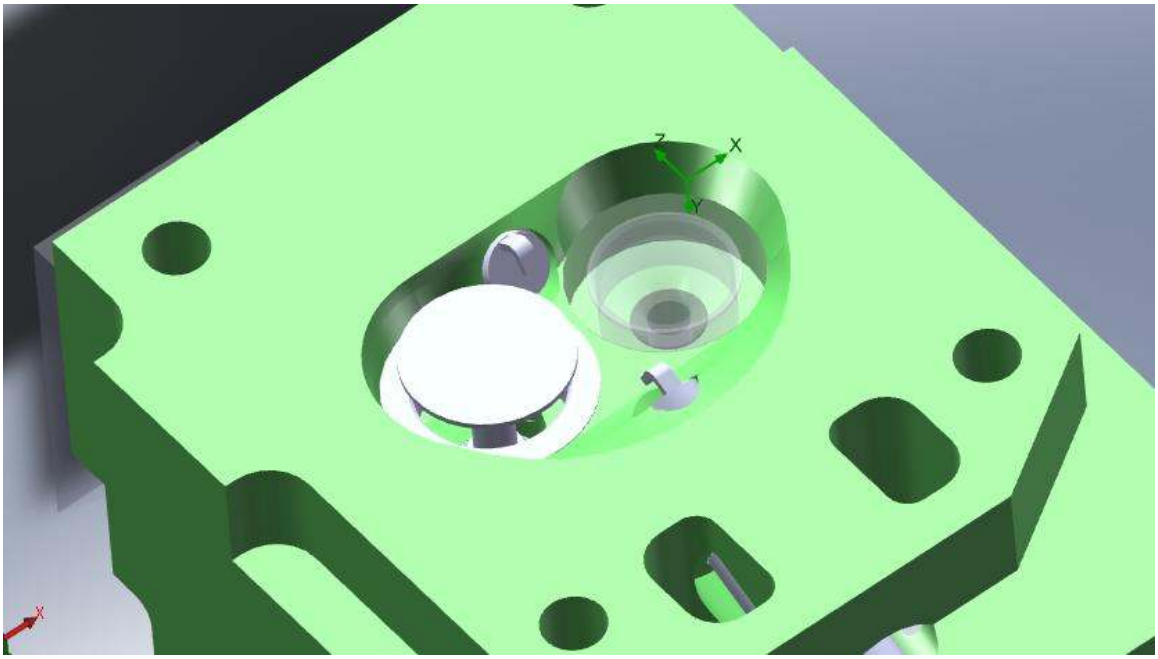

Figure 14 - Iteration 6 – Bottom View, No Streamlines

In the next set of figures, the streamlines for the front (figure 15) and side (figure 16) can be seen. Since the combustion chamber was now closer to a bathtub shape, the air exited the port and was deflected down instead of wrapping around the cylinder and causing swirl. In figure 17, a cutaway of the cylinder can be seen. It appears that some streamlines get trapped or may stagnate on the port side of the intake valve. The streamline shown after making a loop travels straight down into the cylinder.

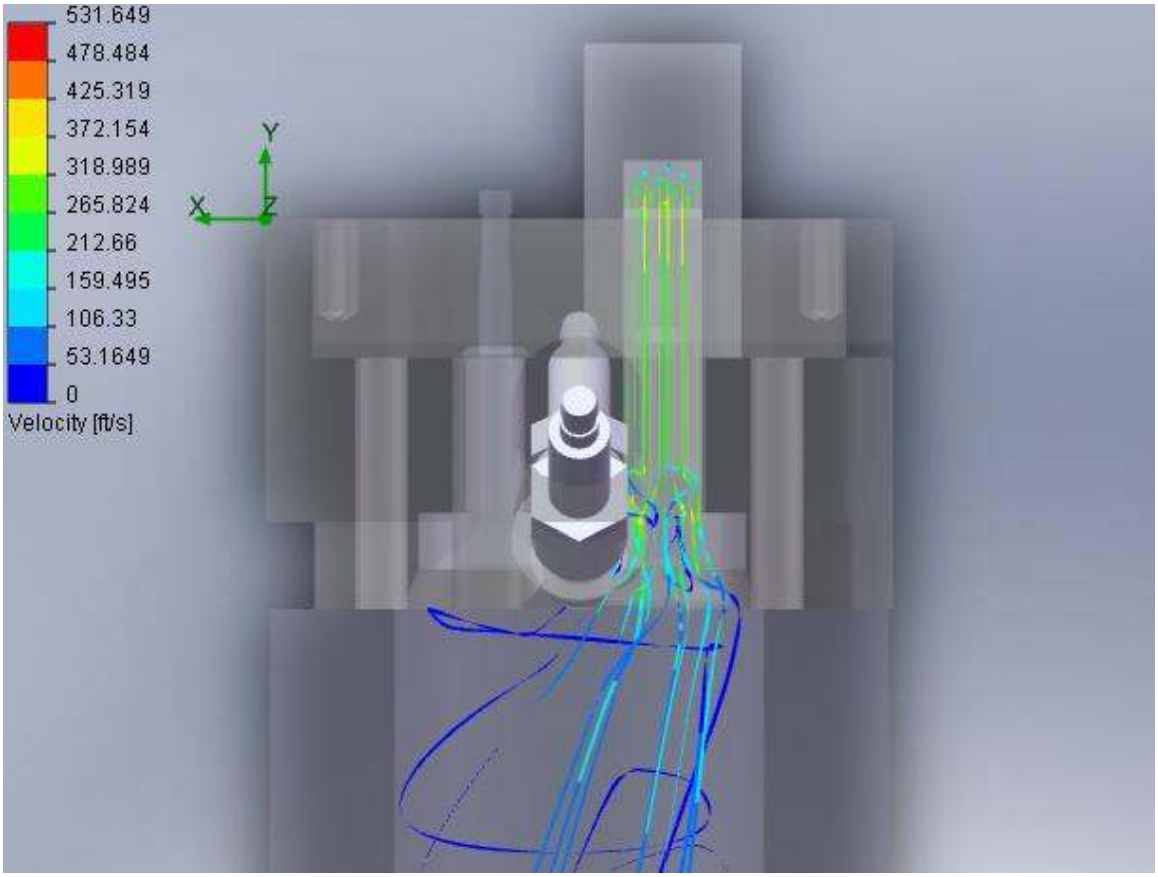

Figure 15 – Iteration 6 - Rear View

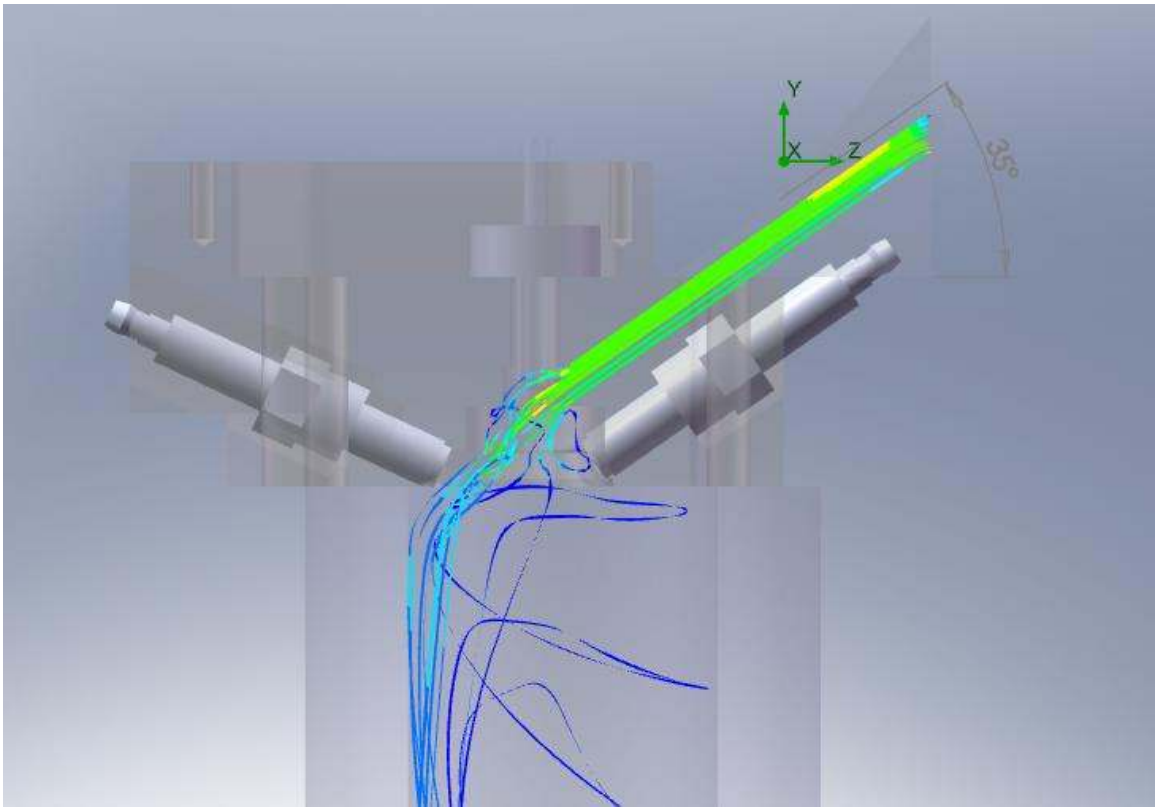

Figure 16– Iteration 6 - Side View

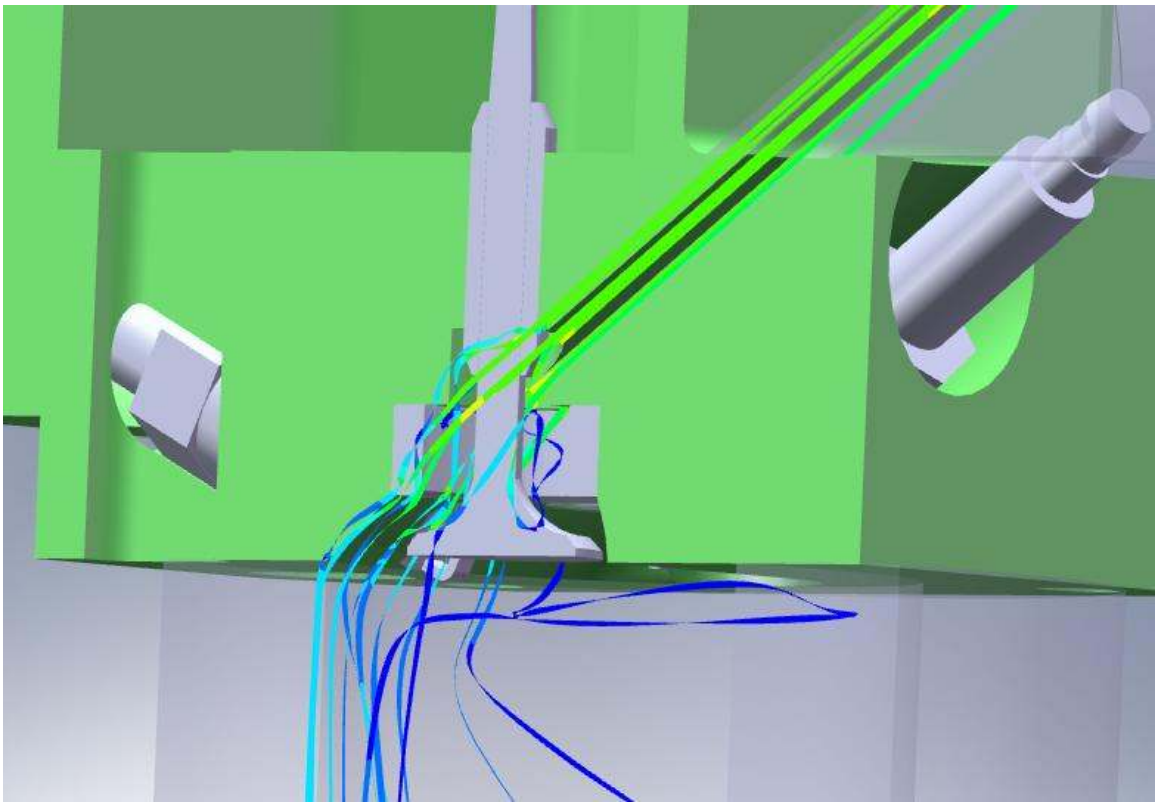

Figure 17– Iteration 6 - Cutaway

The next iteration needed to generate far more swirl. Offsetting the port to begin creation of a helical port was investigated. The seventh iteration utilized a .5” tall and .25” wide intake runner. It was offset so that the outside edge was tangent with the outside of the valve pocket. The results for the front, side, and cutaway can be seen in figures 18, 19, and 20. The swirl pattern is well developed and propagates down through almost the entire length of the cylinder. The stagnation points that were seen in earlier iterations have completely disappeared. In figure 20, there is an increase in velocity as the flow exits the runner and enters the valve pocket. The flow rate in the seventh iteration was 9.8 CFM and the swirl ratio was 1.19. In the eighth iteration the sharp edge that caused this was removed. The results of the smoothed out valve pocket can be seen in figures 21, 22, 23, and 24. The flow rate was 10.1 CFM and the swirl ratio 1.89.

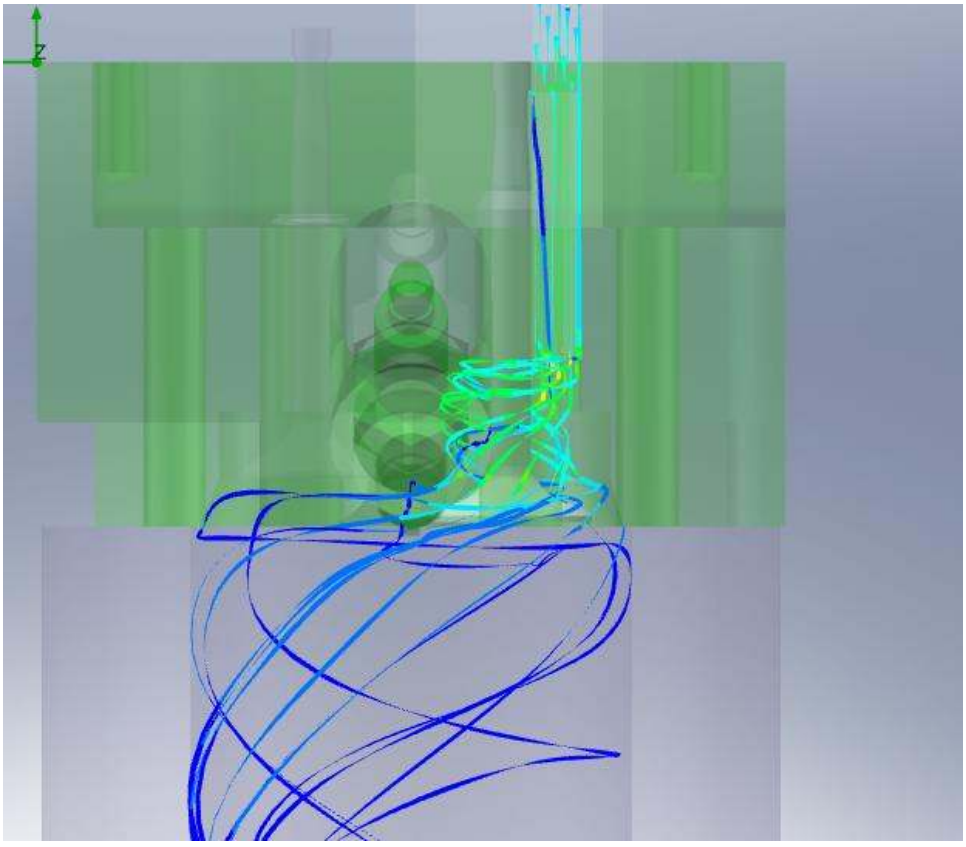

Figure 18 – Iteration 7 – Rear View

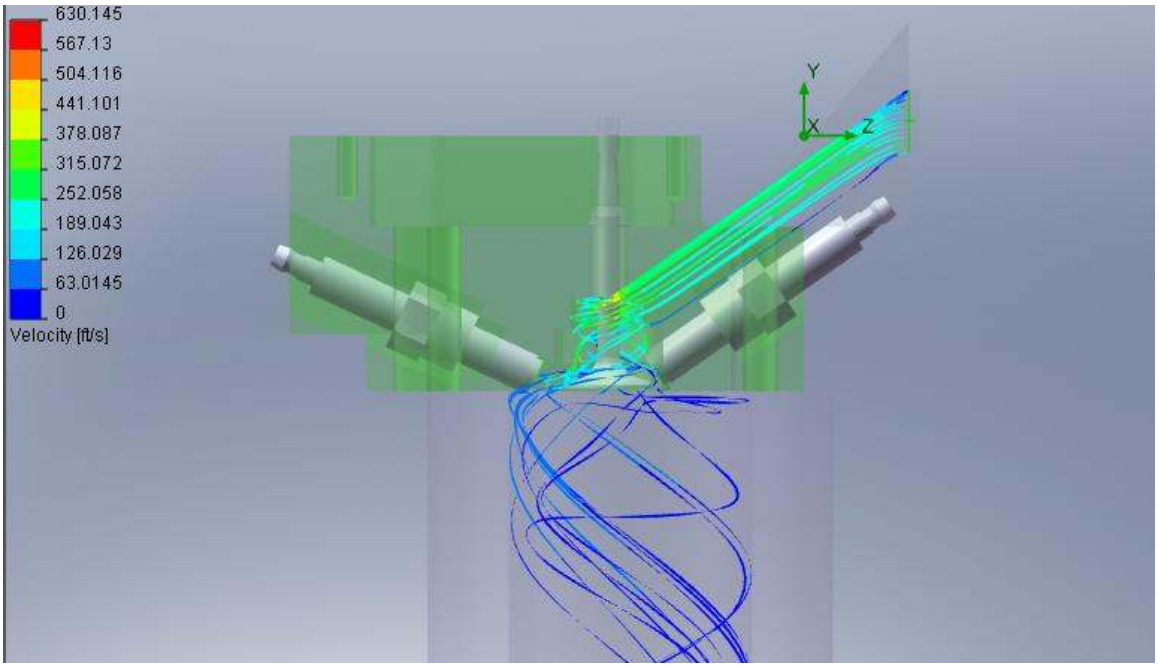

Figure 19– Iteration 7 - Side View

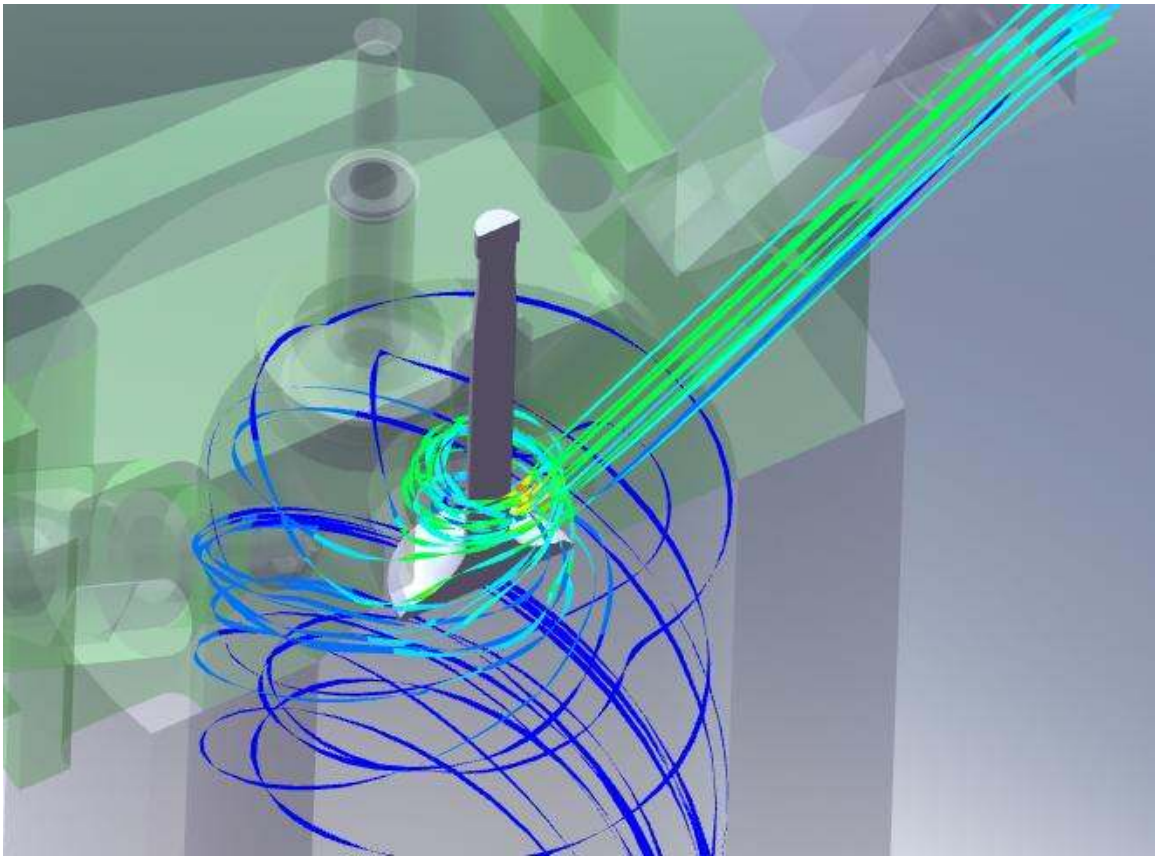

Figure 20– Iteration 7 - Isometric View Cutaway

In figure 21, the cross-section of the intake runner shows how more material has been removed at the transition between runner and valve pocket. In the views with streamlines, the previous spike in velocity at the transition is reduced. The swirl is much tighter in the cylinder. In addition to the transition being added, a helical cut was added so that the air could spiral out of the valve pocket.

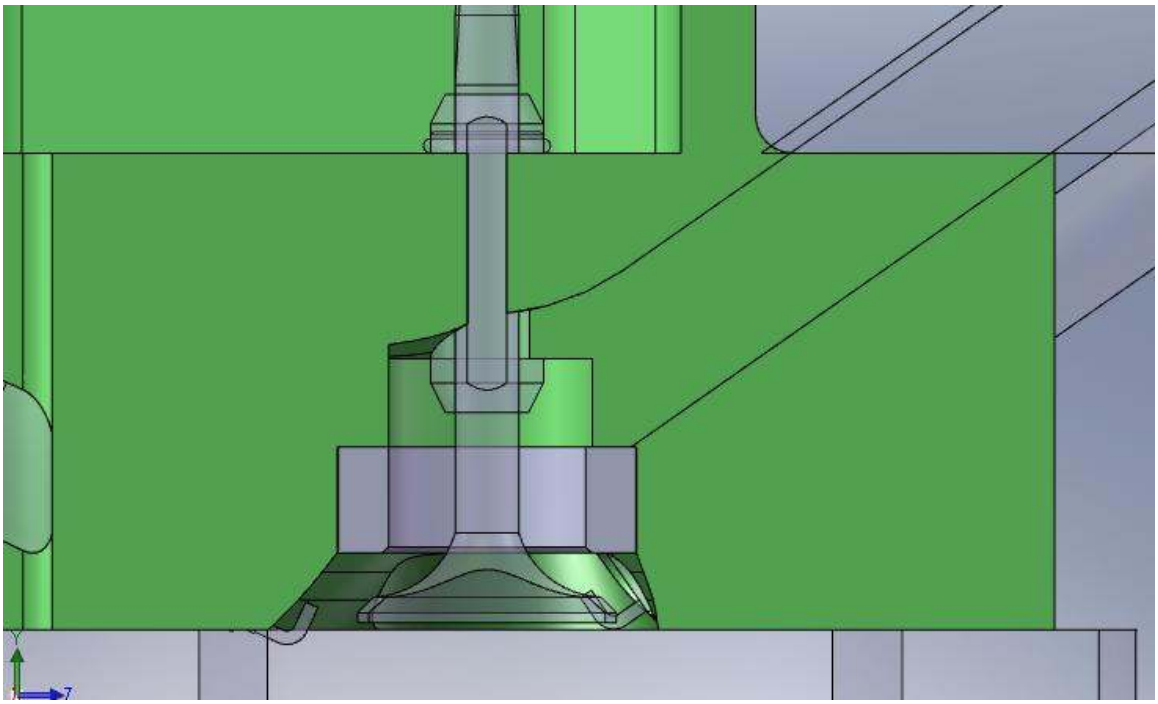

Figure 21 – Iteration 8 – Side View

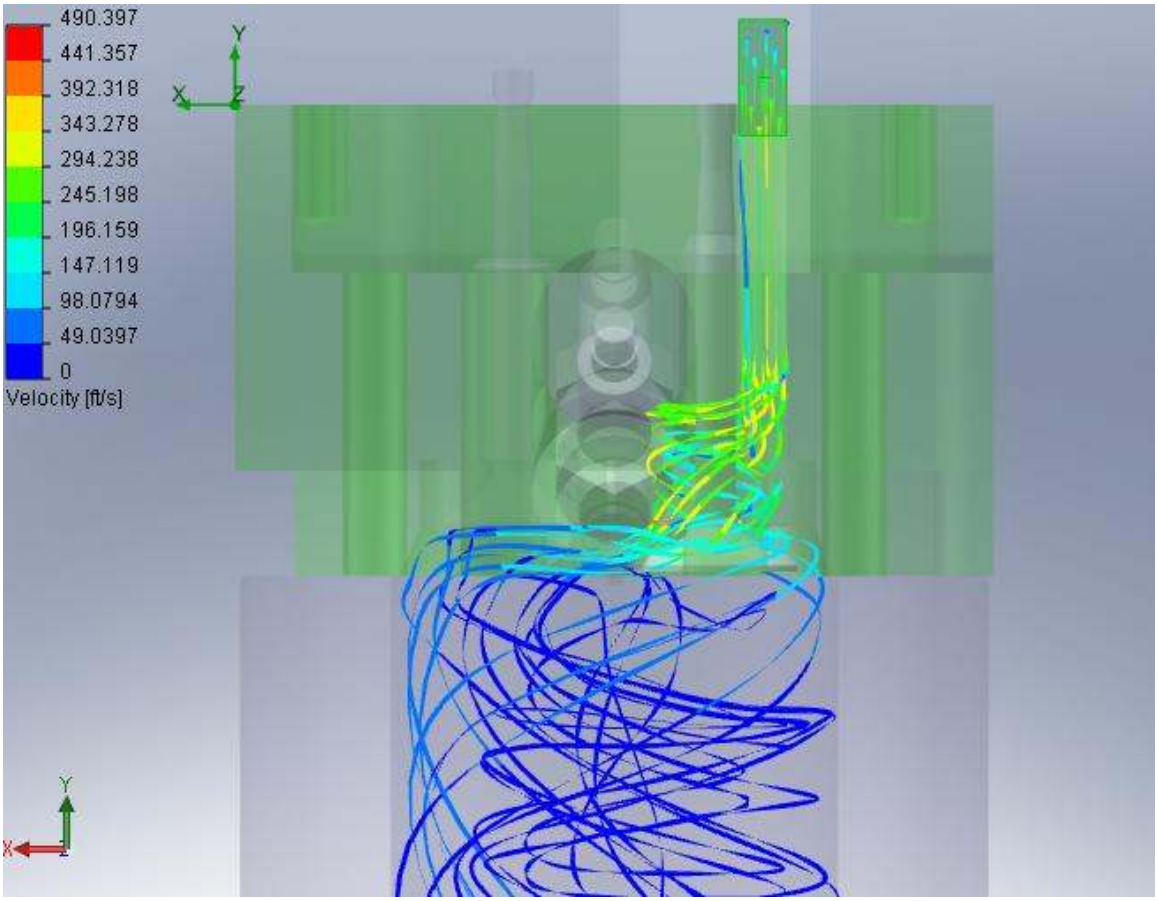

Figure 22 – Iteration 8 – Rear View

Axially directed flow is present, but much stronger swirl is present. The swirl rotates about the valve and starts to swirl close to the cylinder head once it enters the cylinder.

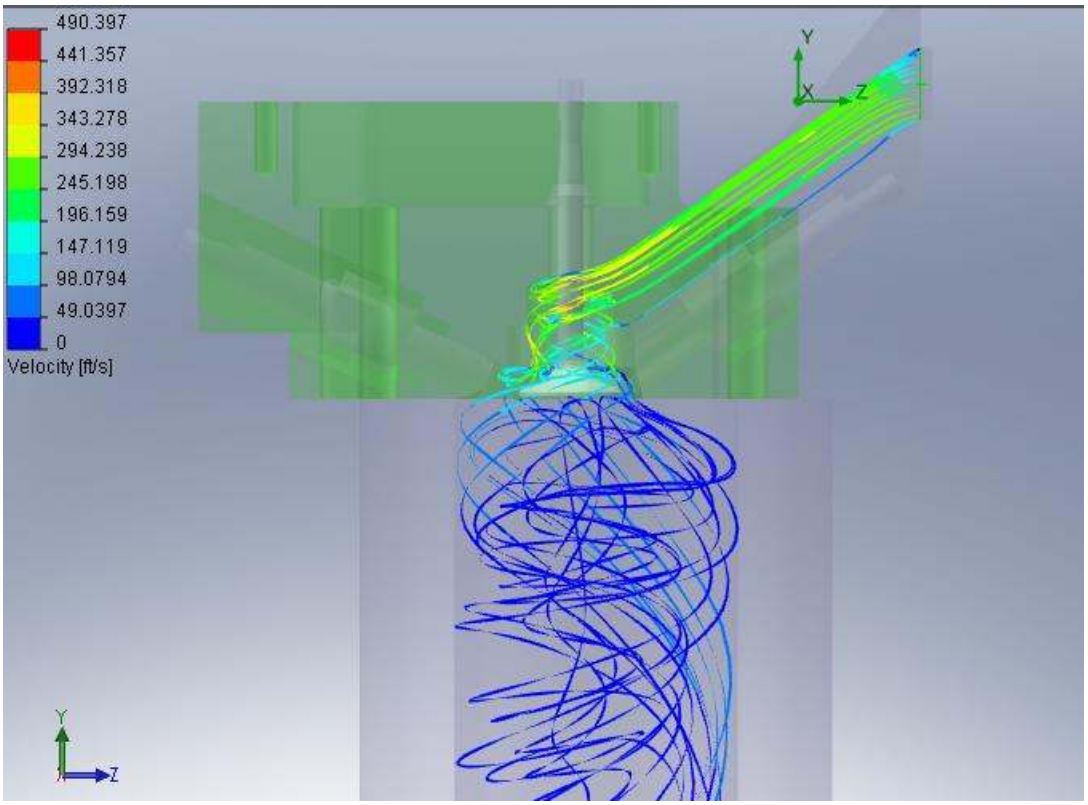

Figure 23 – Iteration 8 – Side View

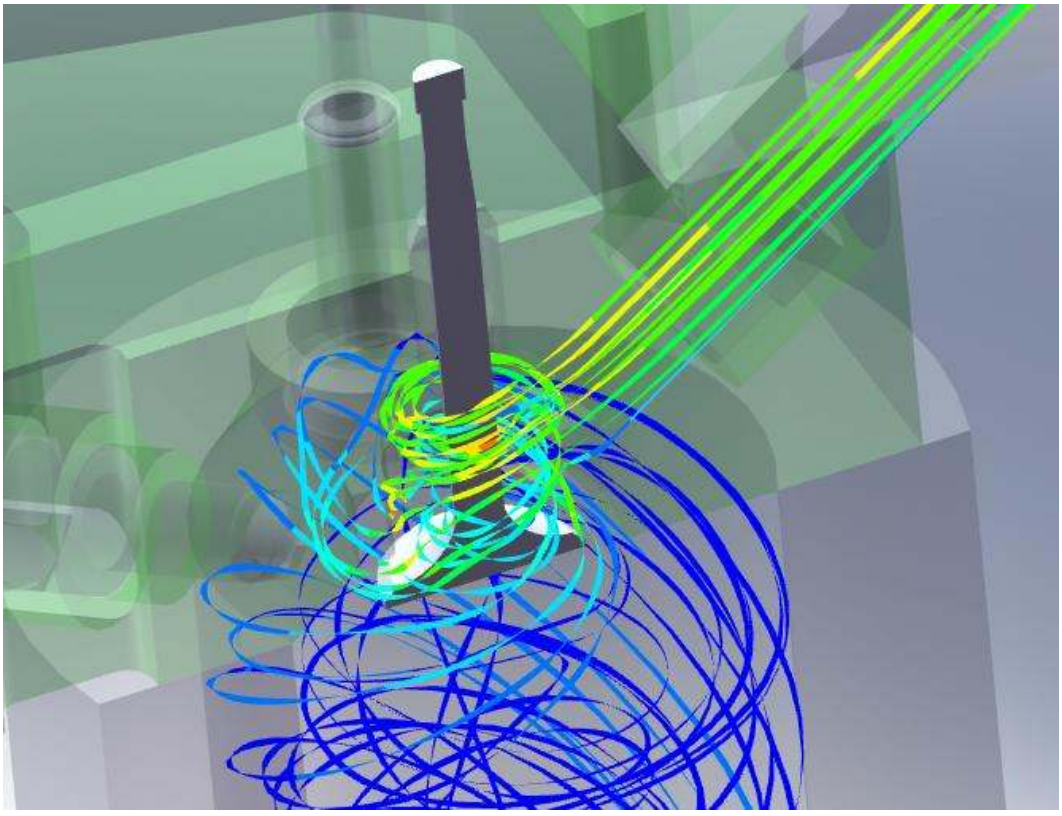

Figure 24 – Iteration 8 – Side Cutaway

It was thought that the use of a horizontal intake runner would not impede flow and reduce difficulties during fabrication. These results for iteration nine can be seen in figures 25, 26, and 27. The runner cross-sectional dimensions were not changed. The flow rate for the ninth iteration was 10.3 CFM and the swirl was 1.91. Since there was adequate swirl being developed, it was time to focus on generating enough airflow to feed the engine. The original cylinder head under the same conditions allowed for about 25 CFM of flow. In order to allow for adequate flow, the runner was widened to be .5” by .5”. These results for iteration ten can be seen in figures 28, 29 and 30. Due to the location of one of the head bolts, the centerline could not be made tangent with the outside of the valve pocket, so the runner was pulled toward the center of the valve. Due to the change in shape, the helical cut was removed and much of the swirl was lost. With the cross-sectional area of the runner doubled the flow rate picked up to 23.1 CFM. However, the swirl ratio dropped to 1.51. This was still insufficient airflow to allow adequate breathing capacity to the engine.

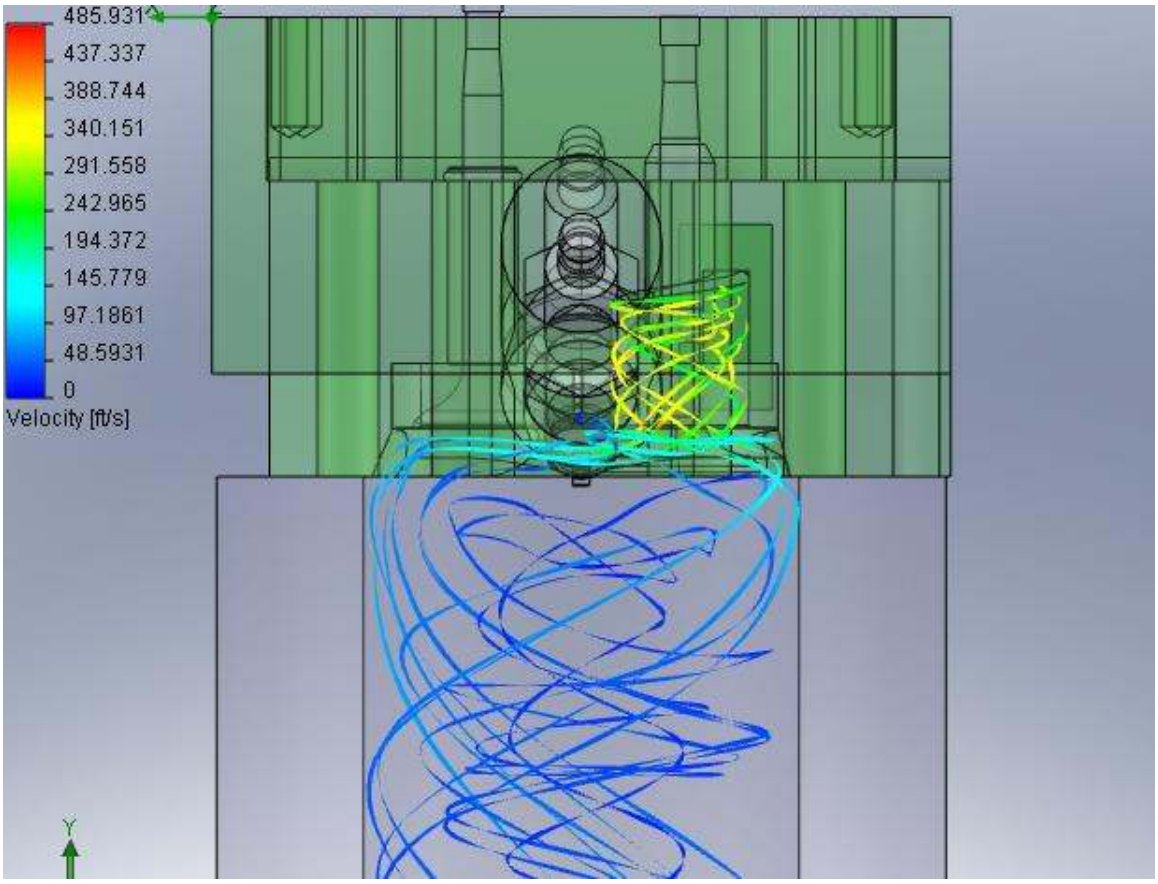

Figure 25 – Iteration 9 – Rear View

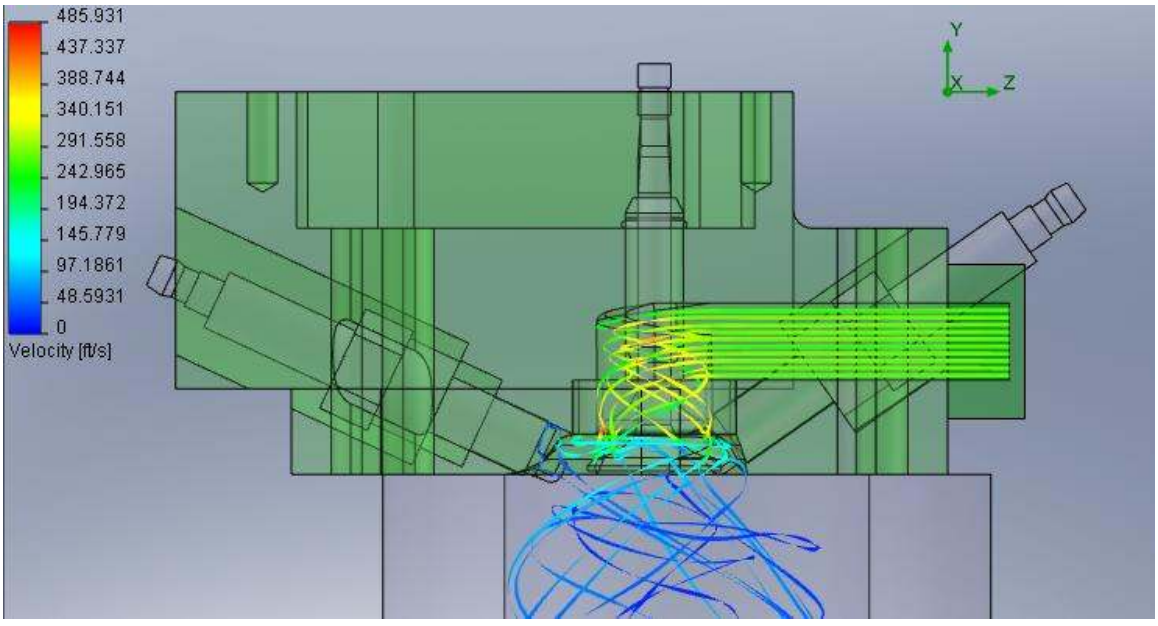

Figure 26 – Iteration 9 – Side View

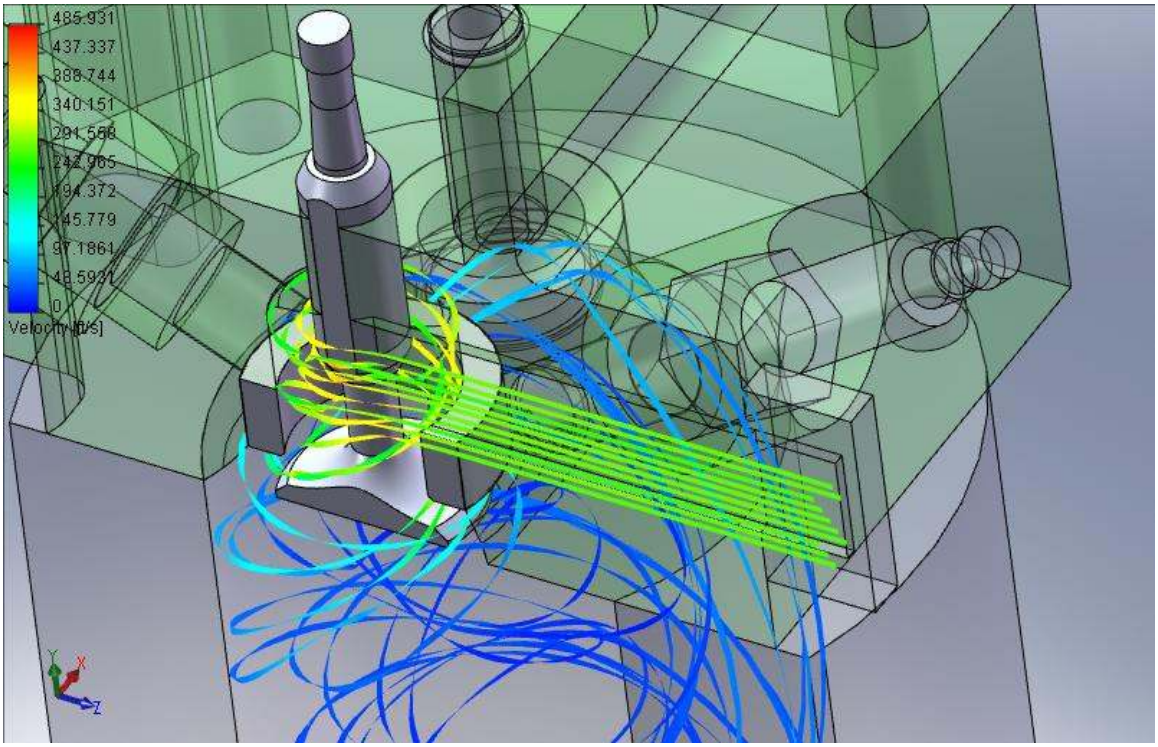

Figure 27 – Iteration 9 – Side View Cutaway

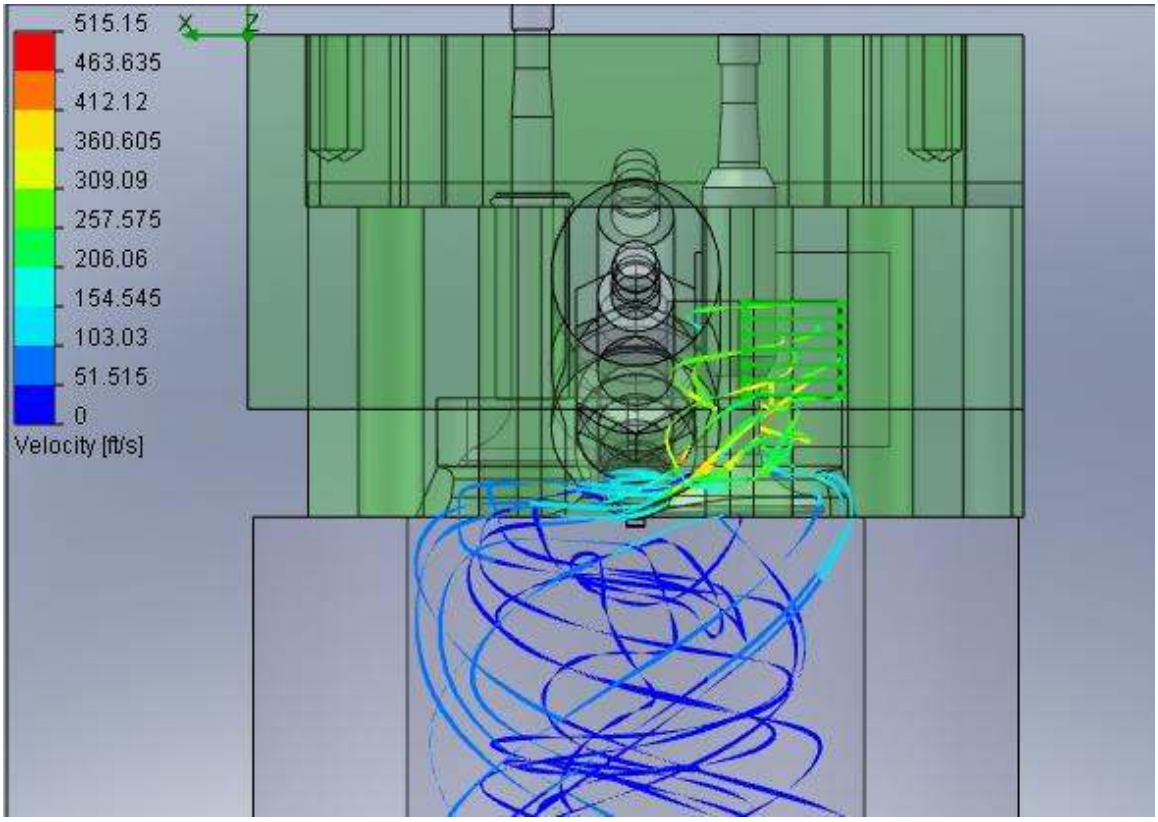

Figure 28 – Iteration 10 – Rear View

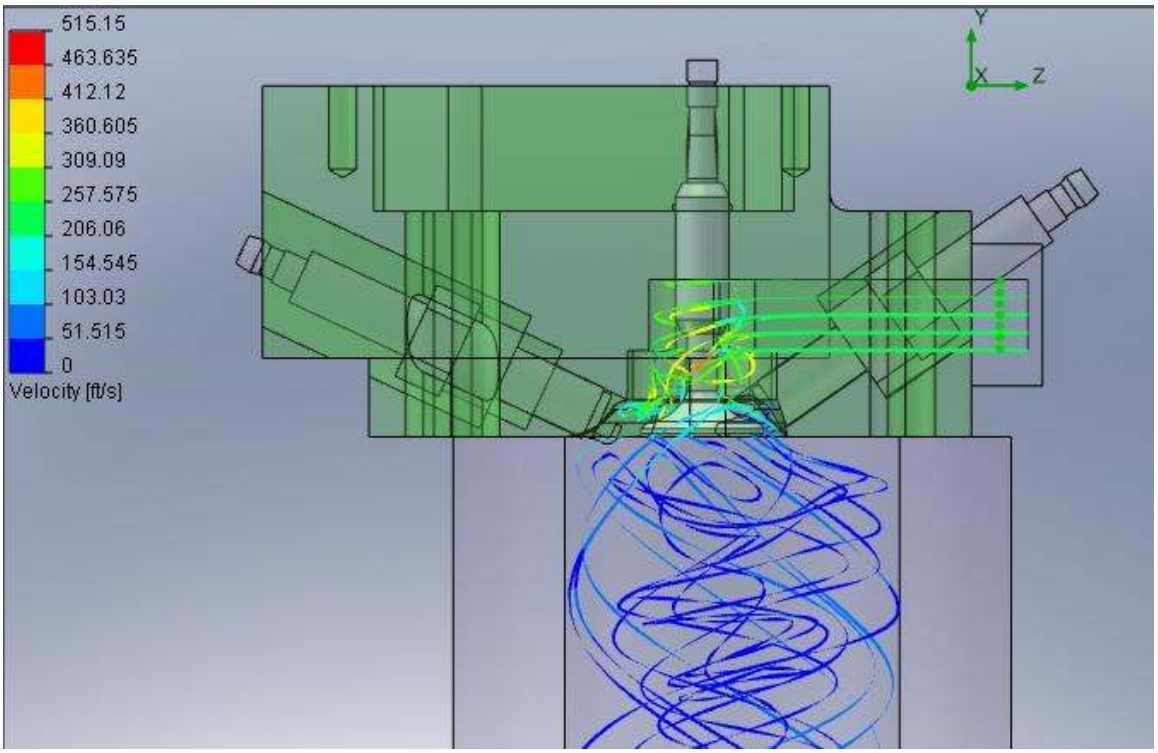

Figure 29 – Iteration 10 – Side View

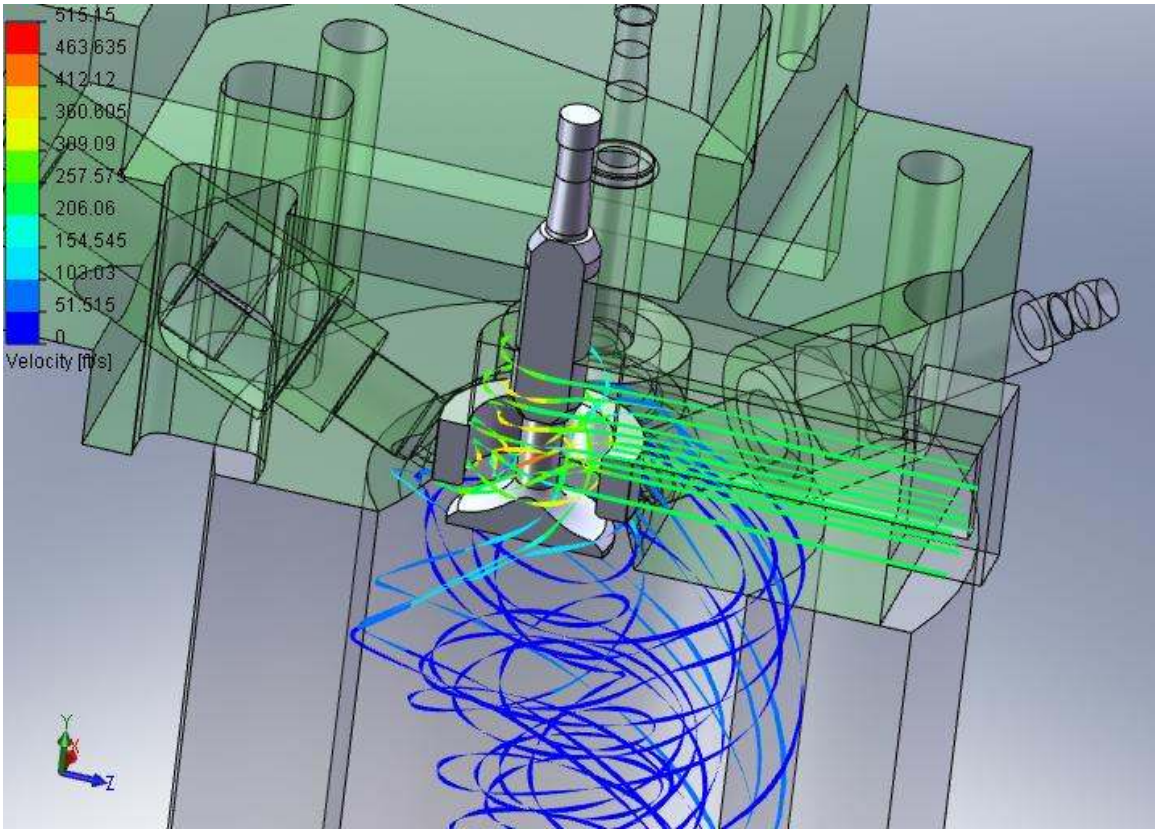

Figure 30 – Iteration 10 – Side View Cutaway

Since the runner was much longer than the original stock head, it is conceivable that some of the stock heads high flow rate was due to its short runner length. The next iteration used the same runner geometry, except the entrance was on the adjacent face and was as close to tangent on the cylinder wall as possible. The runner was slightly shorter. The results for the 11th iteration can be seen in figures 31, 32, 33, and 34. The change increased the flow rate to 27.2 CFM unfortunately some of the organized swirl was lost and the cylinder became much more turbulent. The swirl ratio was 1.21.

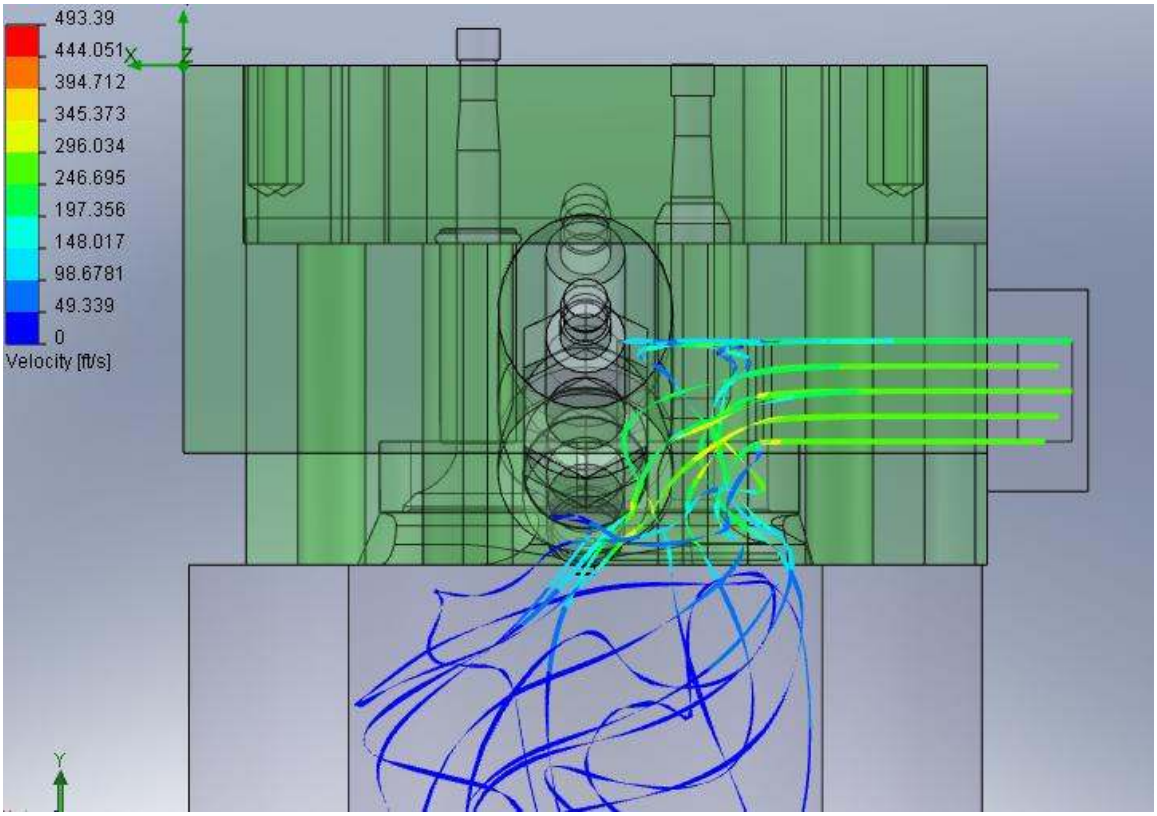

Figure 31 – Iteration 11 – Rear View

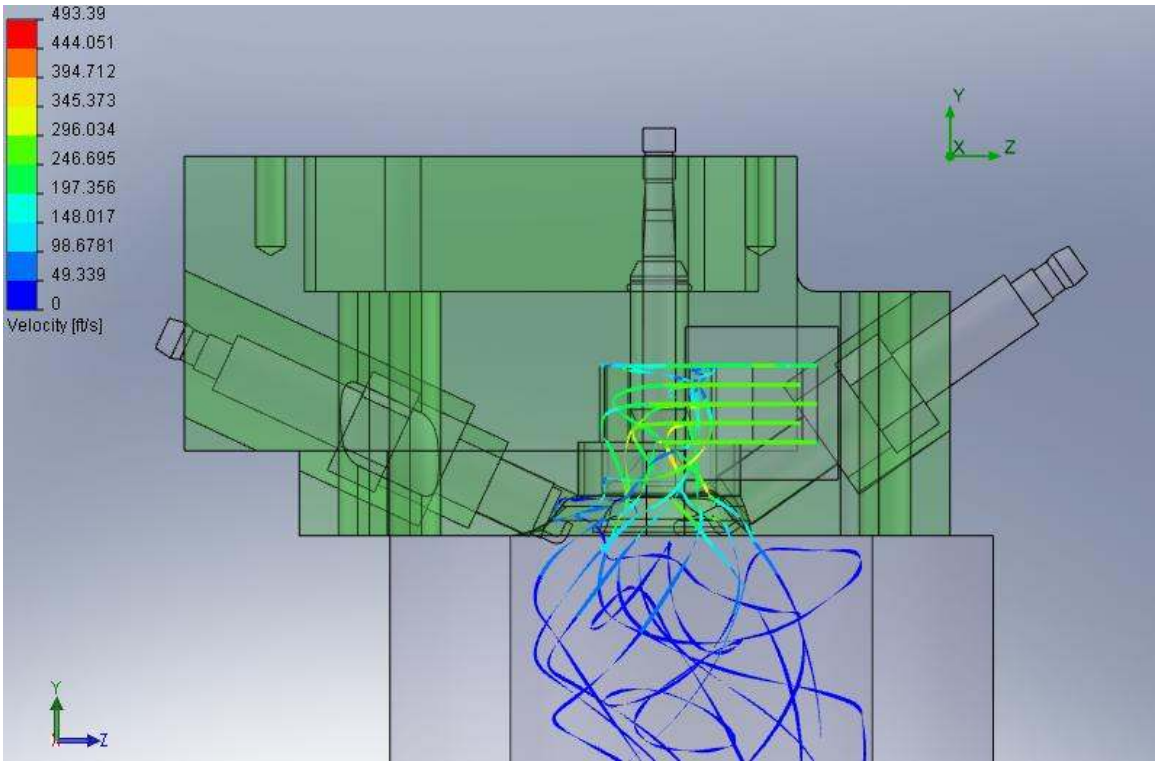

Figure 32 – Iteration 11 – Side View

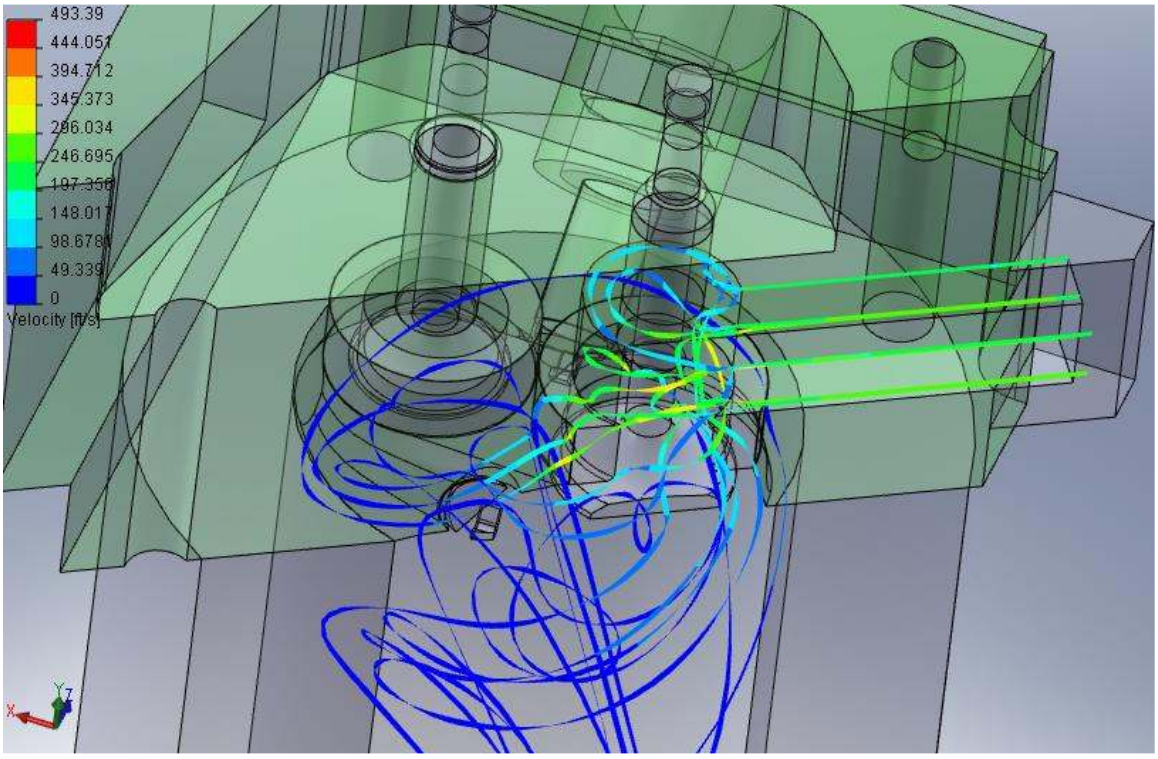

Figure 33 – Iteration 11 – Side Cutaway

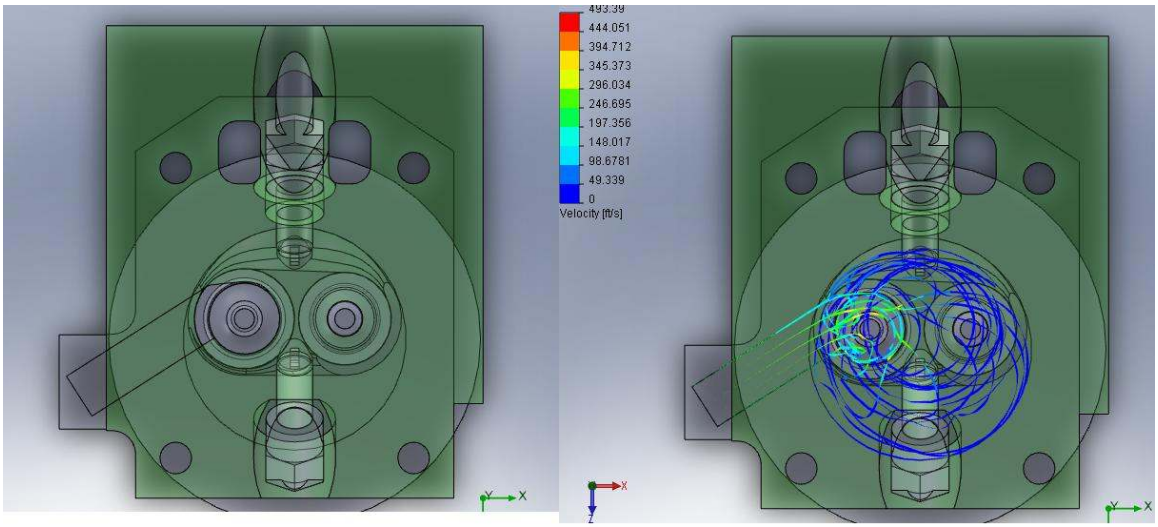

Figure 34 – Iteration 11 – Top View

To allow for more air to flow through the cylinder, the valve seat was rounded to allow the air to flow more smoothly. The results for removal of the material in the valve seat can be seen in figures 35, 36, 37, and 38. This removal of a small amount of material in the valve seat allowed the flow to jump to 29.5 CFM. The flow was much less chaotic and the swirl was much better defined. However, it did not become uniform until it had traveled down the cylinder about ¼ of a bore diameter. The swirl ratio for the 12th iteration was 1.62.

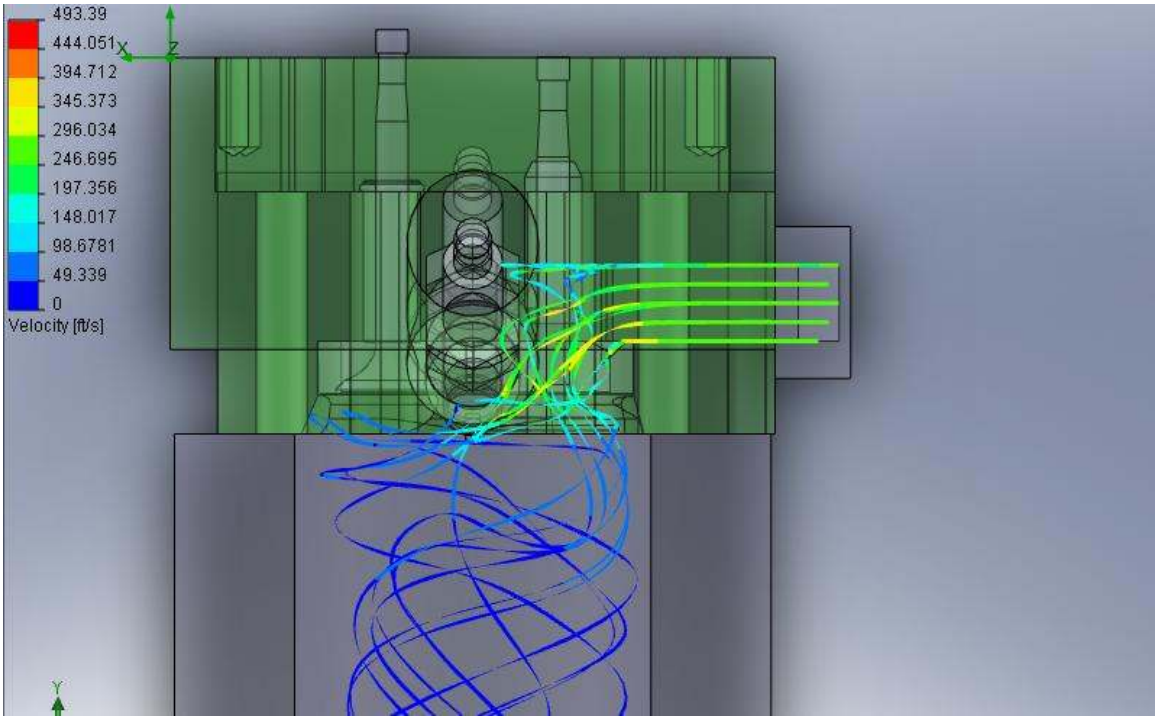

Figure 35 – Iteration 12 – Front View

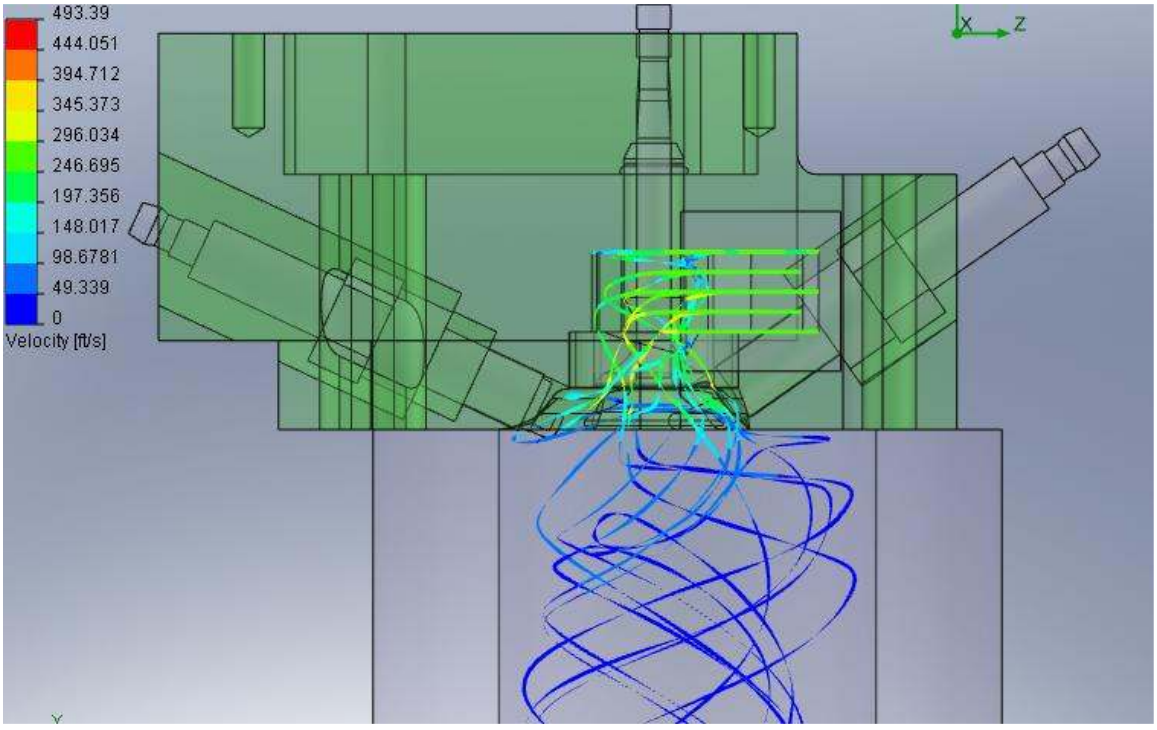

Figure 36 – Iteration 12 – Side View

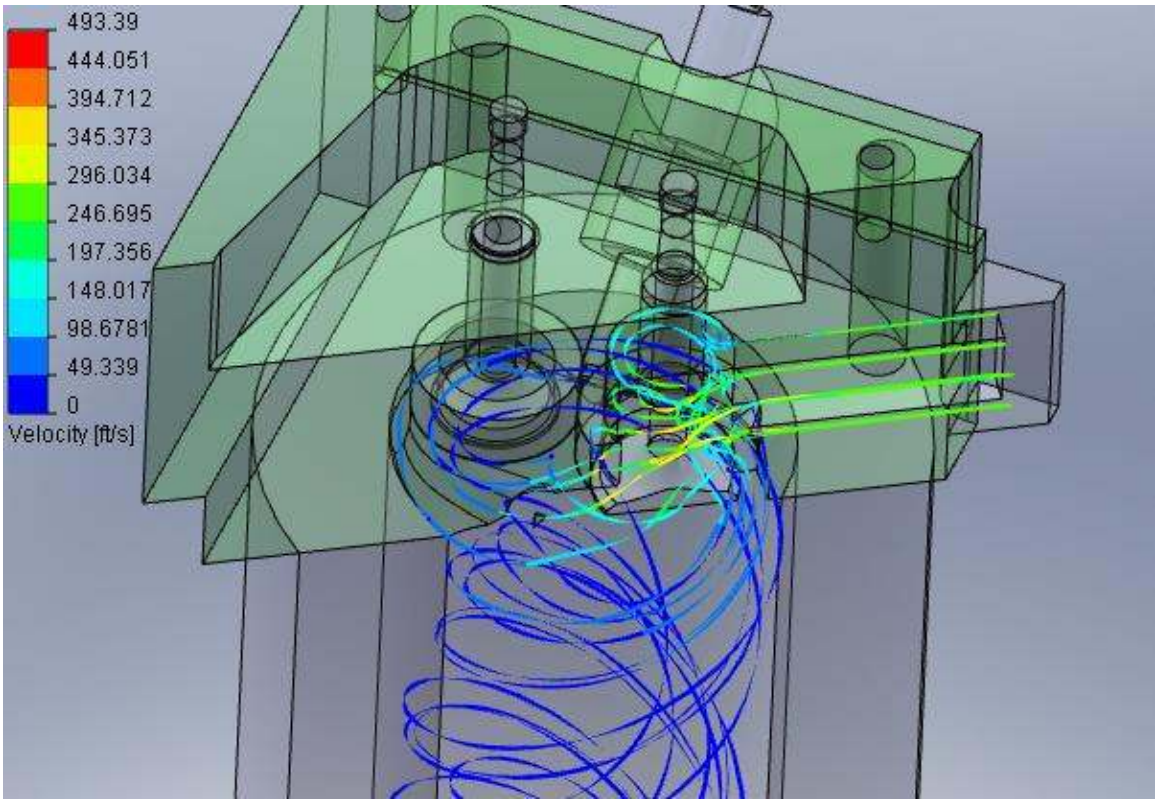

Figure 37 – Iteration 12 – Side View Cutaway

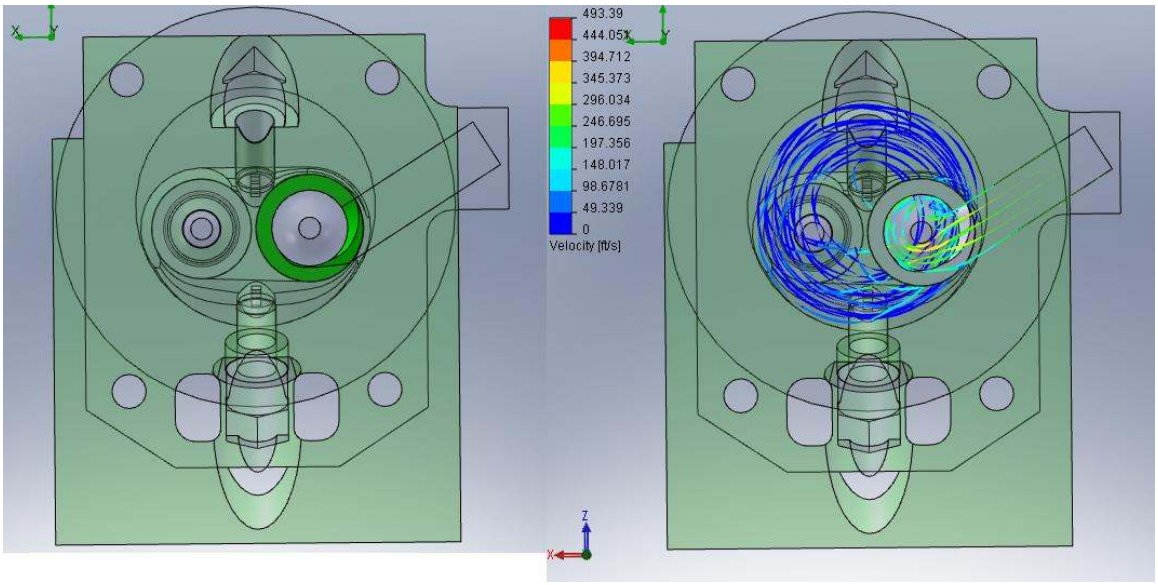

Figure 38 – Iteration 12 – Top View

The 13th iteration was designed to increase the flow rate further. The area of the runner was expanded to be .75” wide and the angle was shifted so it would hit the cylinder wall more tangentially. To achieve this, the runner was shortened and material was removed

from the head for a future mating surface. The results are shown in figures 39, 40, 41 and 42. The changes are most apparent in figure 42. The swirl does not develop strongly, but the flow rate has increased to 33.1 CFM and the swirl ratio was 1.43.

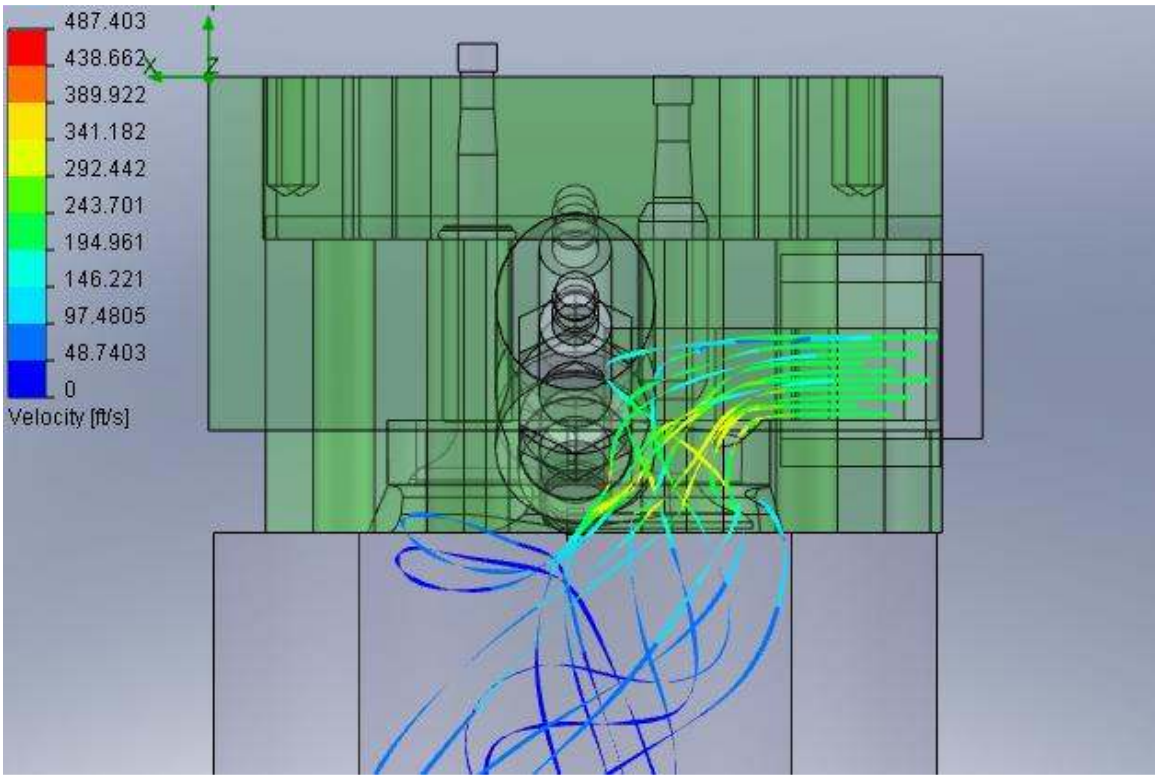

Figure 39 – Iteration 13 – Front View

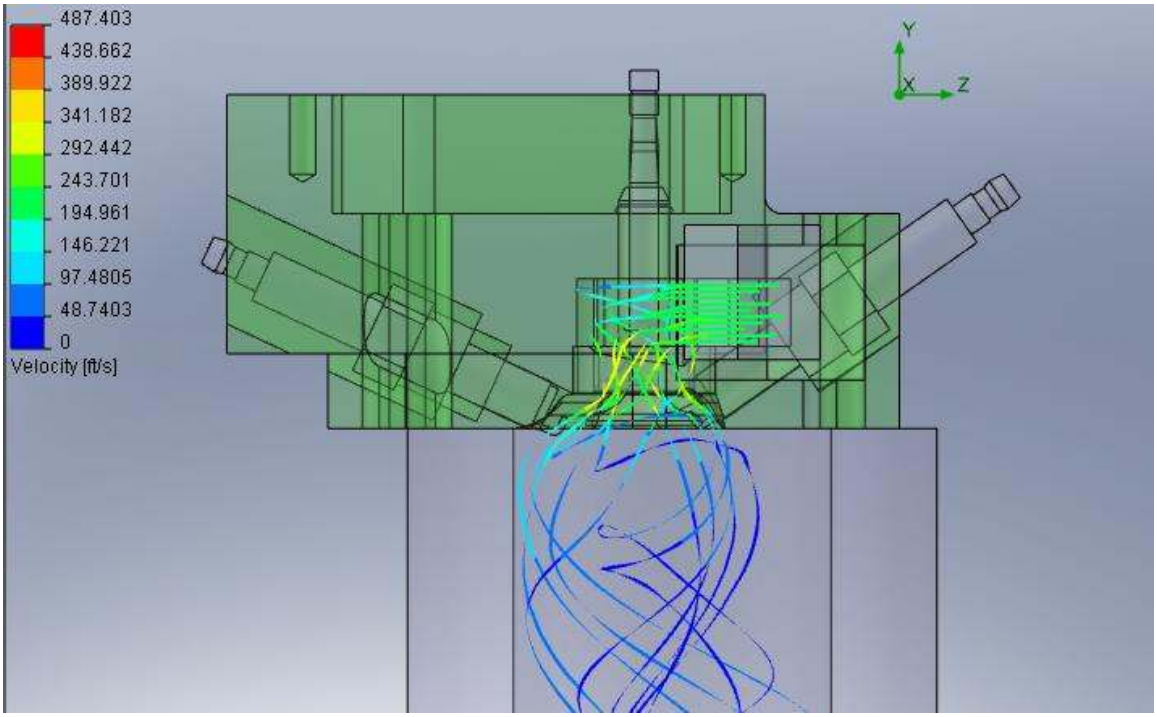

Figure 40 – Iteration 13 – Side View

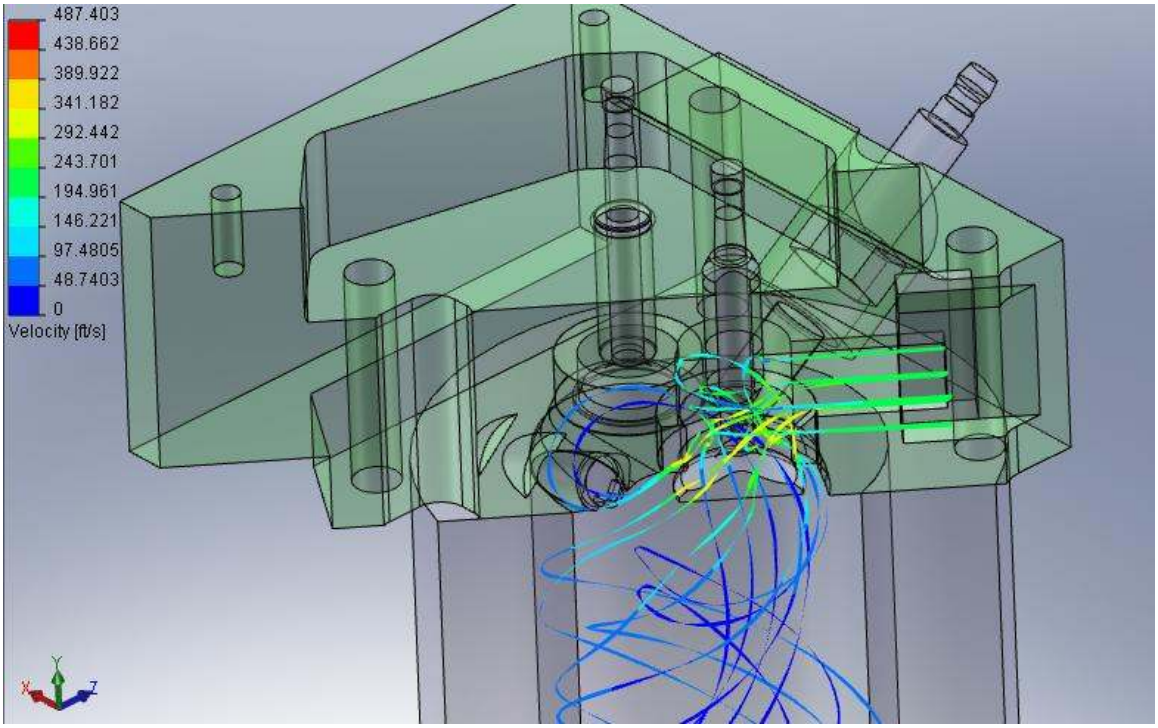

Figure 41 – Iteration 13 – Side View Cutaway

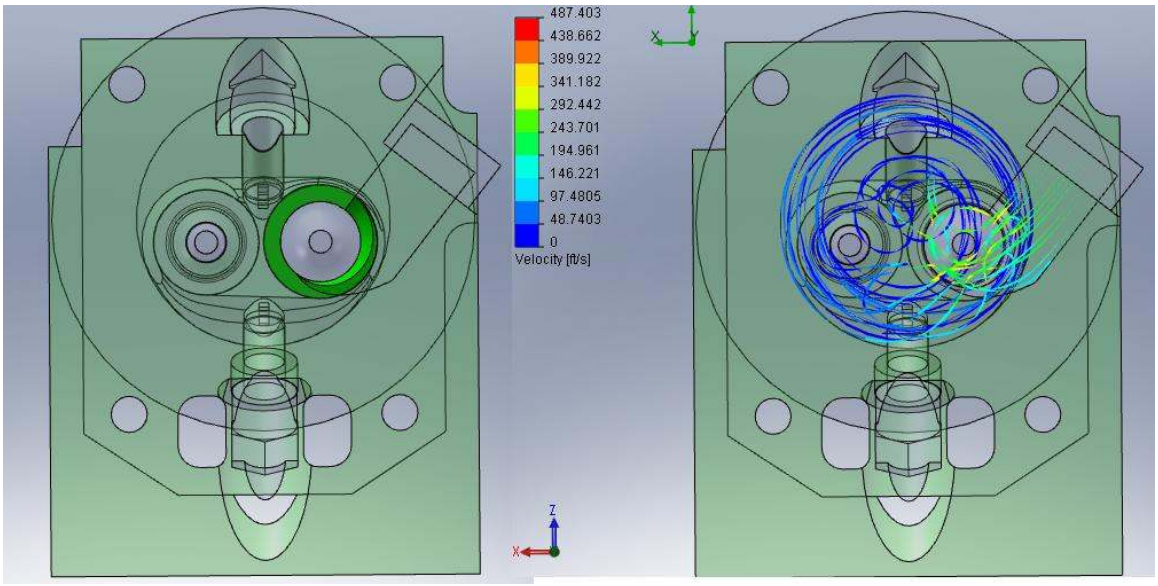

Figure 42 – Iteration 13 – Top View

The addition of a helical roof in the valve pocket can be seen in figures 43, 44, 45, and 46. The swirl here was well-developed and the flow rate had only dropped to 31.7 CFM. In iteration 14, the swirl ratio had increased to 2.46. The helical roof can be seen to greatly increase swirl.

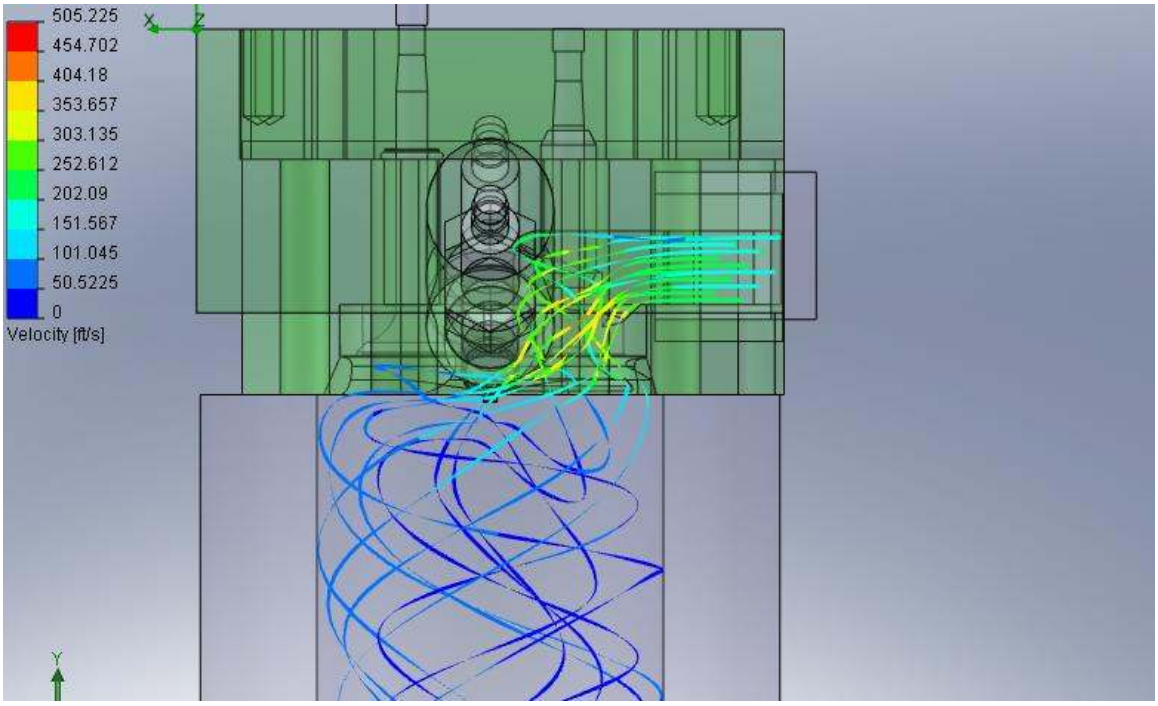

Figure 43 – Iteration 14 – Front View

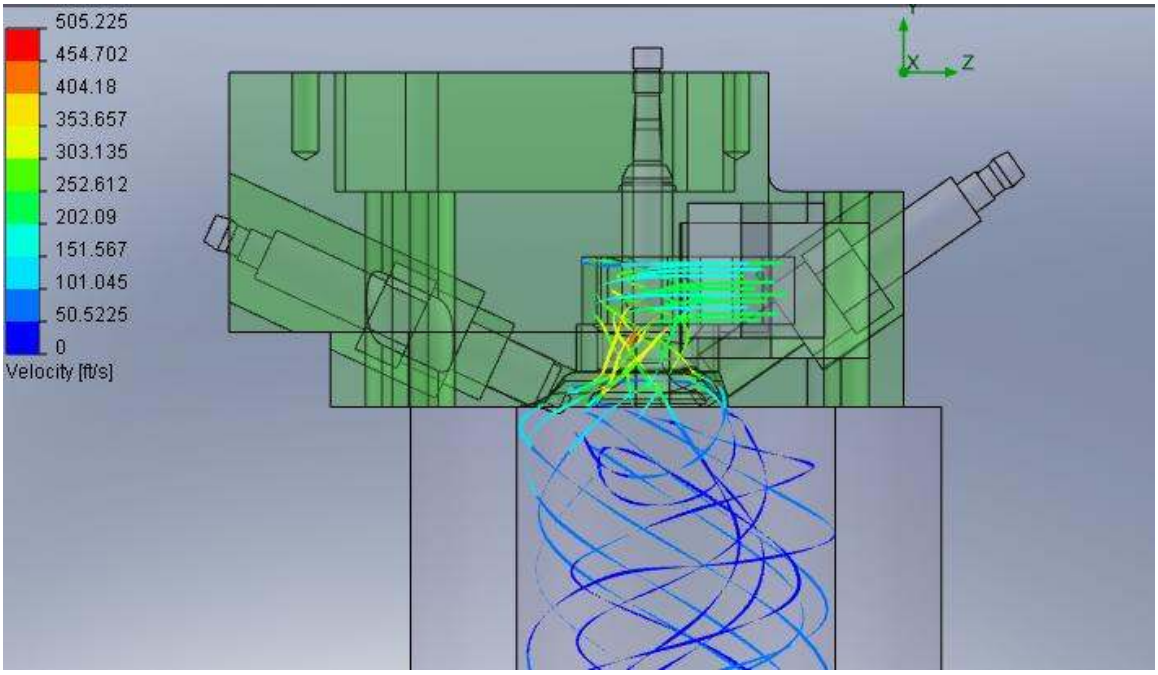

Figure 44 – Iteration 14 – Side View

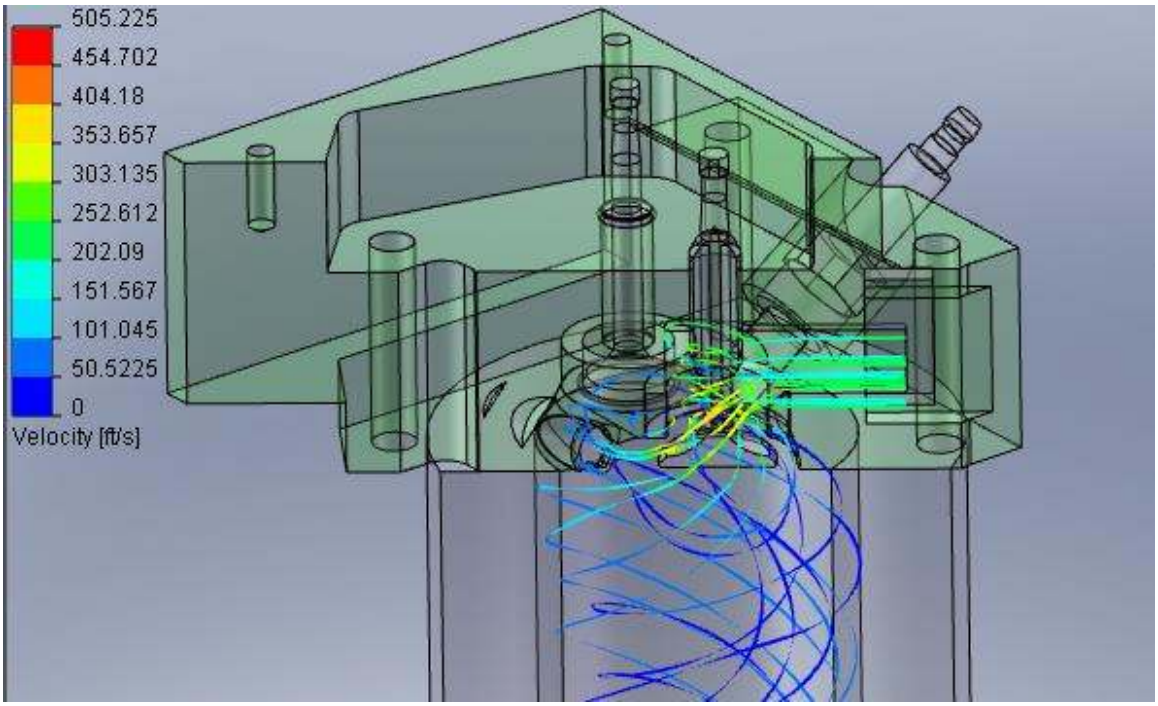

Figure 45 – Iteration 14 – Side Cutaway

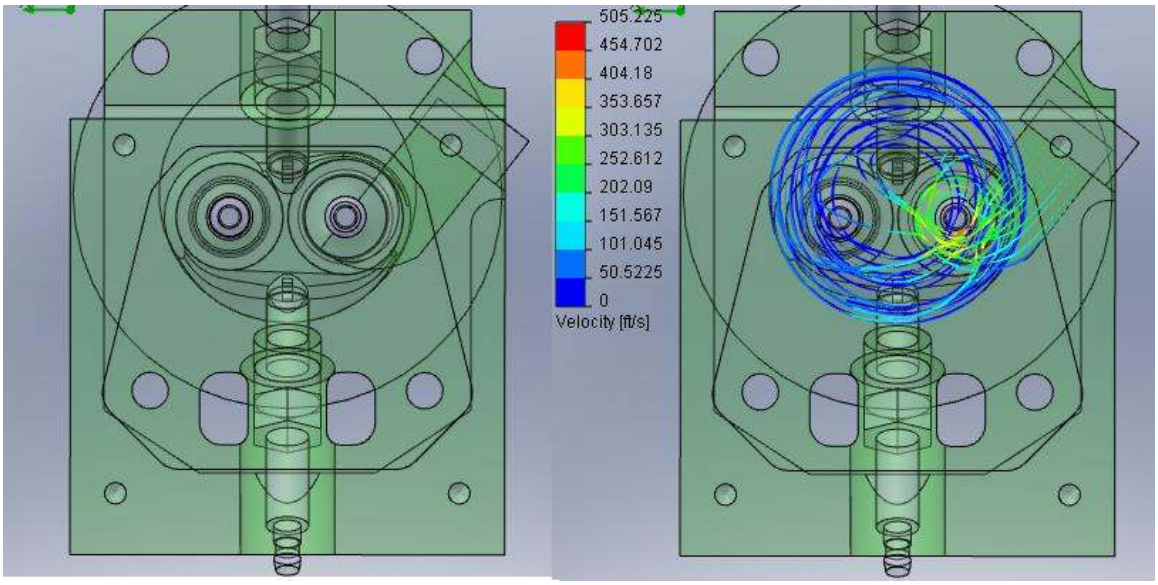

Figure 46 – Iteration 14 – Top View

The intent of the next iteration was to further develop the swirl. If the runner was constricted near the valve pocket, it may increase the velocity slightly and make more swirl. The intake runner was constricted to .5" wide at the entrance to the valve pocket. These results for iteration 15 can be seen in figures 47, 48, 49 and 50. The flow rate for the narrowed runner was 25.1 CFM slightly lower than before, but not nearly as low as the .5" by .5" runner. The swirl begins to generate inside the combustion chamber and propagates down the cylinder. The swirl ratio was 2.99 in the 15th iteration.

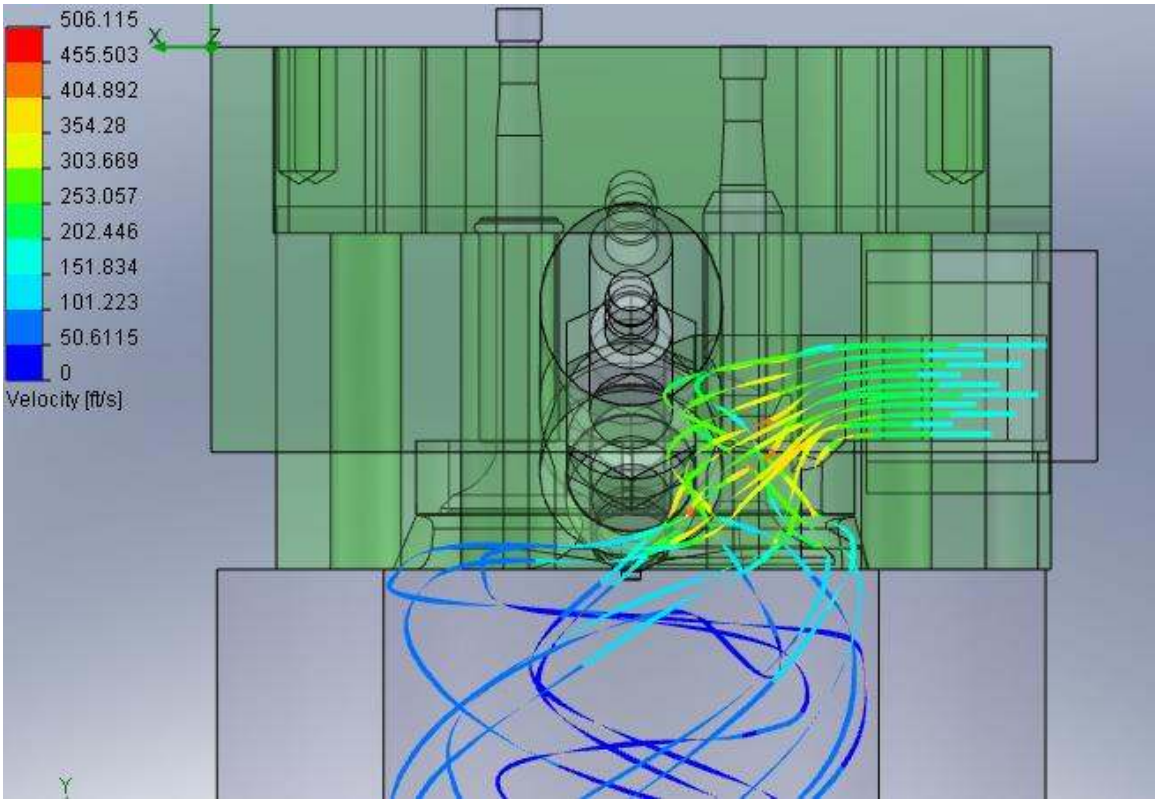

Figure 47 – Iteration 15 – Front View

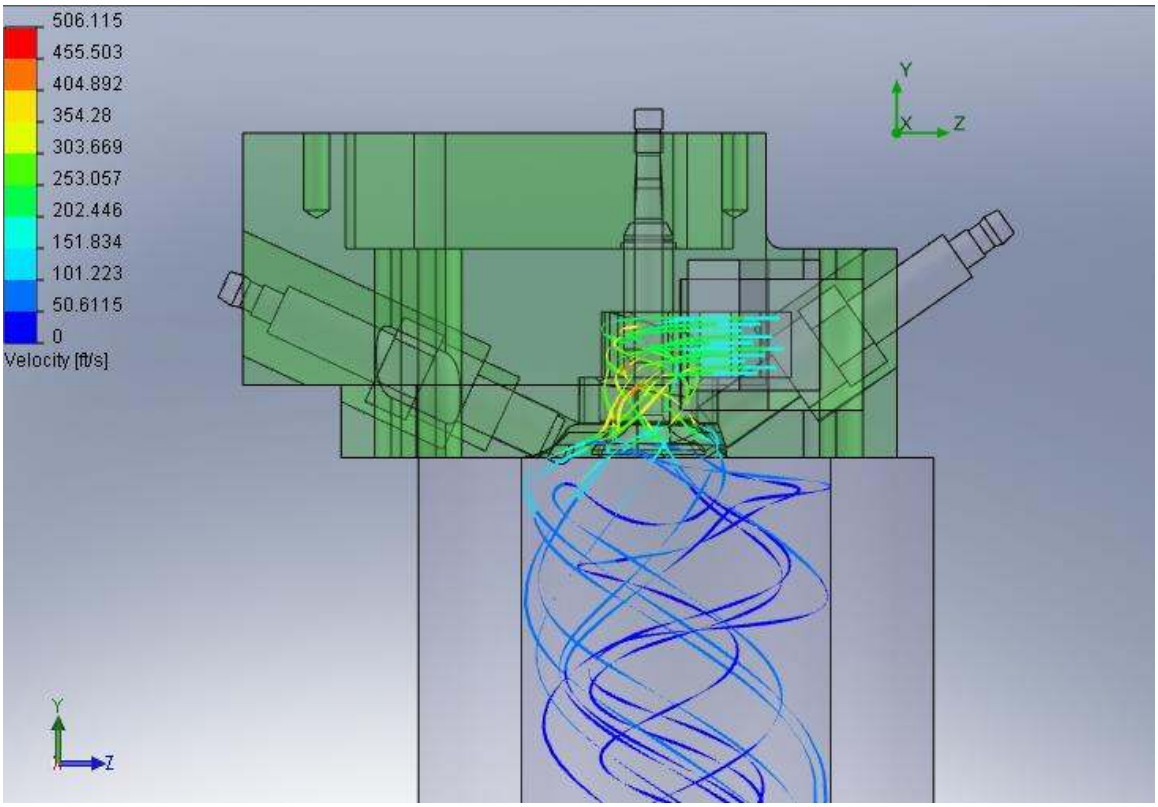

Figure 48 – Iteration 15 – Side View

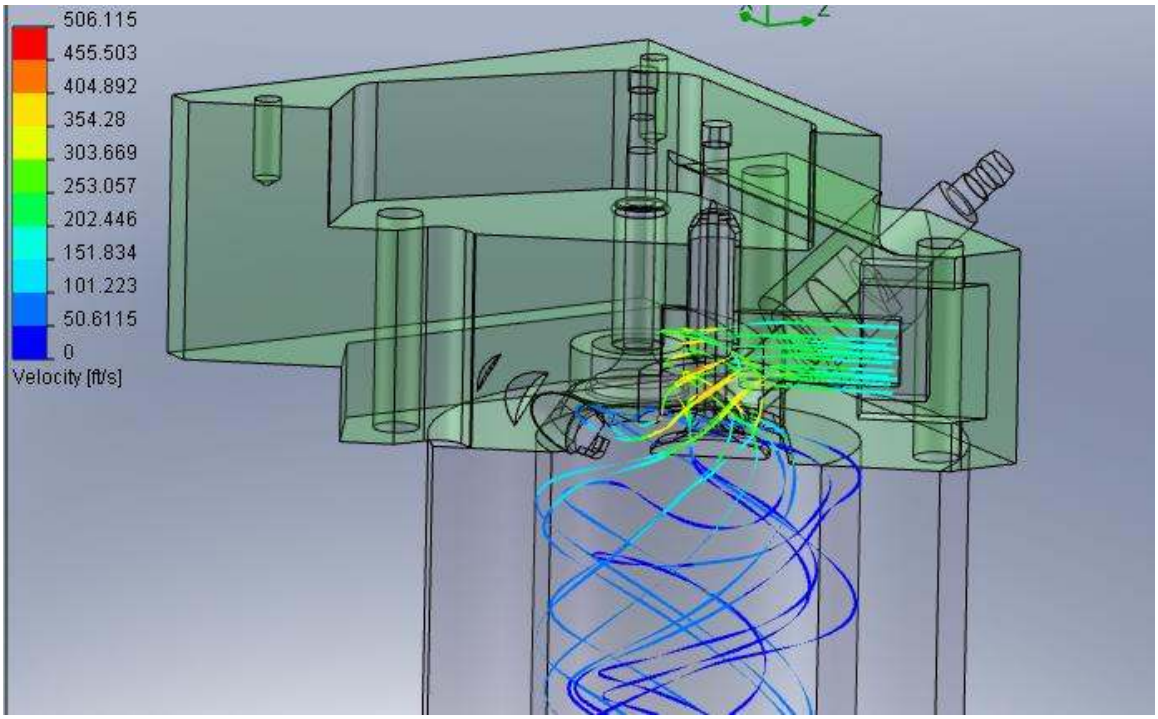

Figure 49 – Iteration 15 – Side View Cutaway

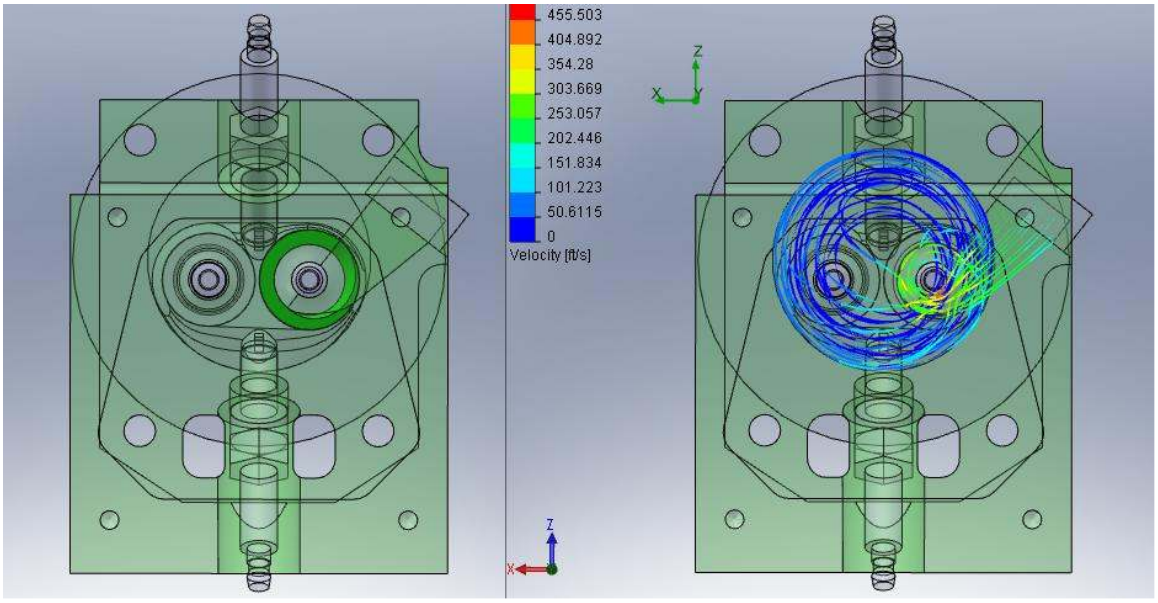

Figure 50 – Iteration 15 – Top View

In the next iteration, a small radius was added to the outside of the helical surface between the helix and the valve pocket vertical wall. The primary reason for adding this radius was to make fabrication easier. The results of iteration 16 can be seen in figures

51, 52, 53, and 54. The flow rate was not greatly affected and dropped to 24.9 CFM. The change caused the swirl ratio to drop to 2.75.

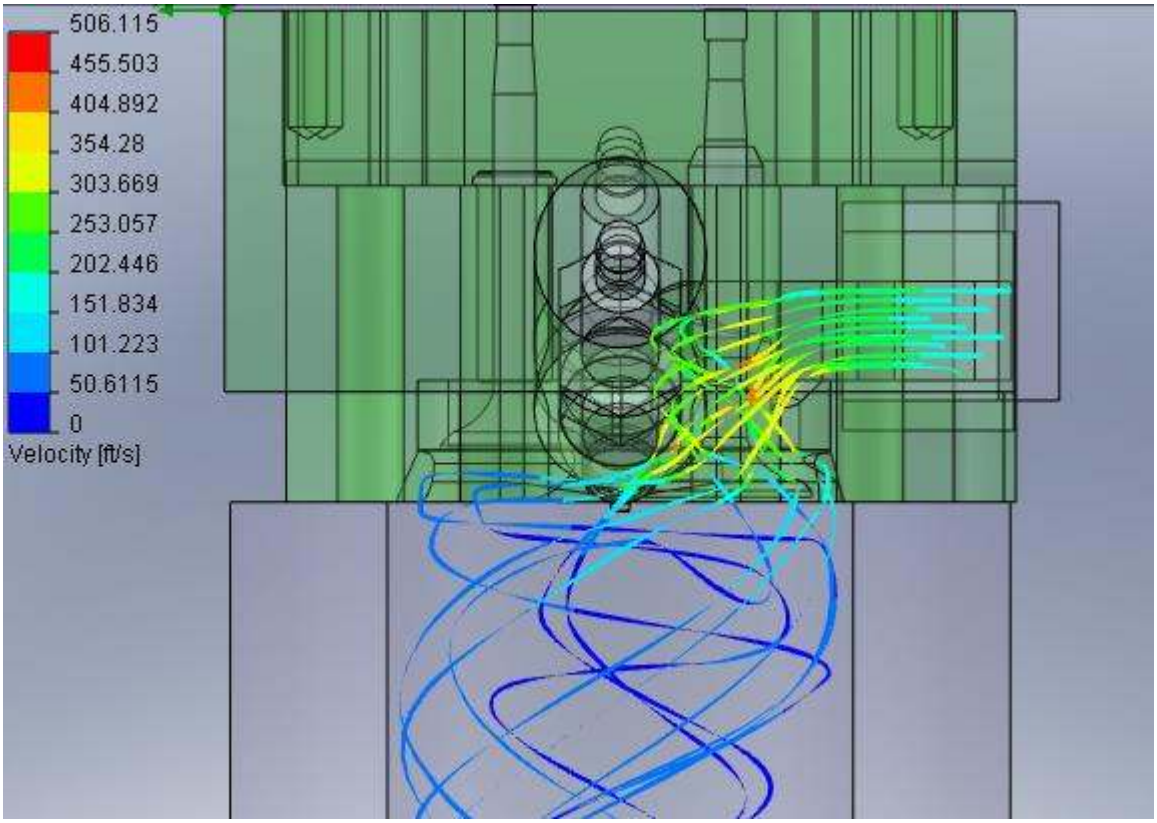

Figure 51 - Iteration 16 – Front View

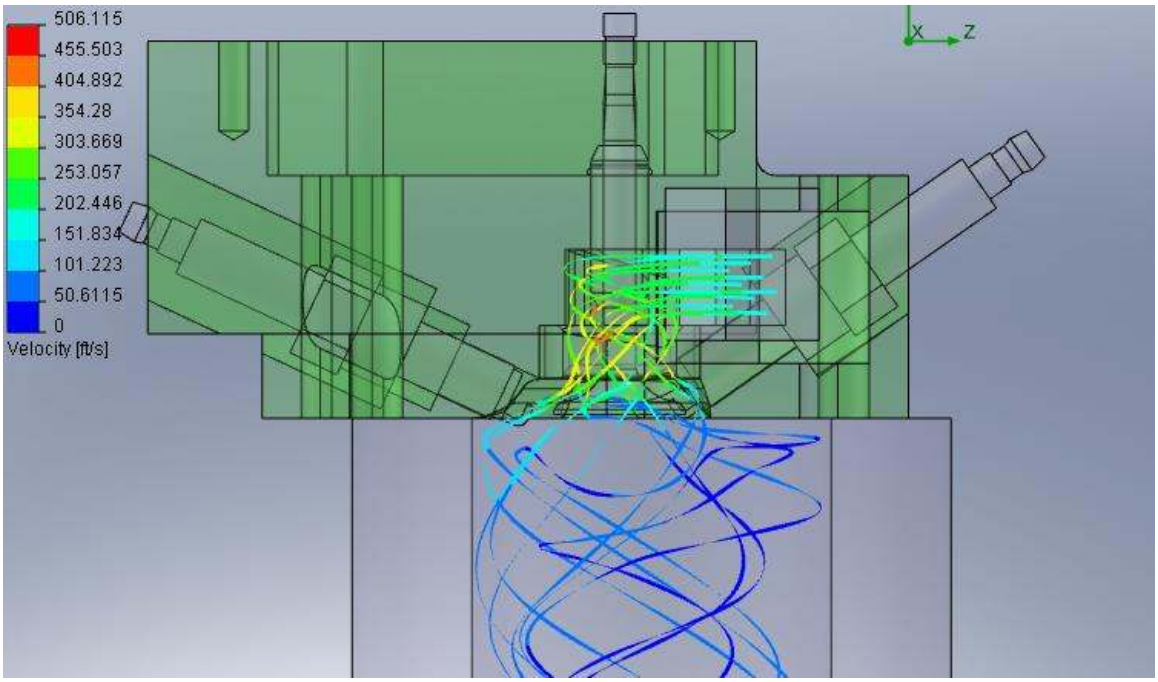

Figure 52 - Iteration 16 – Side View

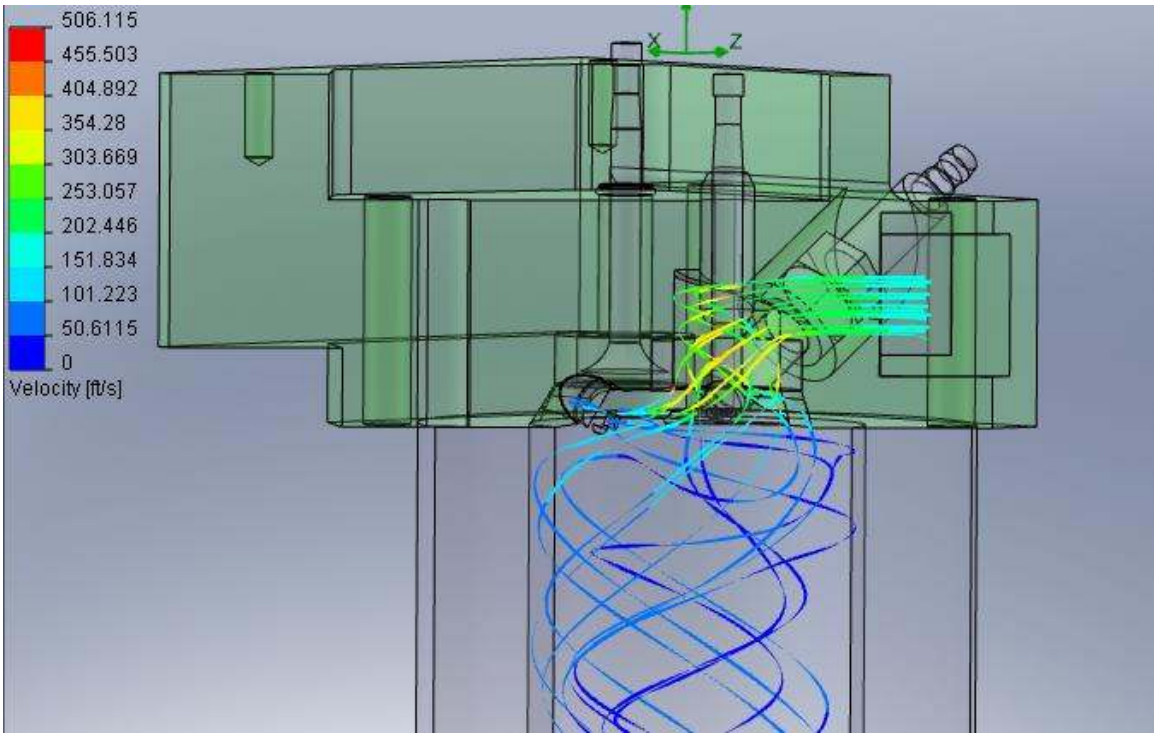

Figure 53 - Iteration 16 – Side View Cutaway

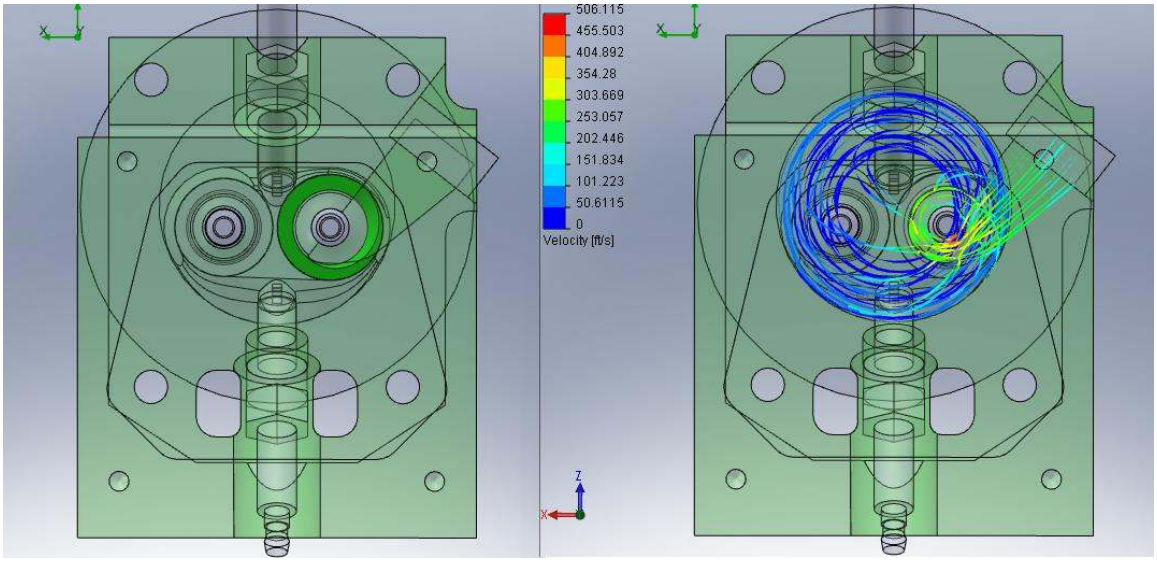

Figure 54 - Iteration 16 – Top View

For the next change, a small deflector was added so that air would pass more freely around the edge of the valve guide. These results for iteration 17 can be seen in figures 55, 56, 57, and 58. The flow rate dropped to 24.7 CFM and the swirl ratio changed slightly to 2.8

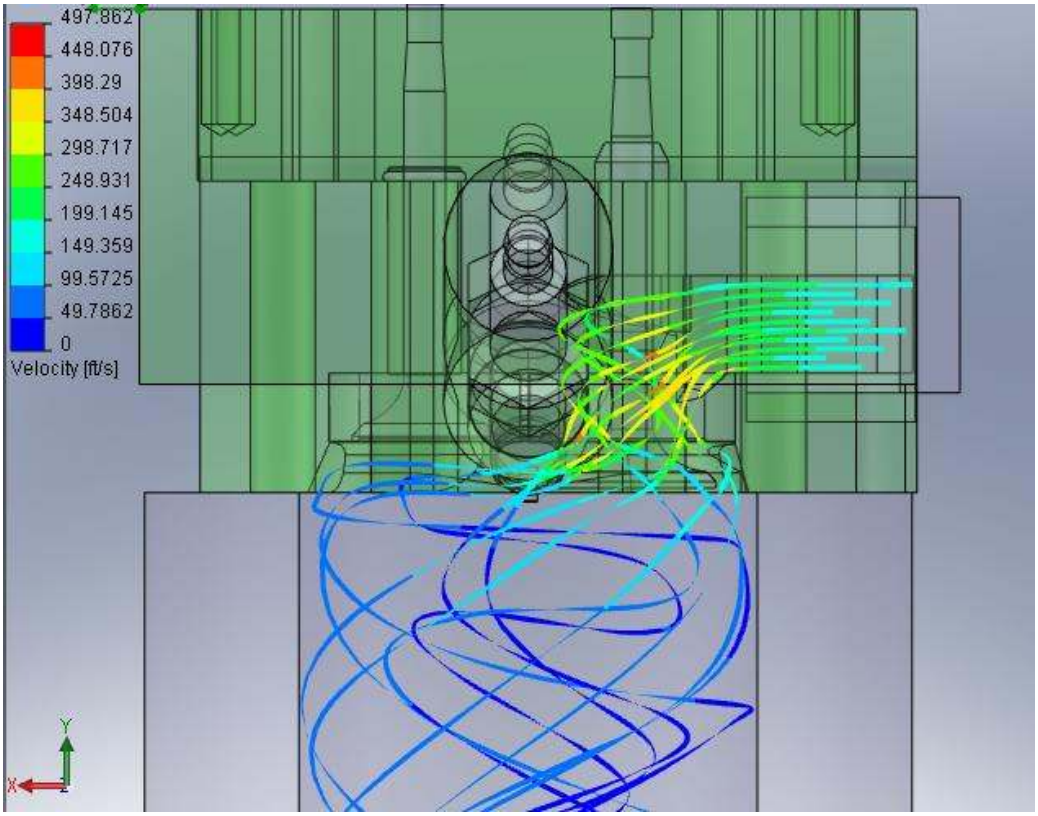

Figure 55 – Iteration 17 – Front View

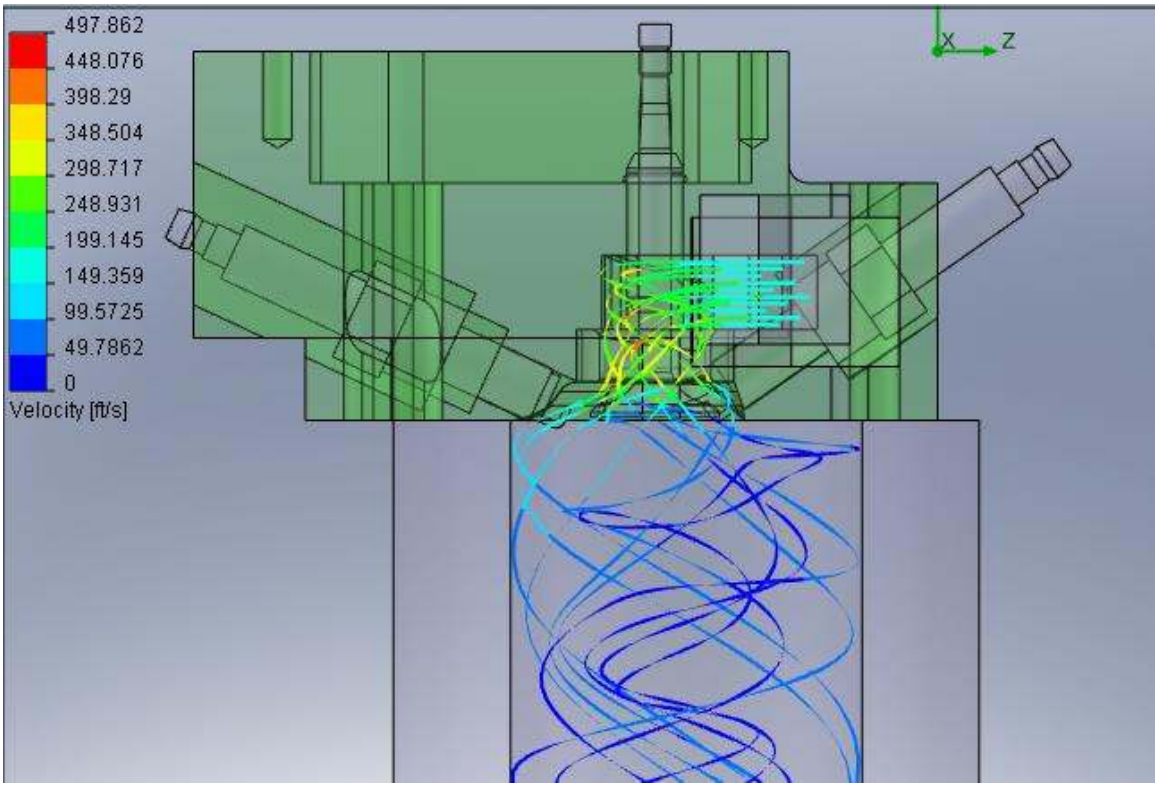

Figure 56 – Iteration 17 – Side View

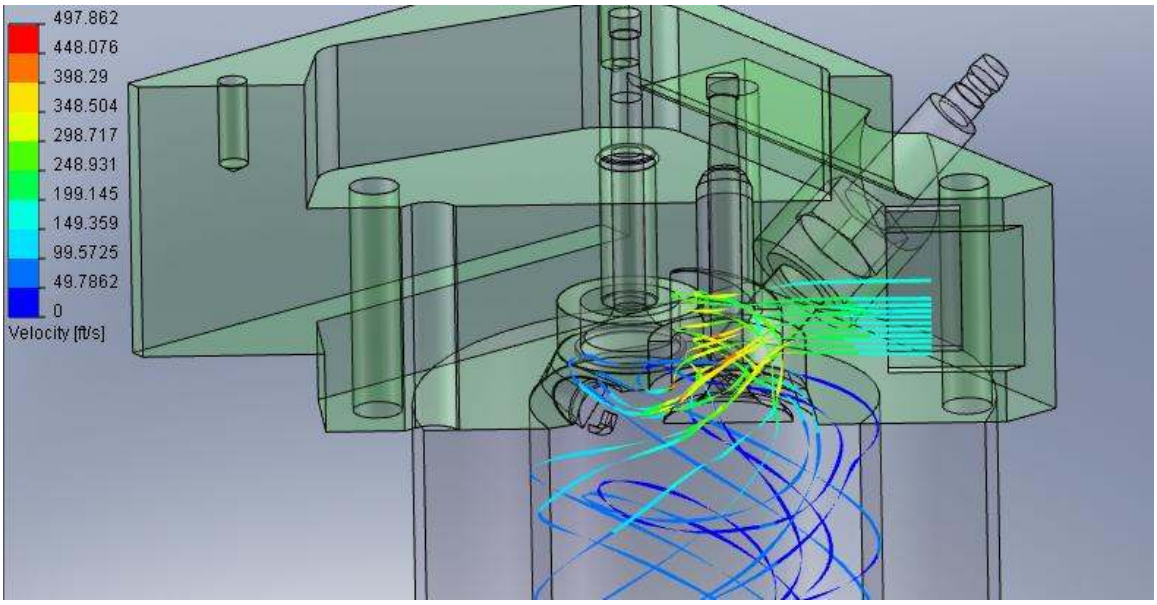

Figure 57 – Iteration 17 – Side View Cutaway

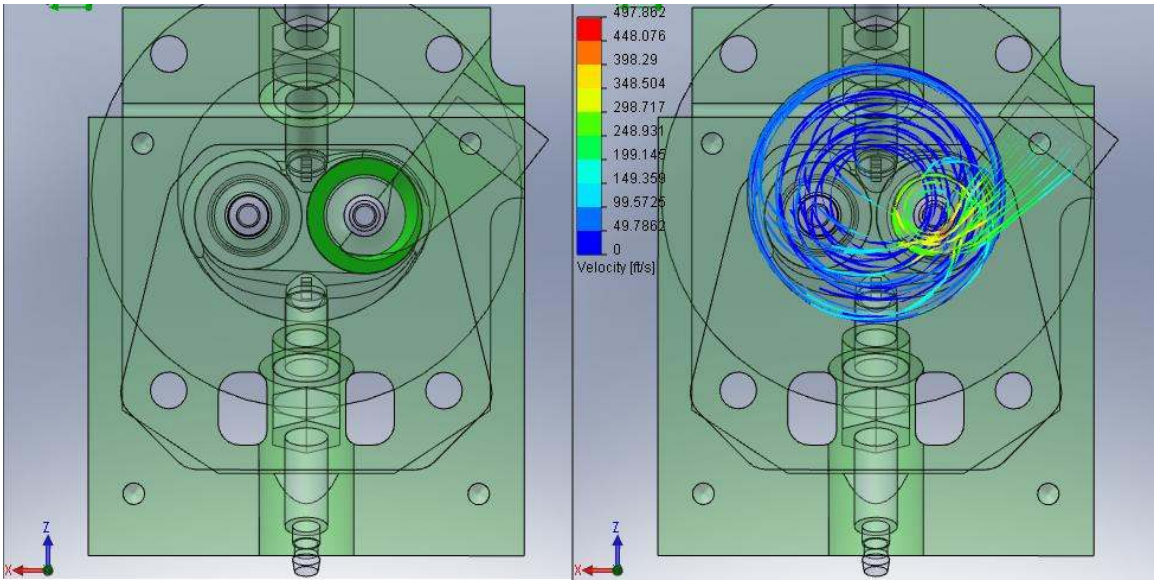

Figure 58 – Iteration 17 – Top View

In the 18th iteration, the deflector was lengthened to see if turbulent losses could be reduced. However, the flow rate dropped further to 23.1 CFM. The results can be seen in figures 59, 60, 61, and 62. The swirl ratio appears similar, but it had dropped slightly to 2.49.

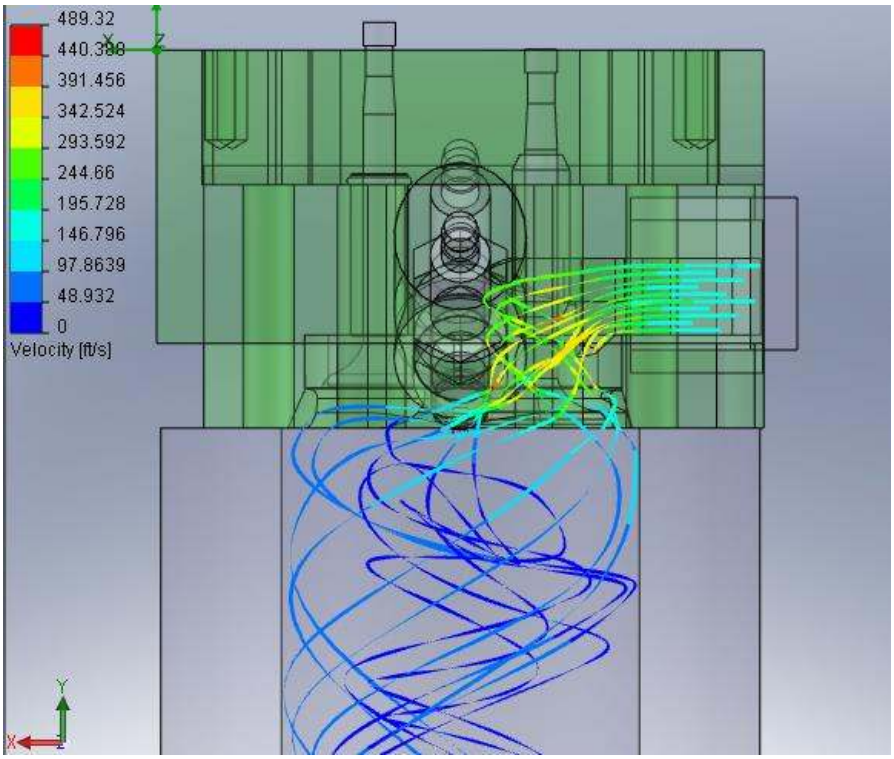

Figure 59 – Iteration 18 – Front View

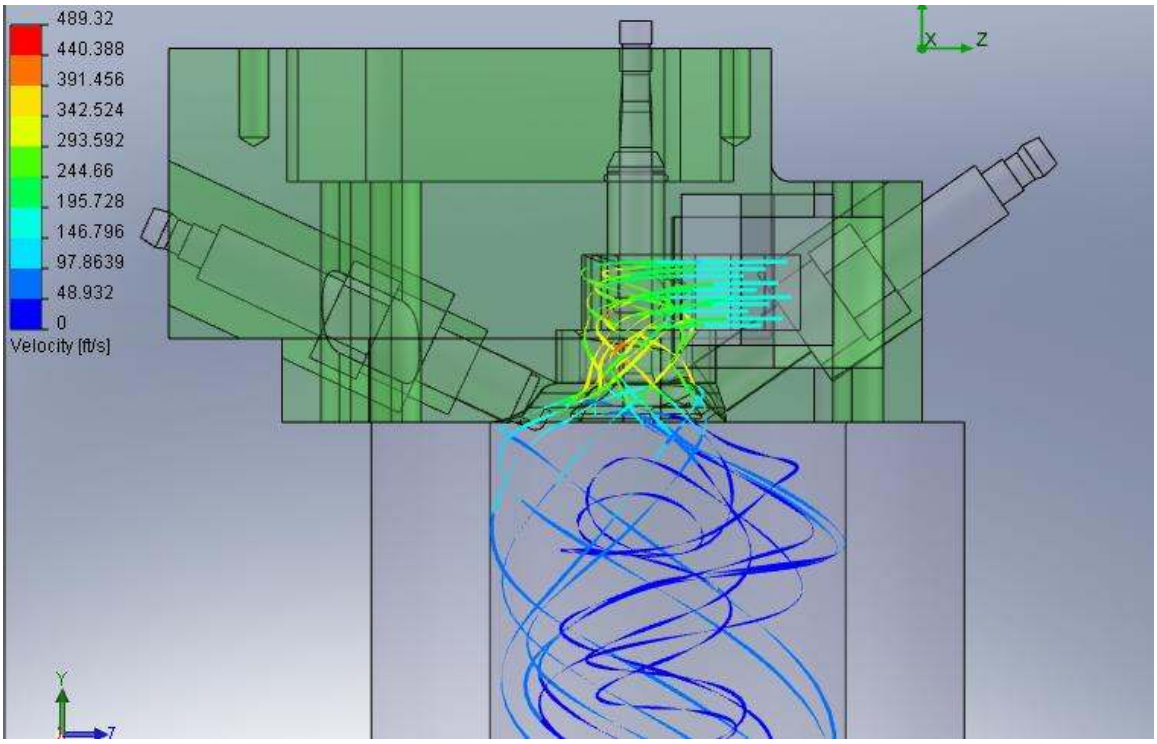

Figure 60 – Iteration 18 – Side View

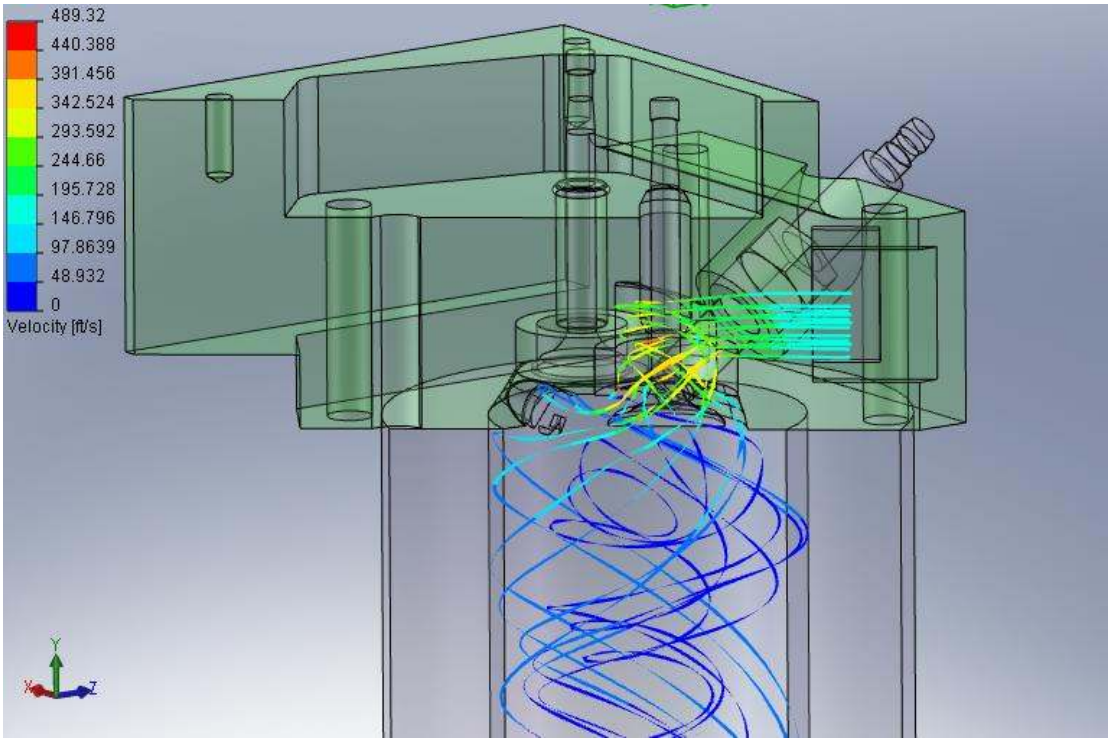

Figure 61 – Iteration 18 – Side View Cutaway

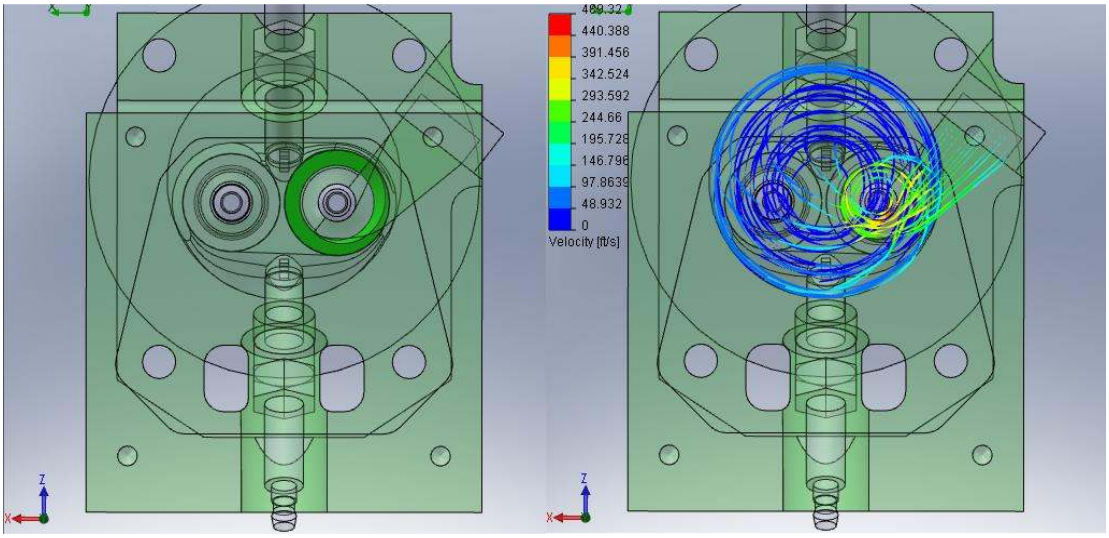

Figure 62 – Iteration 18 – Top View

In an effort to increase the flow rate, the port was widened back to .75”. The results for this change can be seen in figures 63, 64, 65, and 67 can be seen below. The flow rate increased to 25.7 CFM and the swirl pattern became much more pronounced and was evident along the cylinder walls as well as near the center of the cylinder. The swirl ratio was 2.99.

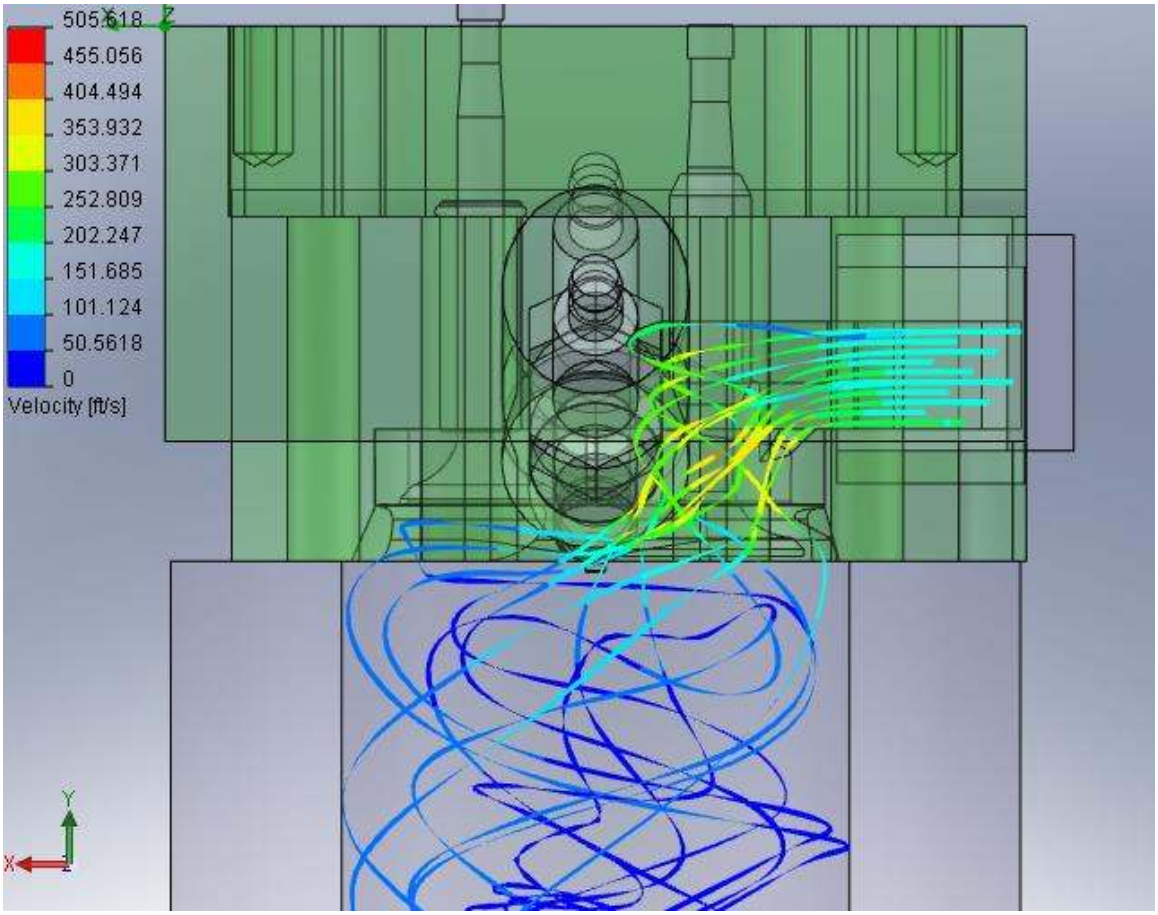

Figure 63 – Iteration 19 – Front View

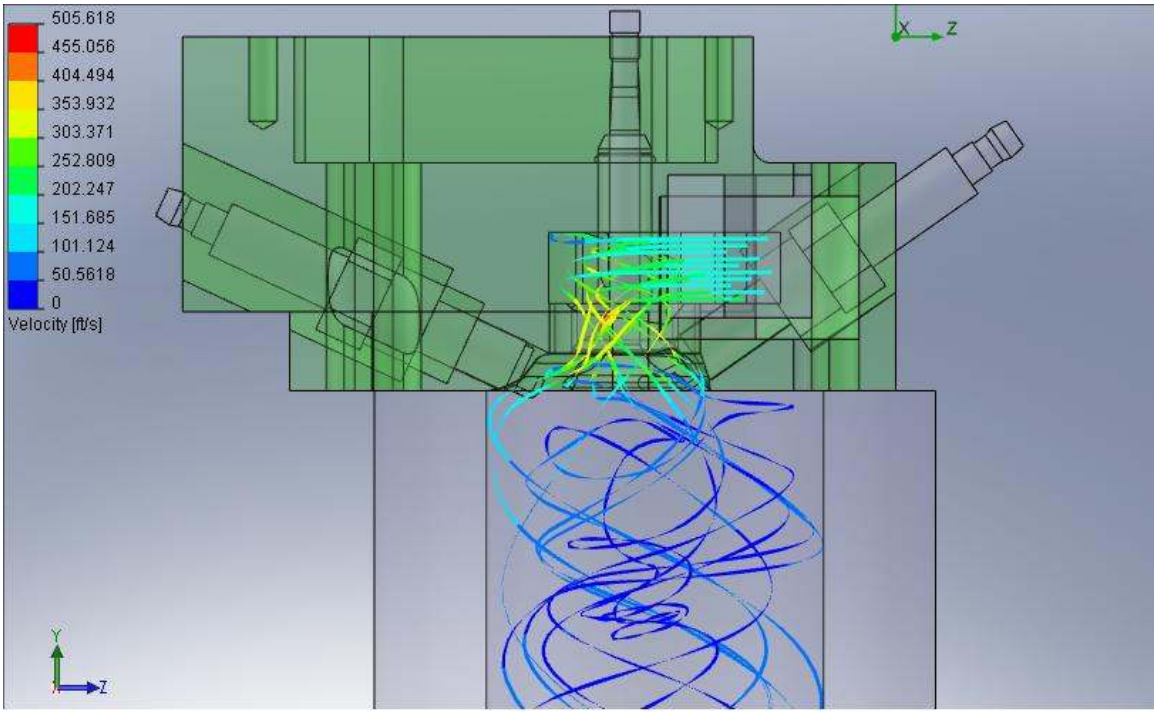

Figure 64 – Iteration 19 – Side View

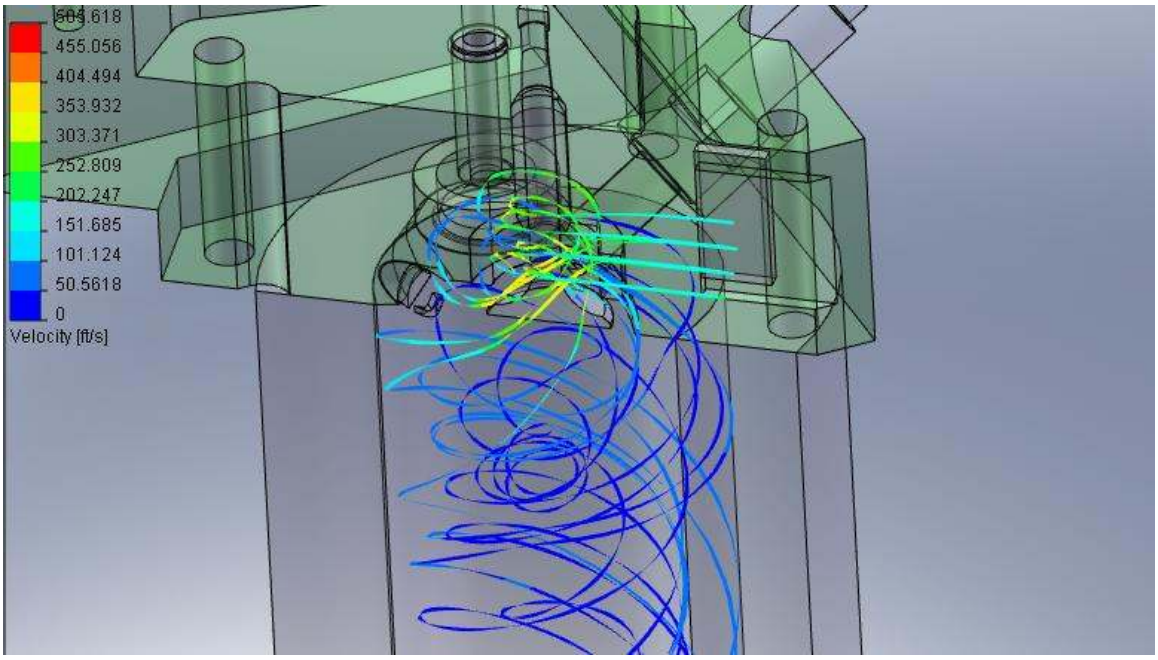

Figure 65 – Iteration 19 – Side View Cutaway

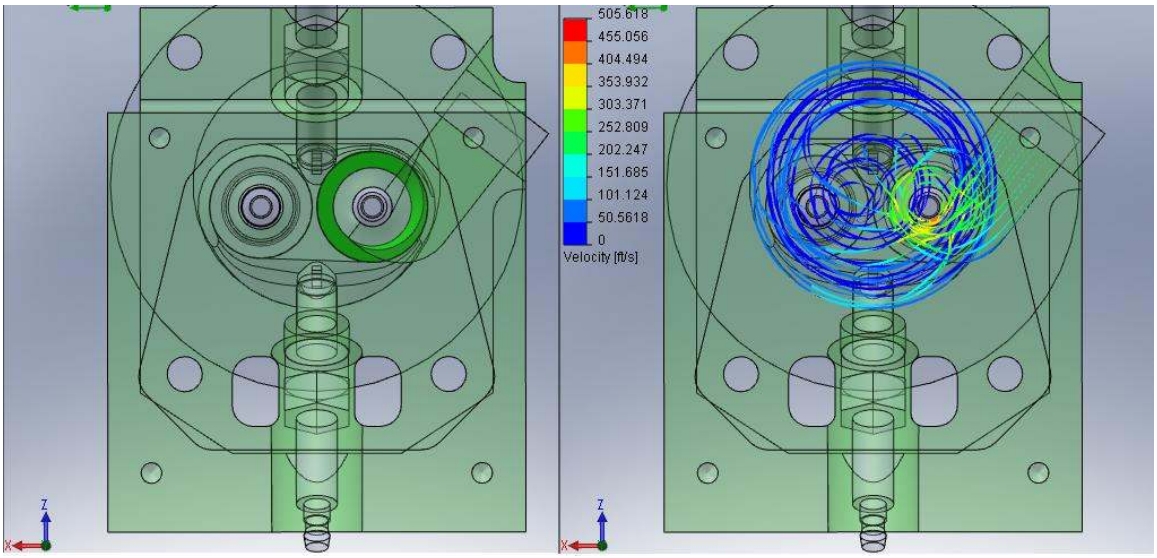

Figure 66 – Iteration 19 – Top View

To produce a cylinder useful for conducting research into the effects of swirl, it is necessary to find a means to vary swirl while the engine is operating. The investigation now shifted to developing a mechanism to reduce the swirl. A .156” diameter orifice was added to the port that would flow air into the valve pocket to reduce the swirl. By adding

the orifice, the swirl ratio dropped to 2.20, and the results can be seen in figures 67, 68, 69, and 70.

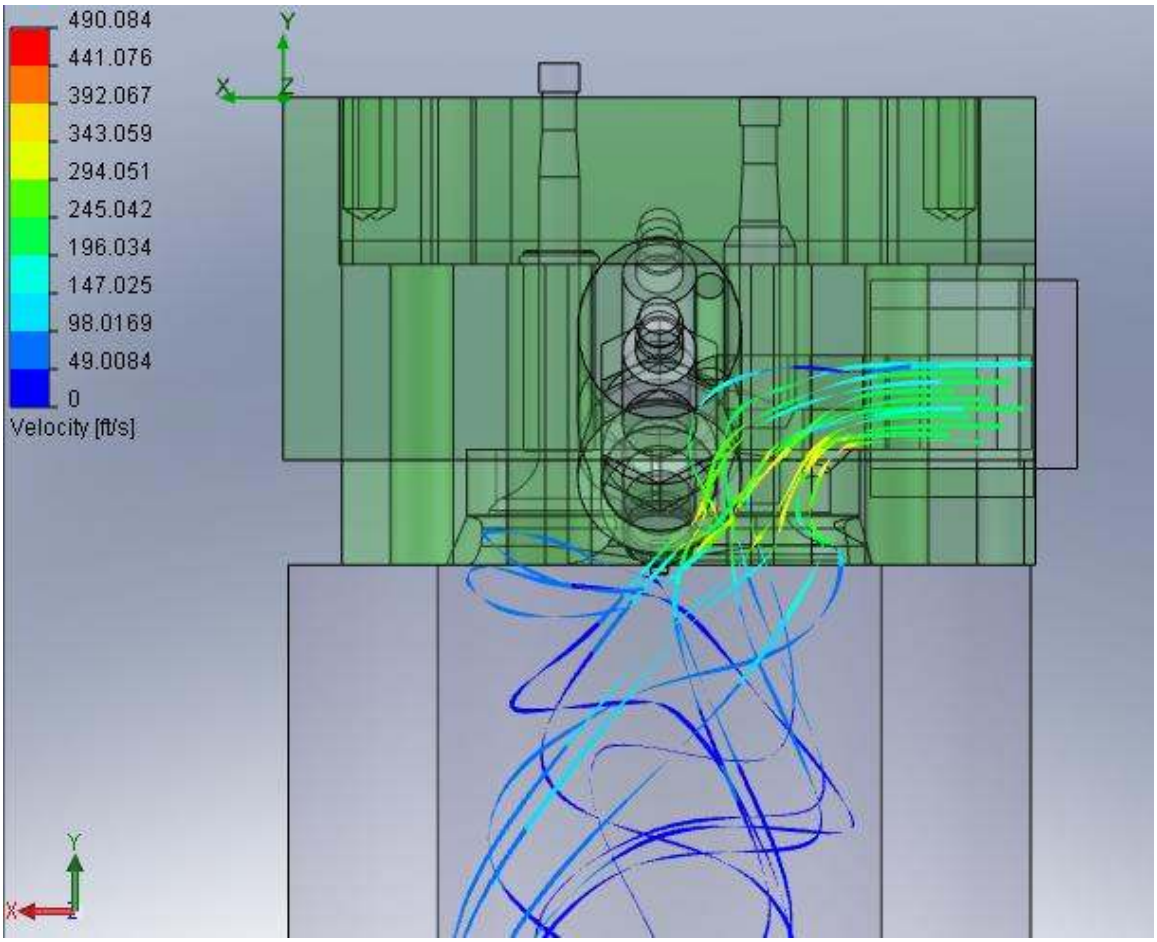

Figure 67 – Iteration 20 – Front View

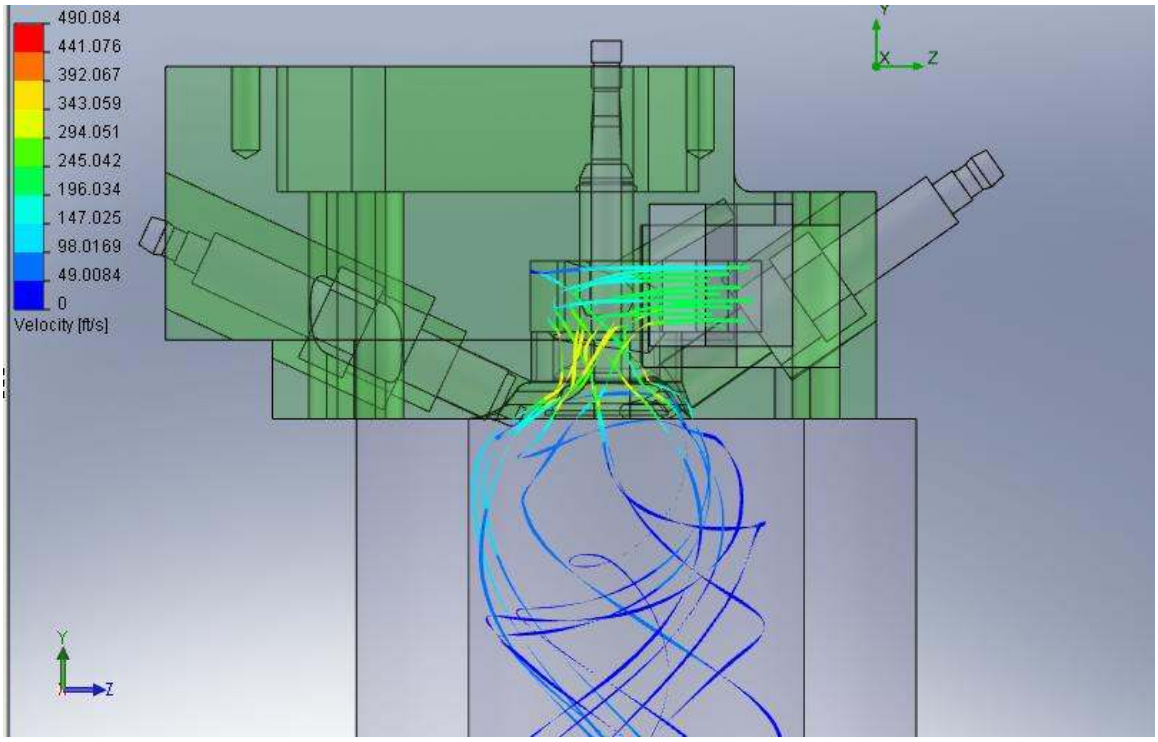

Figure 68 – Iteration 20 – Side View

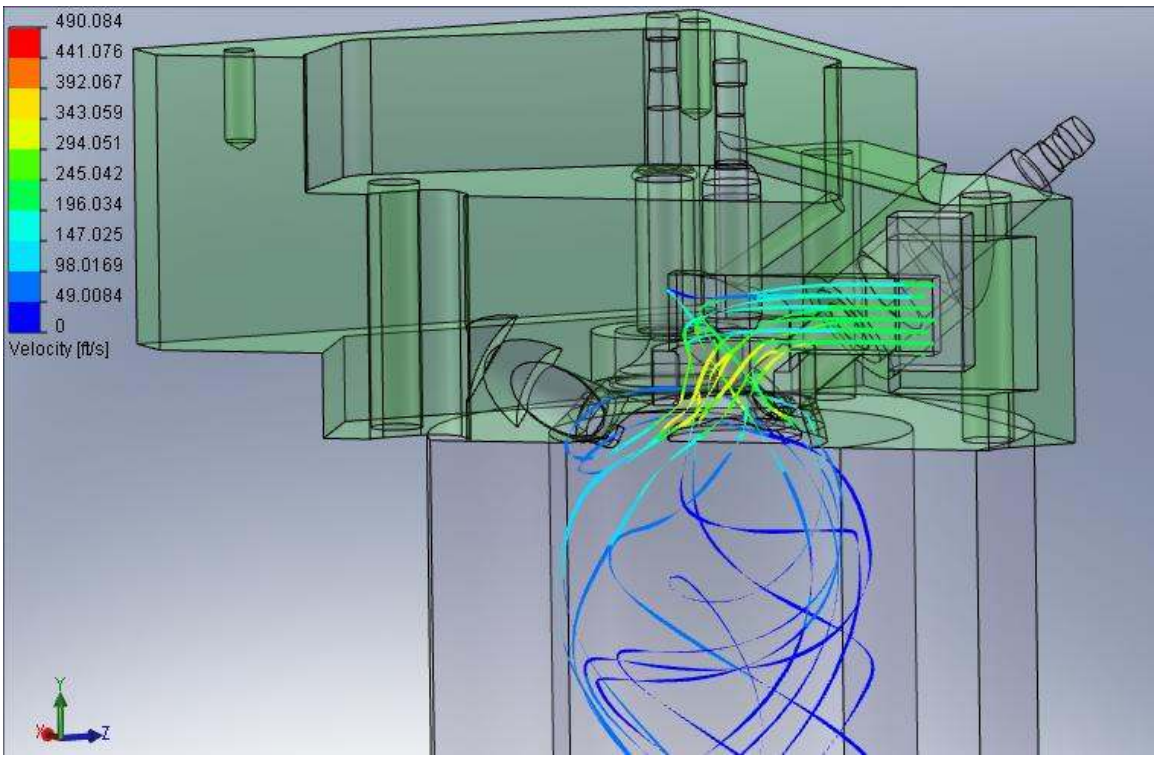

Figure 69 – Iteration 20 – Side View Cutaway

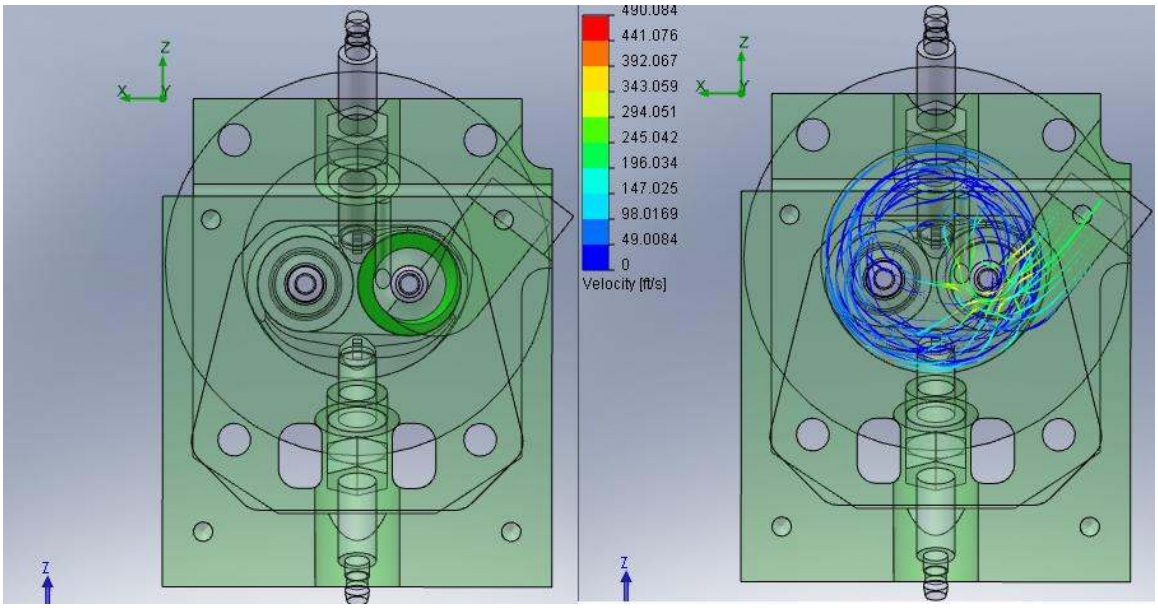

Figure 70 – Iteration 20 – Top View

In iteration 21, the air deflector was removed and the swirl reduction orifice was not used. These results can be seen in figures 71, 72, 73, and 74. The flow rate here is 29.5 CFM. The swirl ratio is well developed throughout the entire length of the cylinder, measuring 2.60.

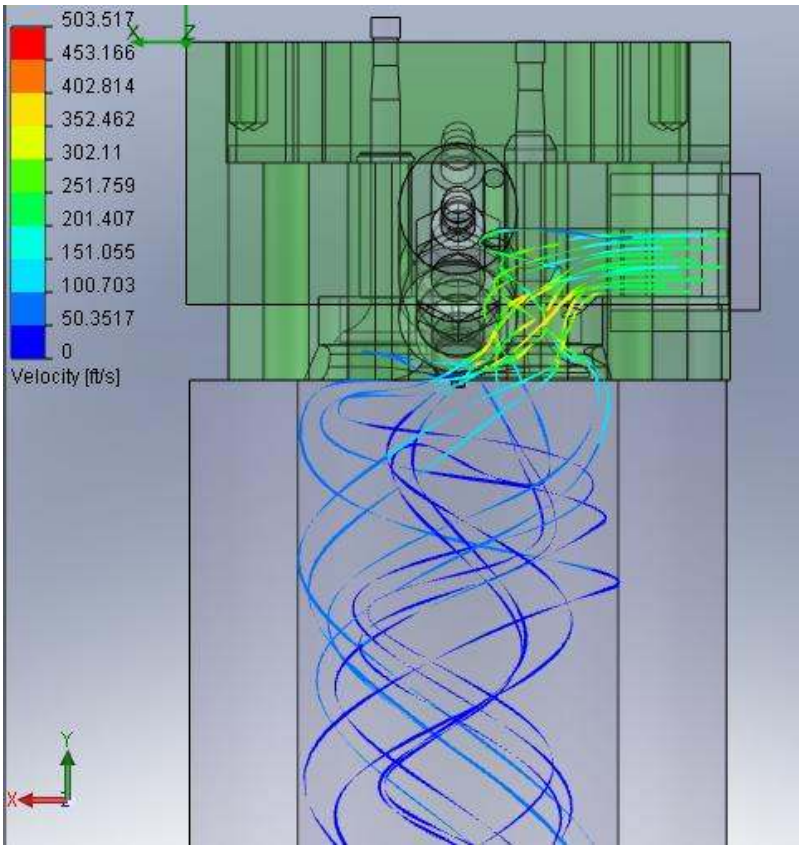

Figure 71 – Iteration 21 – Front View

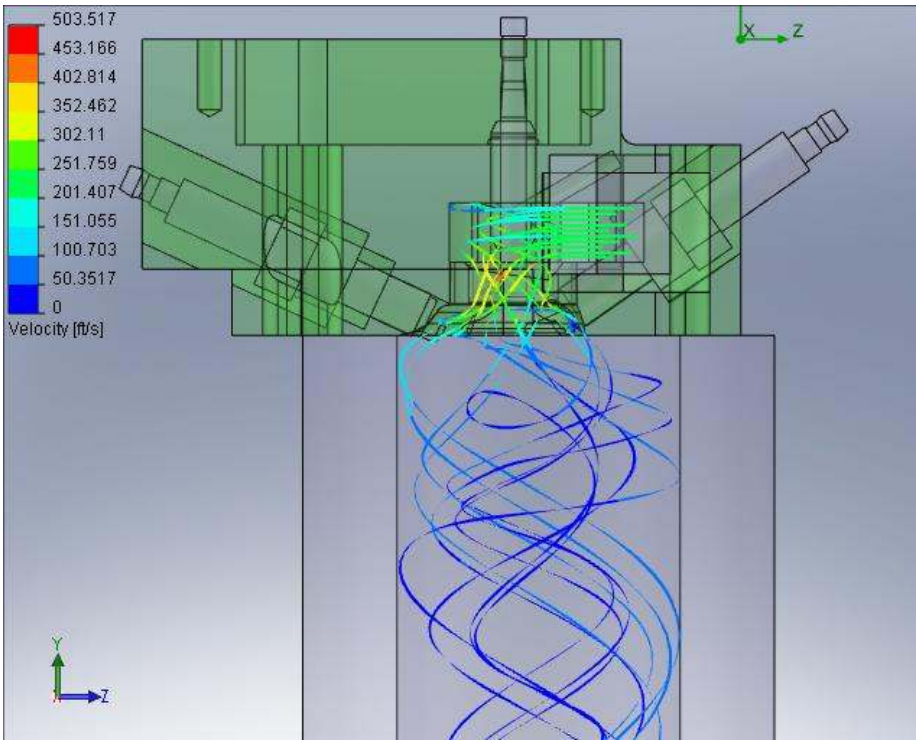

Figure 72 – Iteration 21 – Side View

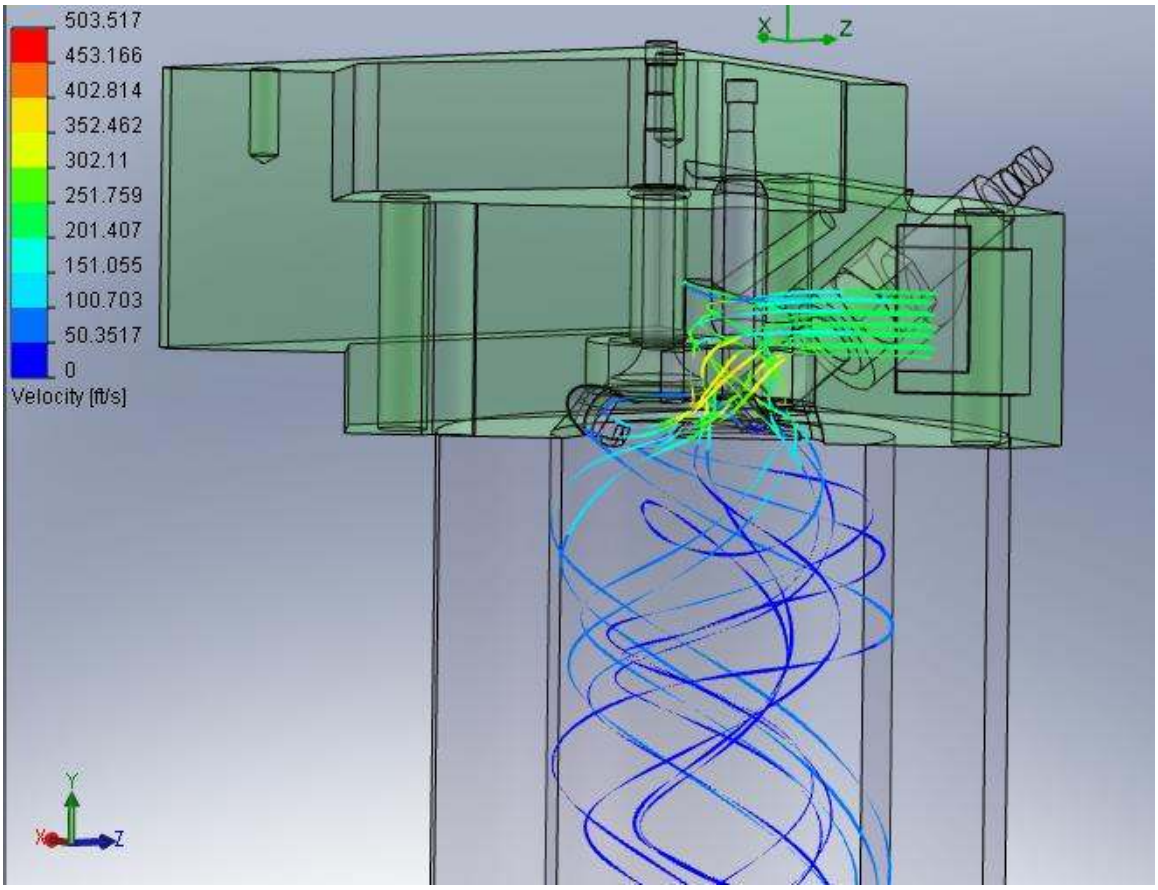

Figure 73 – Iteration 21 – Side View Cutaway

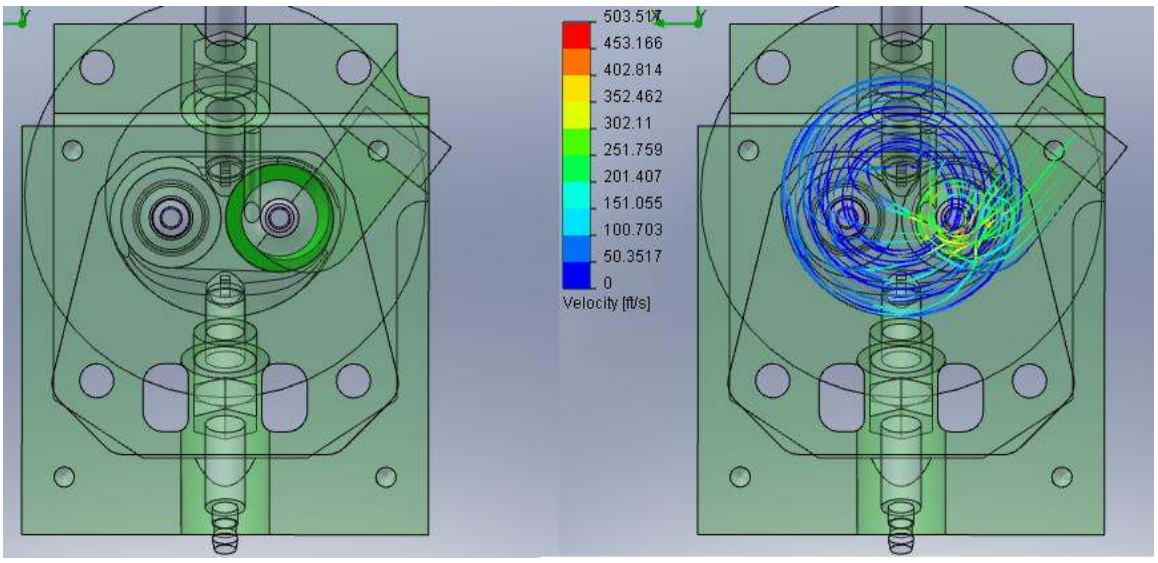

Figure 74 – Iteration 21 – Top View

For iteration 22, the swirl reducing orifice was enabled. These results can be seen in figures 75, 76, 77, and 78. The flow rate was constant and much of the swirl was still present, so the next step will be to further reduce the swirl. The swirl ratio was 1.02

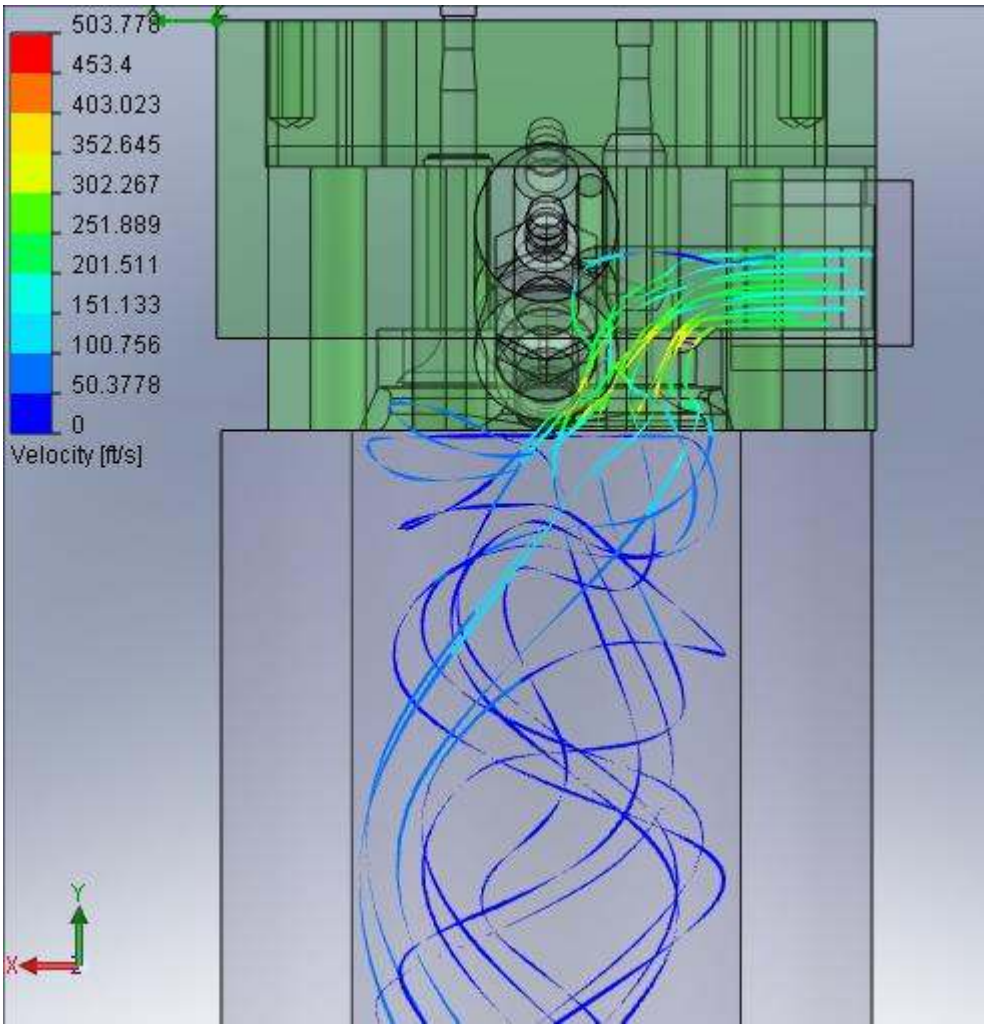

Figure 75 – Iteration 22 – Front View

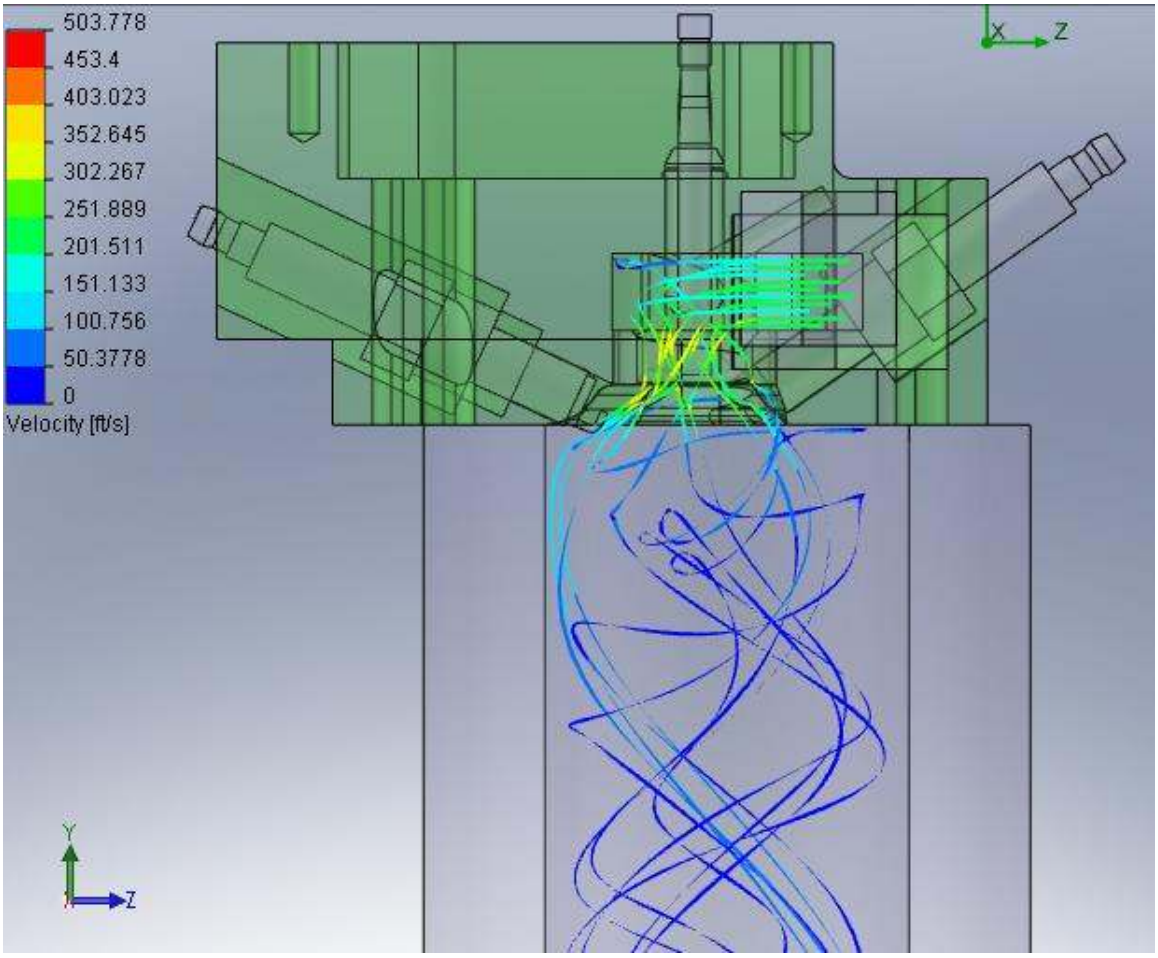

Figure 76 – Iteration 22 – Side View

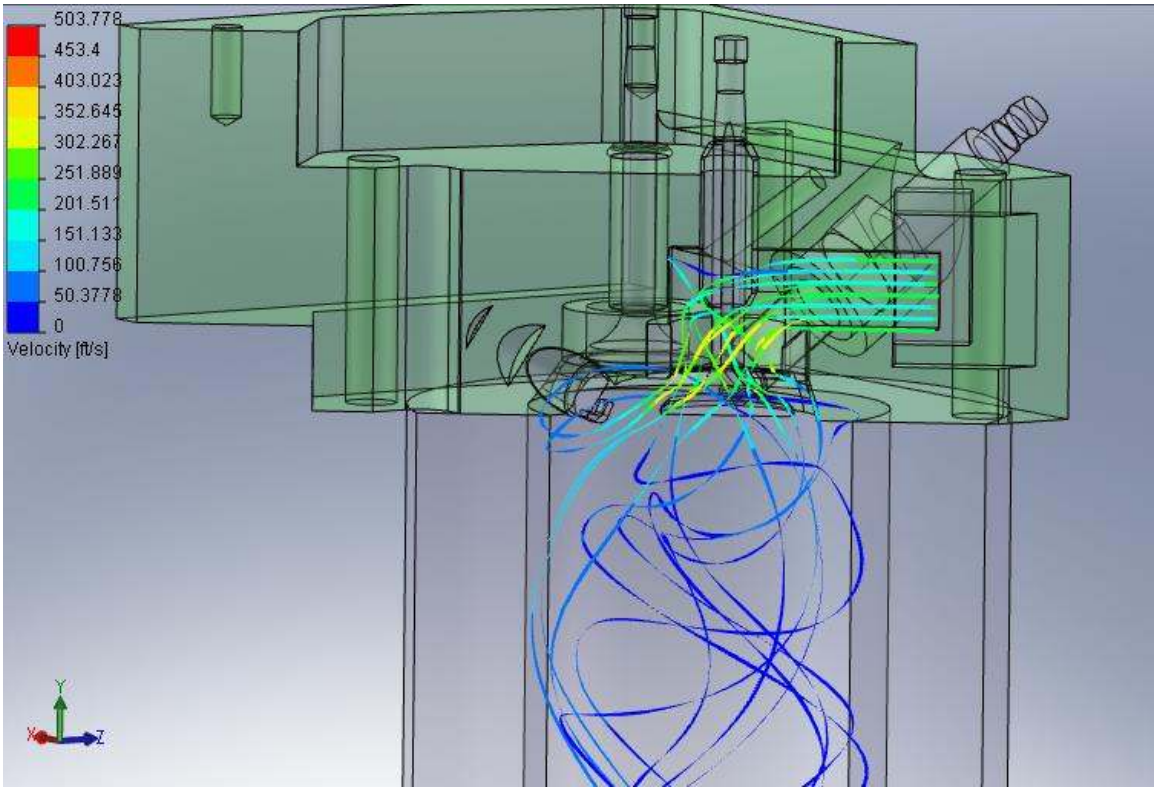

Figure 77 – Iteration 22 – Side View Cutaway

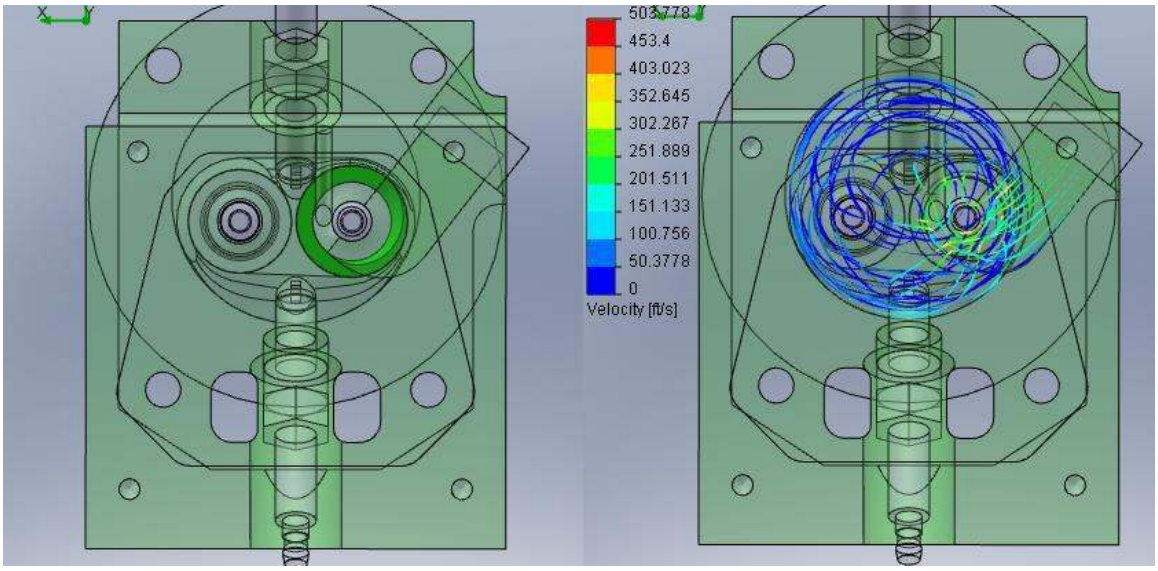

Figure 78 – Iteration 22 – Top View

For iteration 23, the swirl is further reduced using another swirl reducing orifice parallel to the first swirl reducing orifice inlet, but slightly lower. The flow rate remained constant. The results can be seen in figures 79, 80, 81, and 82. The figures show the swirl

pattern has been nearly removed by adding the second swirl reducing orifice. Swirl ratio was .90.

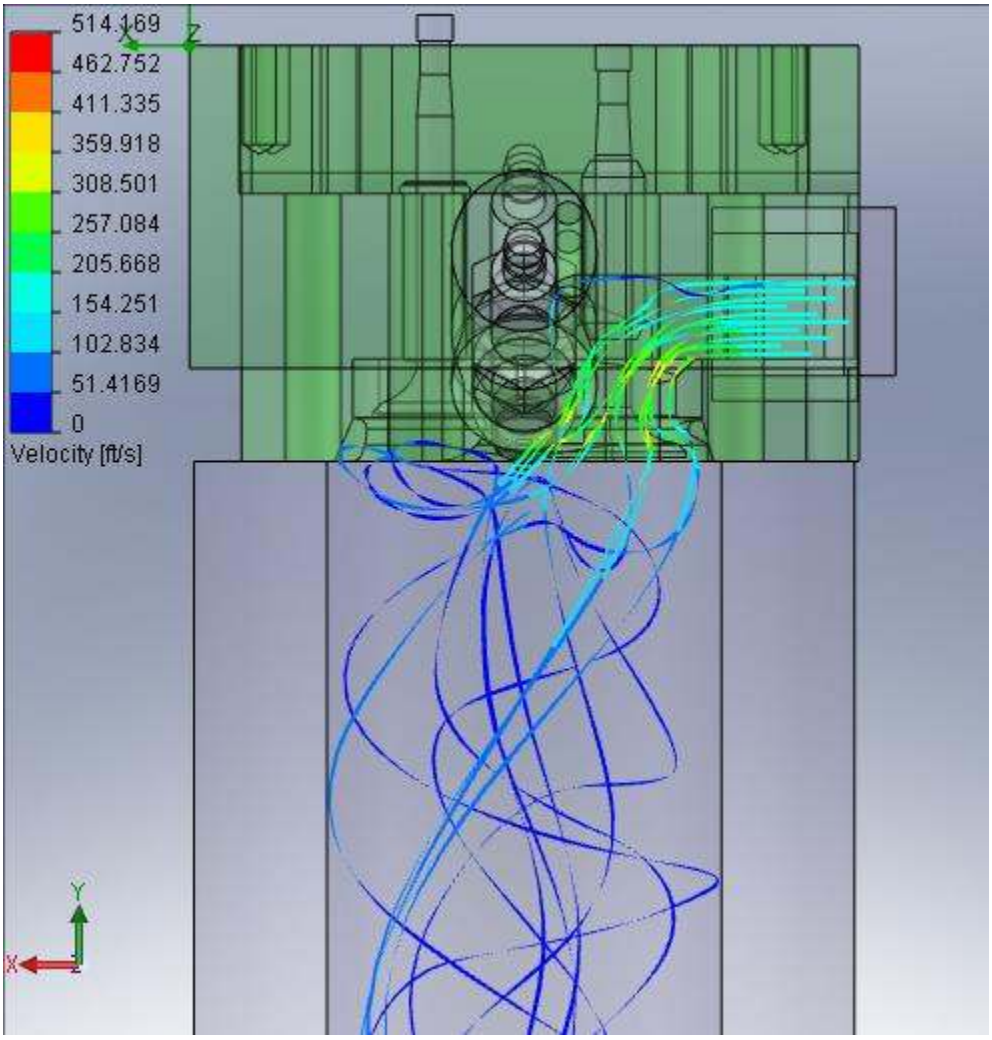

Figure 79 – Iteration 23 – Front View

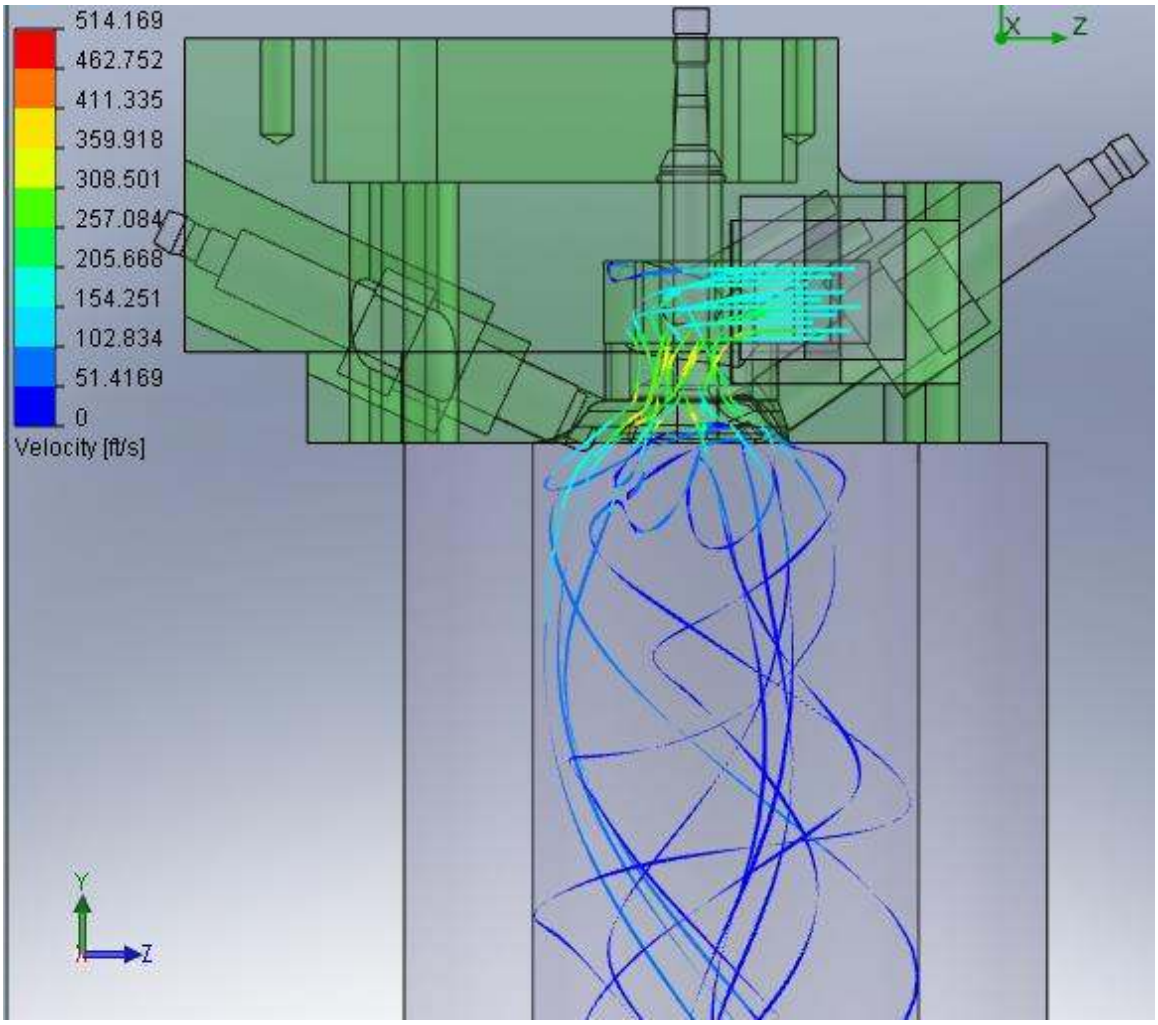

Figure 80 – Iteration 23 – Side View

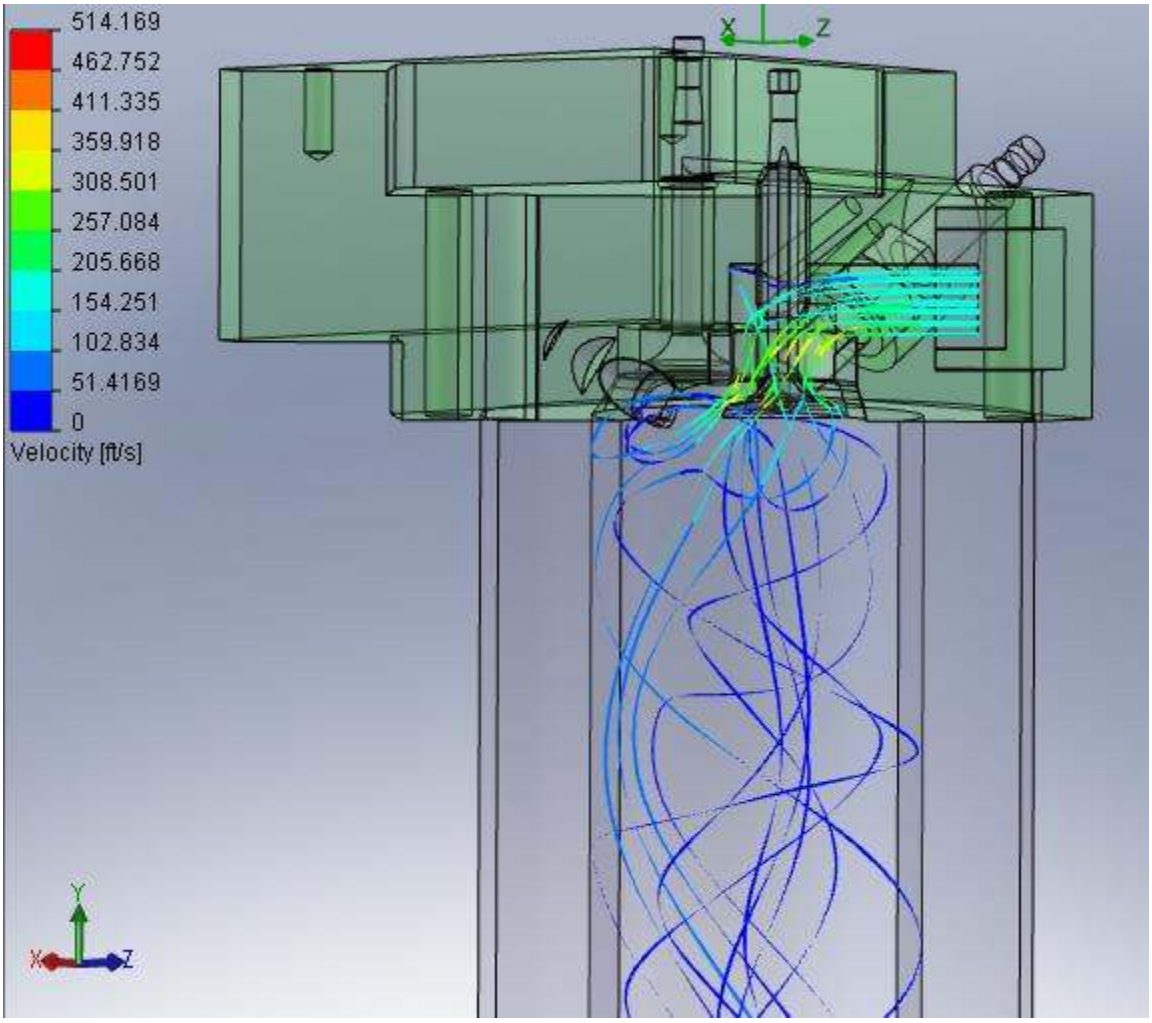

Figure 81 – Iteration 23 – Side View Cutaway

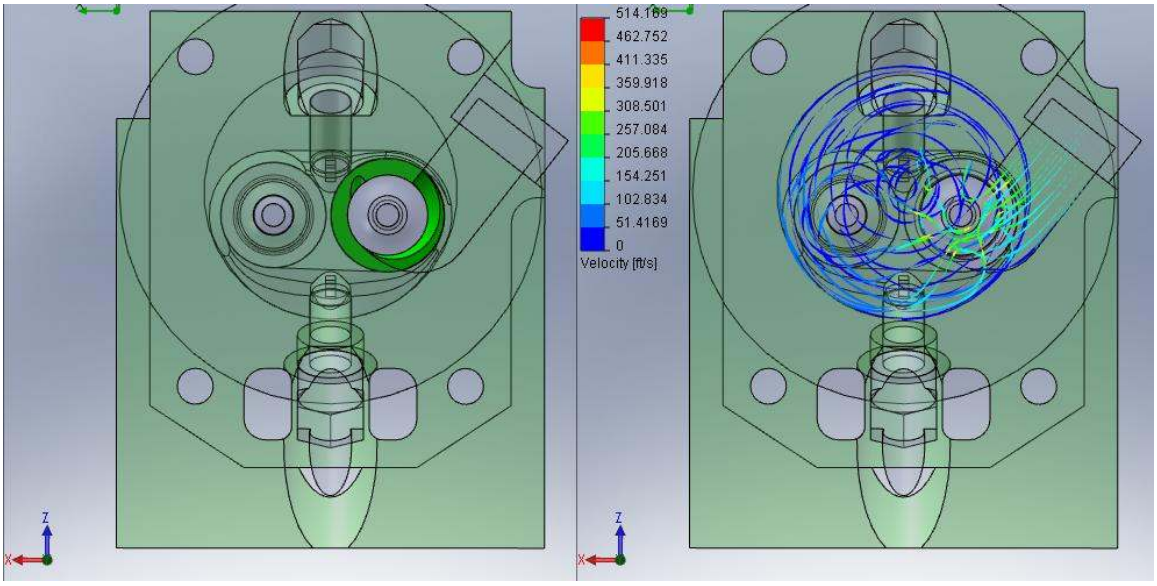

Figure 82 – Iteration 23 – Top View

For iteration 24, the long side radius of the offset port was smoothed and the radius was increased. All of the swirl-reducing ports were removed again. Even with the smoother port, the flow dropped to 27.3 CFM. The swirl ratio here was similar to the previous iteration and was measured at 2.59. The results can be seen in figures 83, 84, 85, and 86.

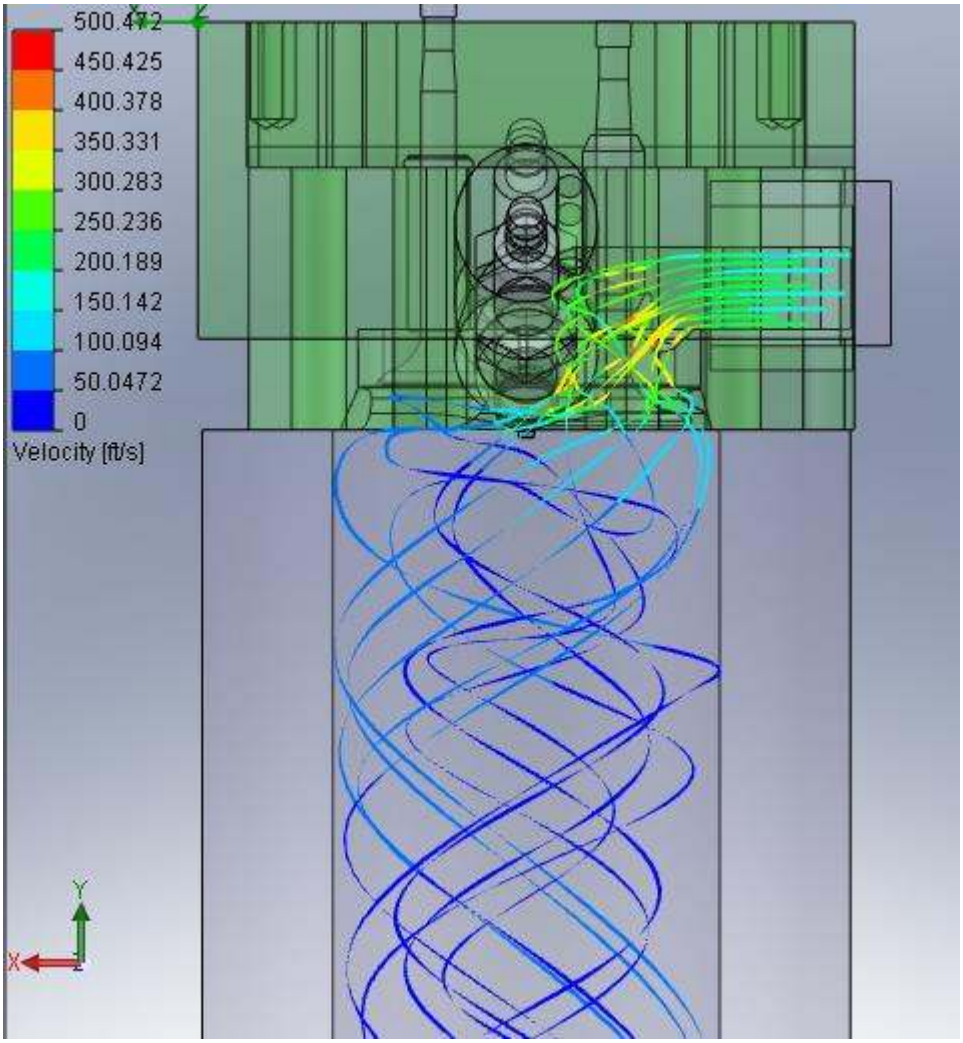

Figure 83 – Iteration 24 – Front View

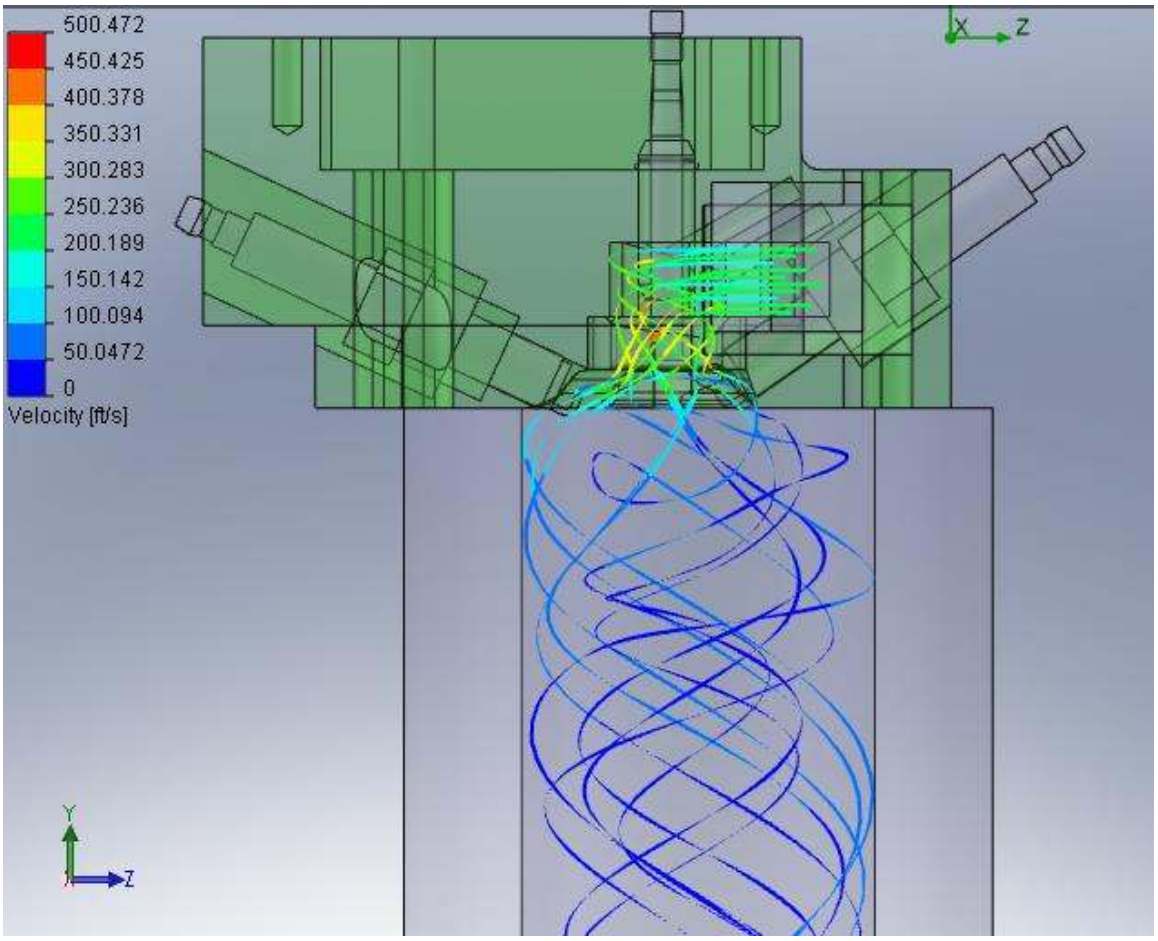

Figure 84 – Iteration 24 – Side View

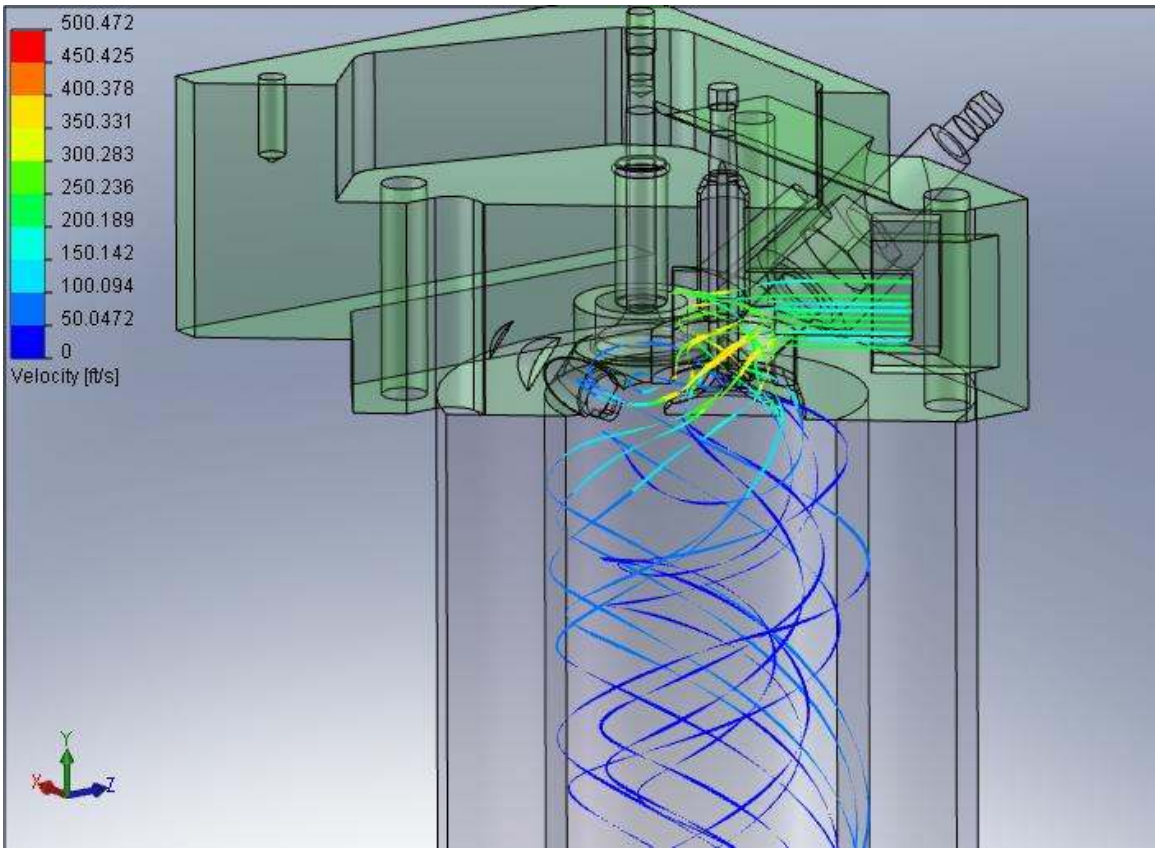

Figure 85 – Iteration 24 – Side View Cutaway

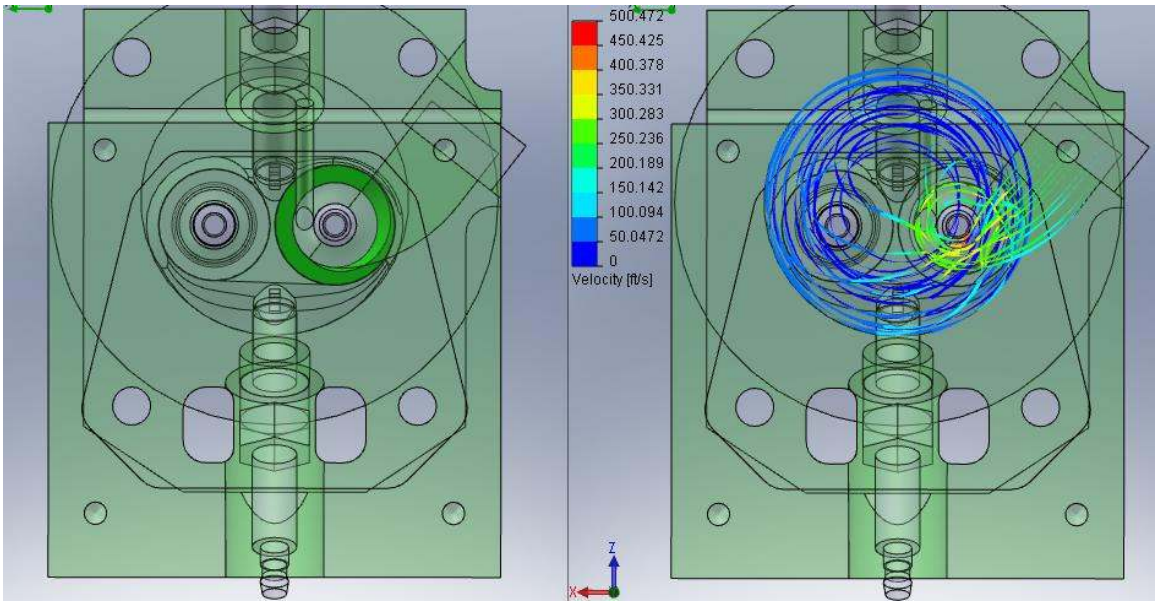

Figure 86 – Iteration 24 – Top View

For the same port design as the previous iteration, iteration 25 shows the effects of activating the swirl reducing ports. The flow rate remained constant and the results can be

seen in figures 87, 88, 89, and 90. Here most of the swirl is reduced, but swirl ratio is still .87.

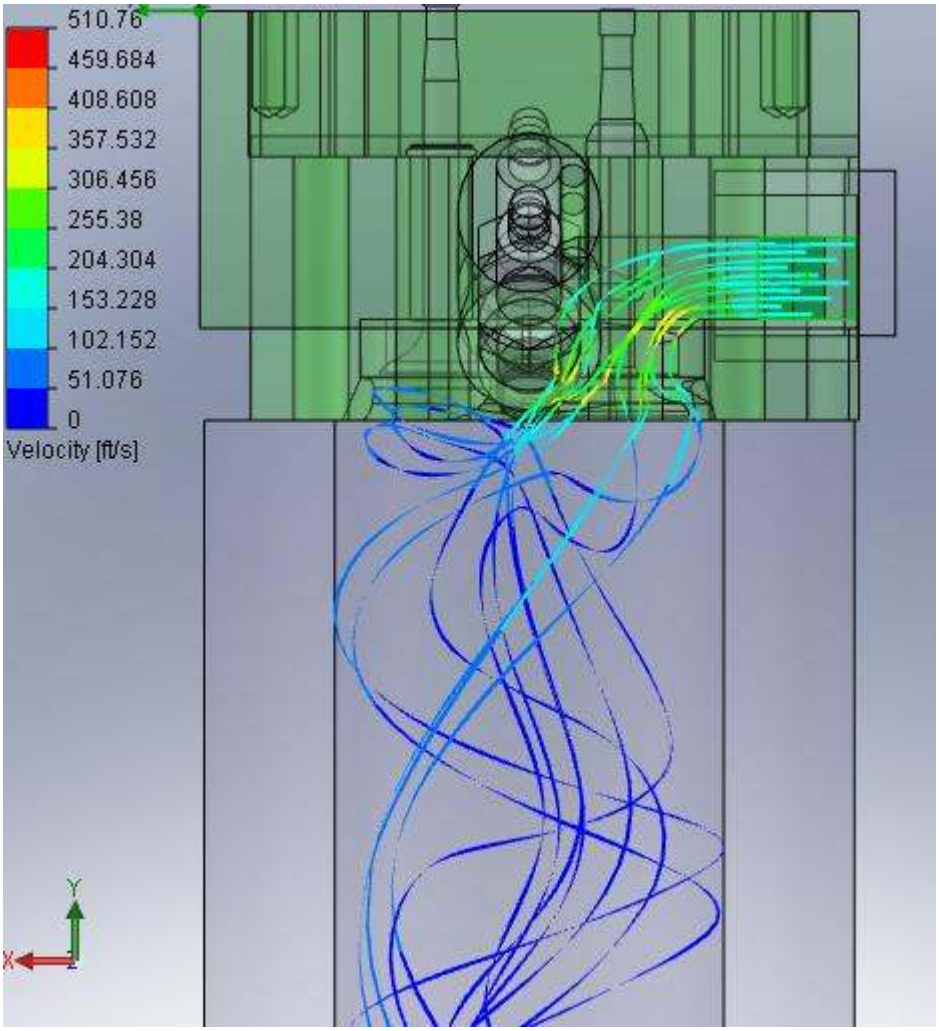

Figure 87 – Iteration 25 – Front View

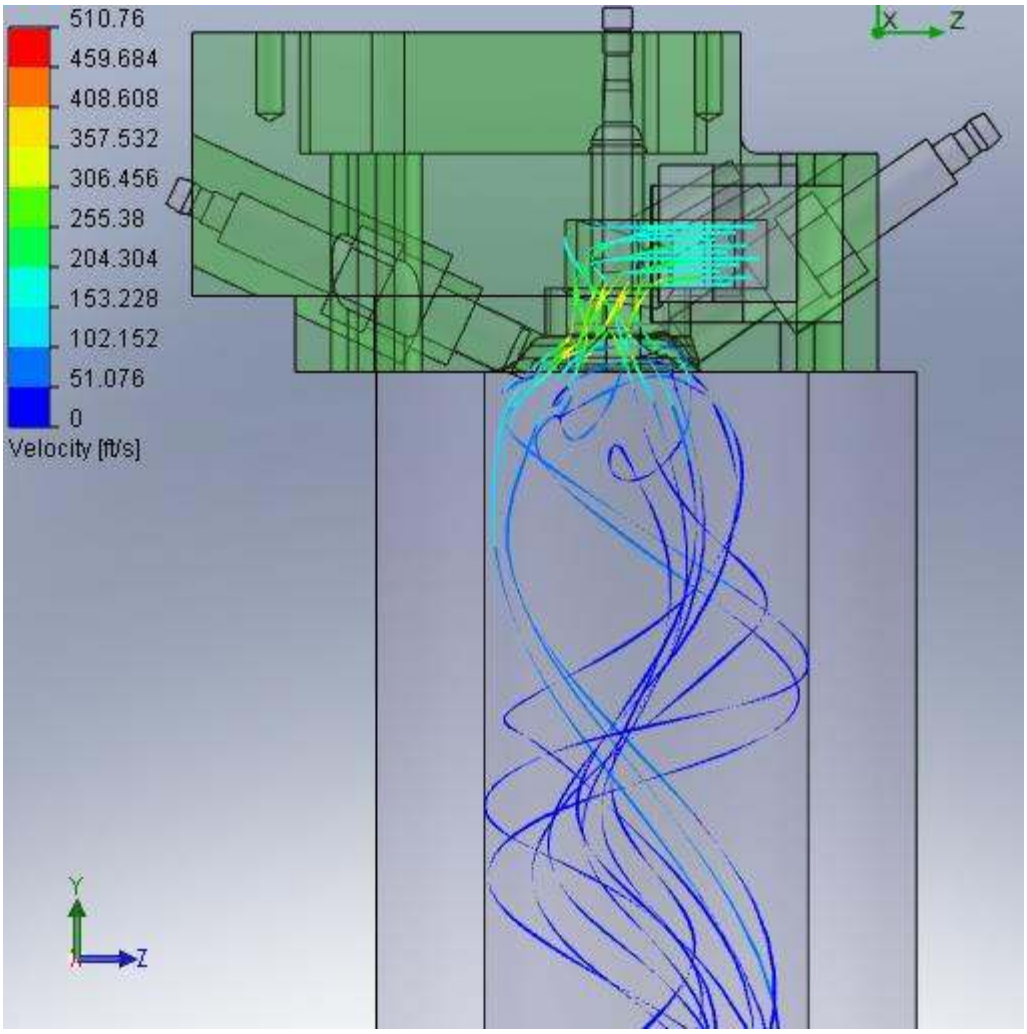

Figure 88 – Iteration 25 – Side View

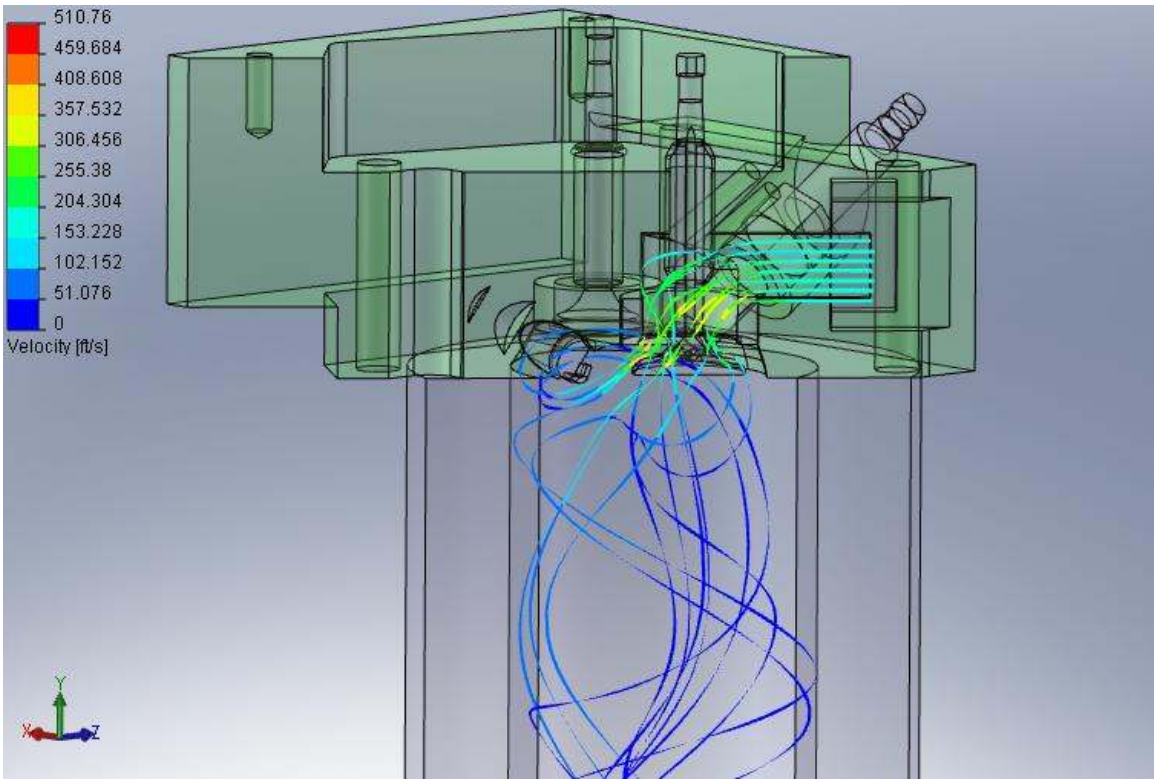

Figure 89 – Iteration 25 – Side View Cutaway

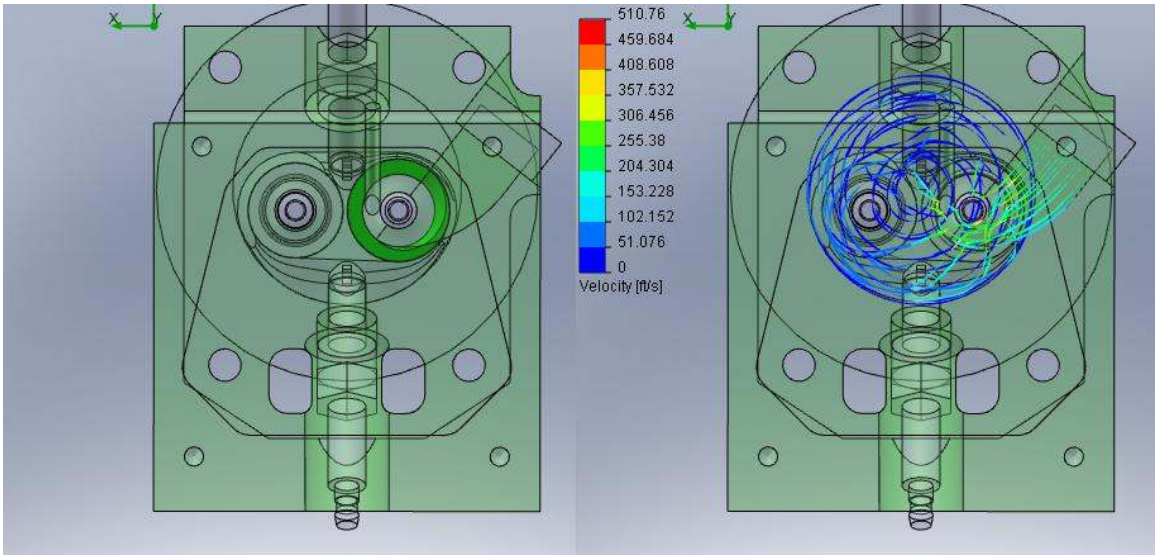

Figure 90 – Iteration 25 – Top View

For iteration 26, the effect of a different swirl-reducing orifice was analyzed. This port was parallel to the face of the head and as close to parallel with the inlet runner as possible without hitting the head bolt. The flow rate produced was constant and the swirl

was reduced, but not eliminated. The results for iteration 26 can be seen in figures 91, 92, 93, and 94. The swirl rate was measured at .96.

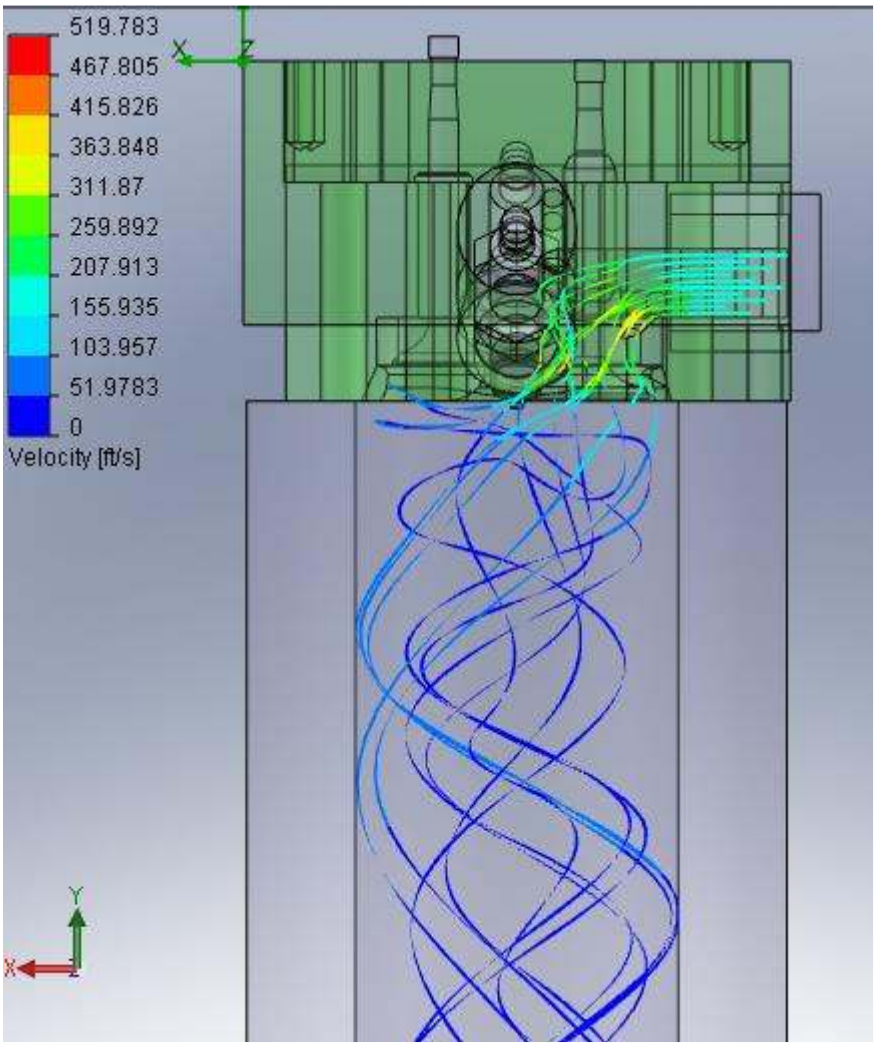

Figure 91 – Iteration 26 – Front View

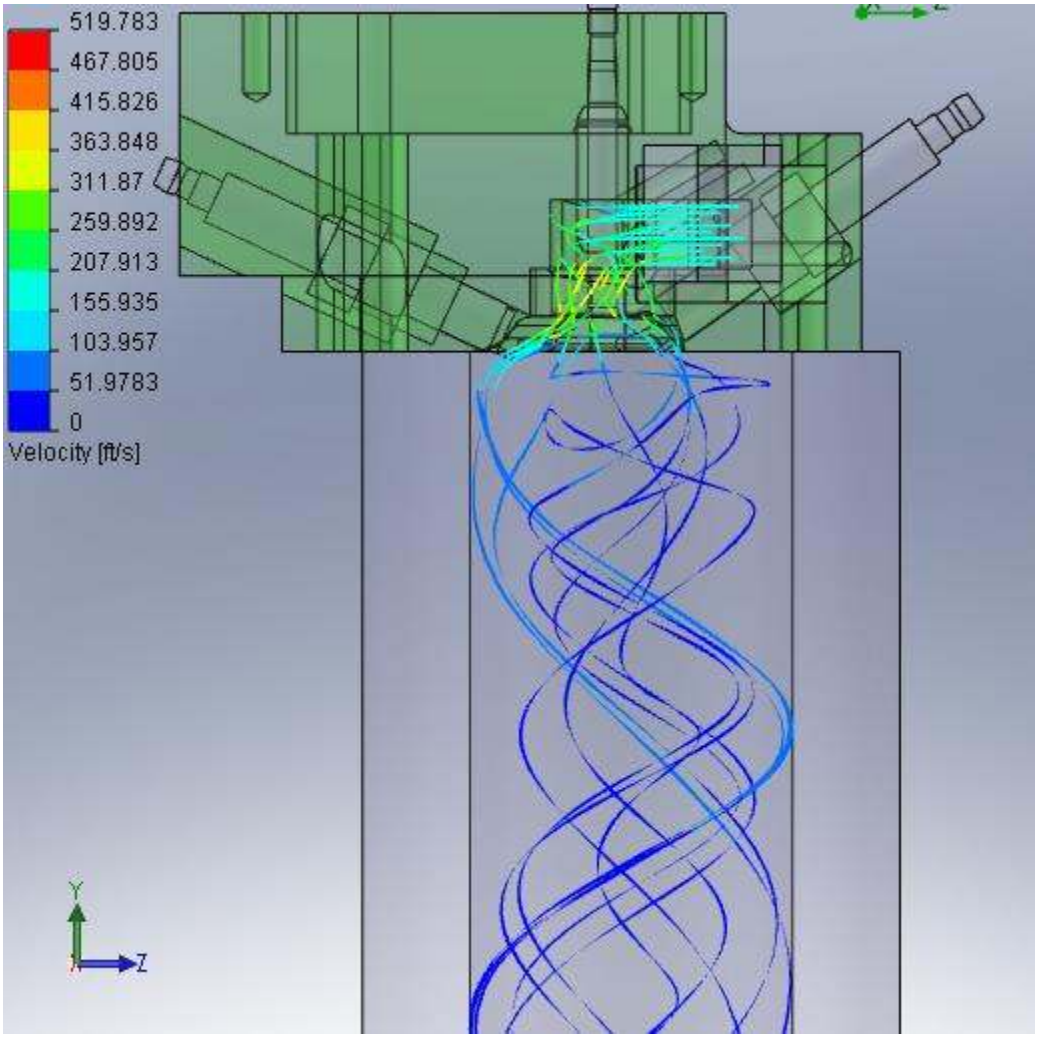

Figure 92 – Iteration 26 – Side View

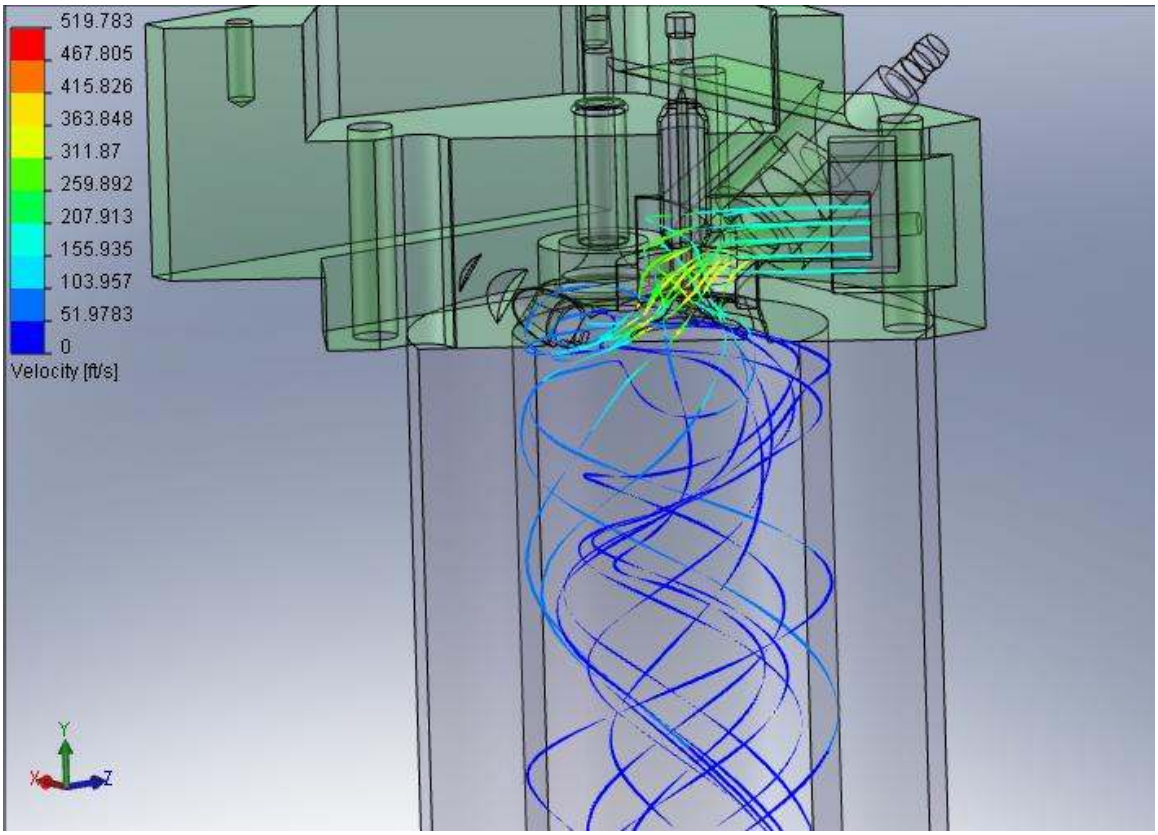

Figure 93 – Iteration 26 – Side View Cutaway

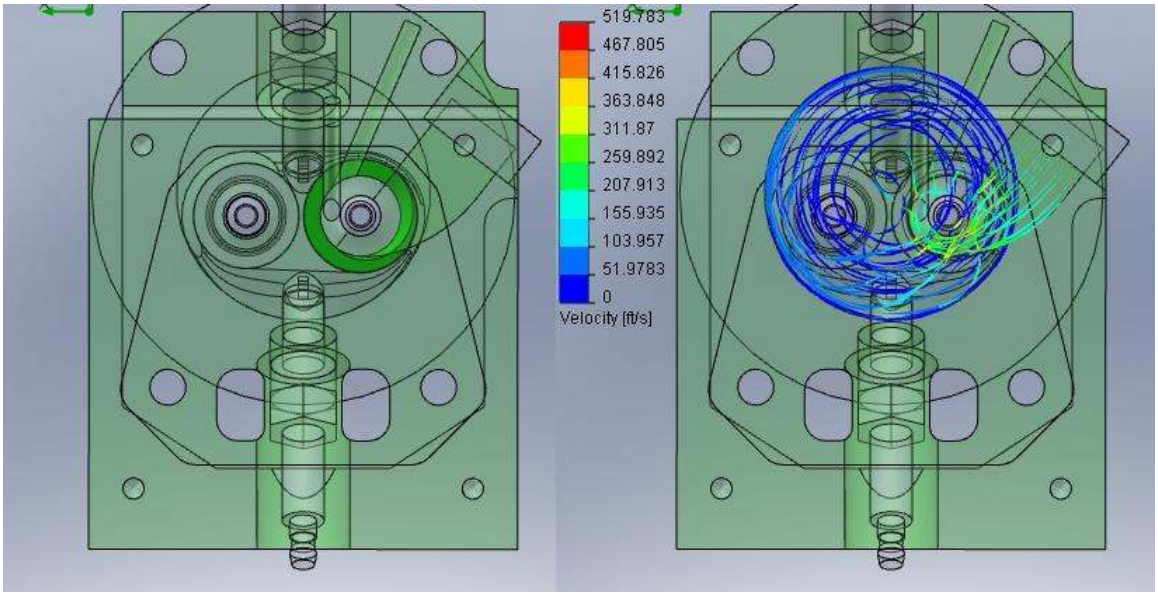

Figure 94 – Iteration 26 – Top View

For the 27th iteration, the runner geometry seen in iteration 23 was used since the results were better than seen in the previous iteration. The 3rd swirl reducing orifice was activated and the first two were deactivated. The flow rate remained constant to what was

seen earlier and the results can be seen in figures 95, 96, 97, and 98. The swirl ratio was .97.

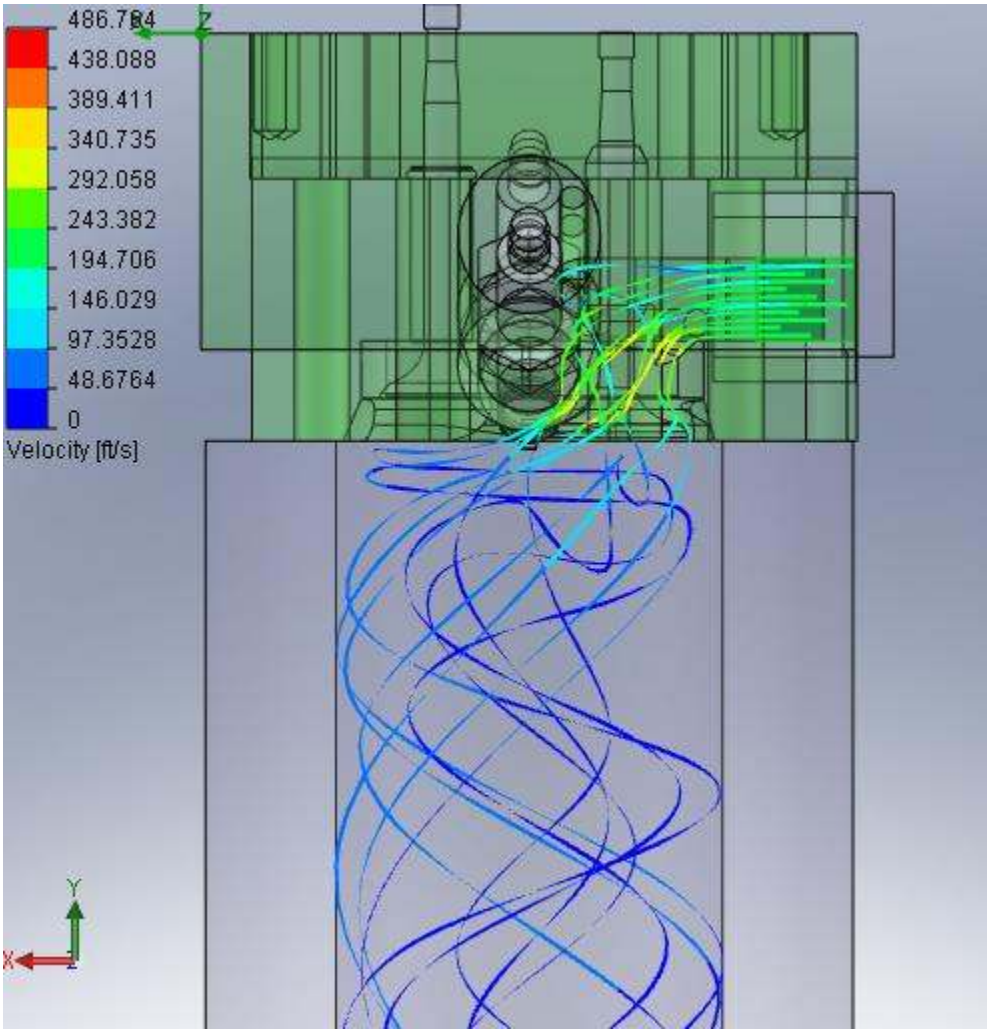

Figure 95 – Iteration 27 – Front View

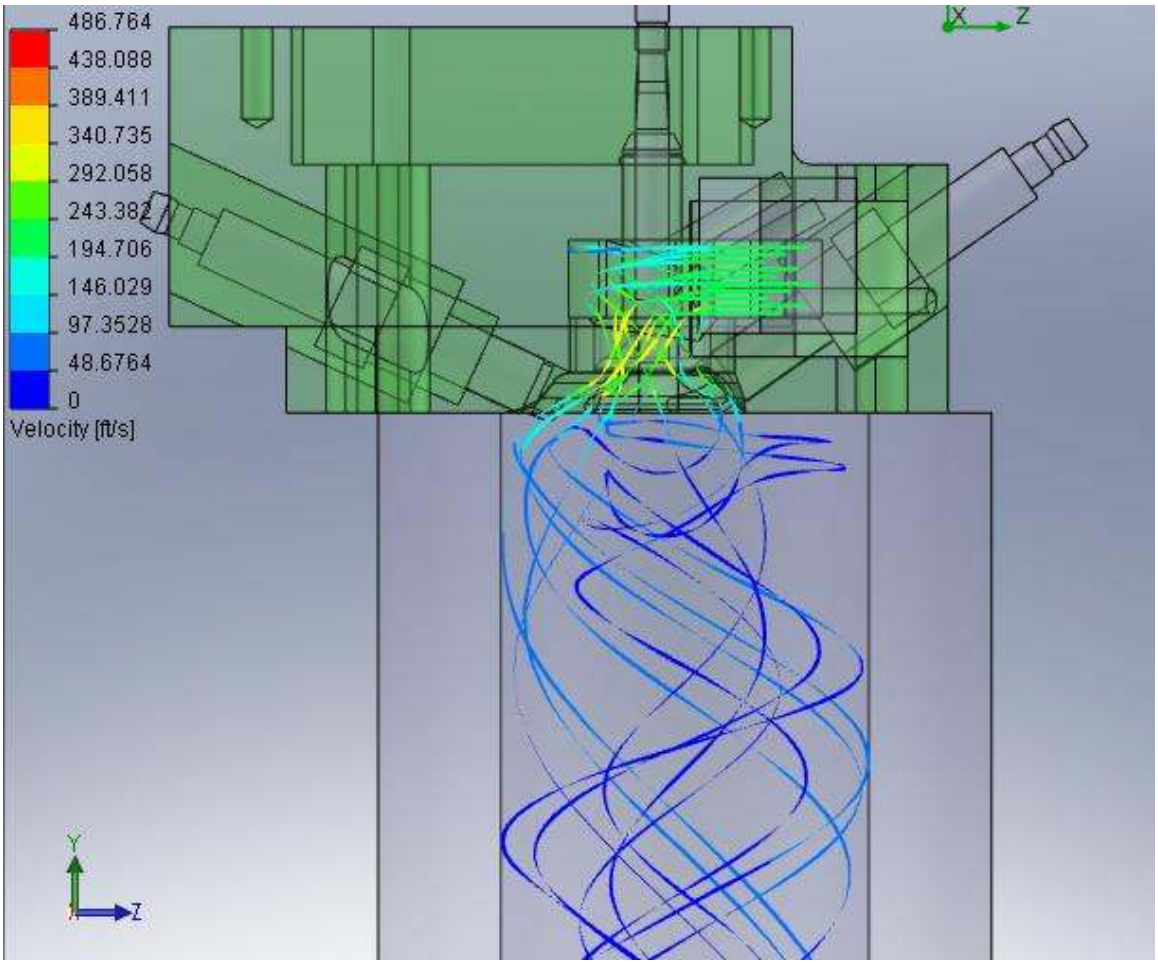

Figure 96 – Iteration 27 – Side View

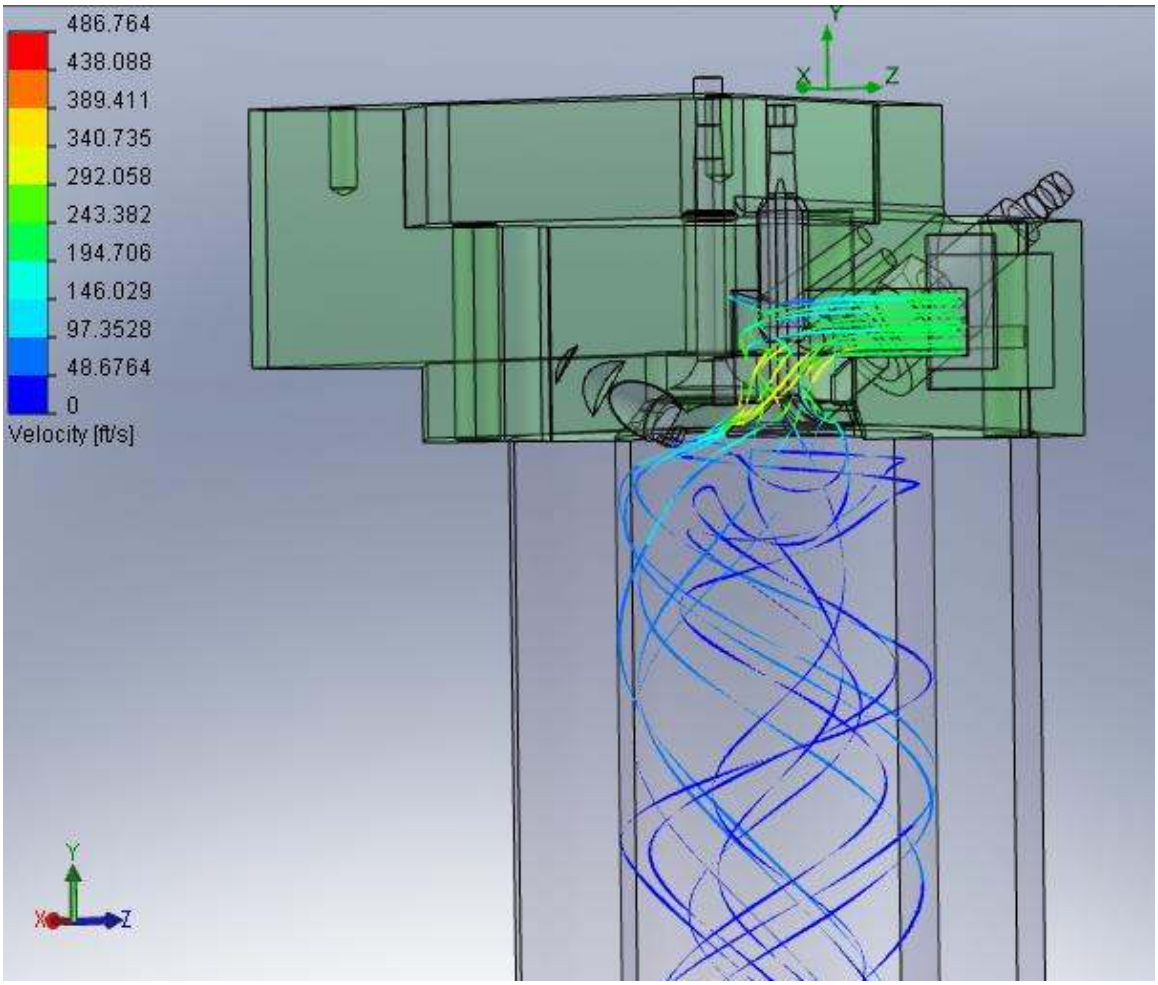

Figure 97 – Iteration 27 – Side View Cutaway

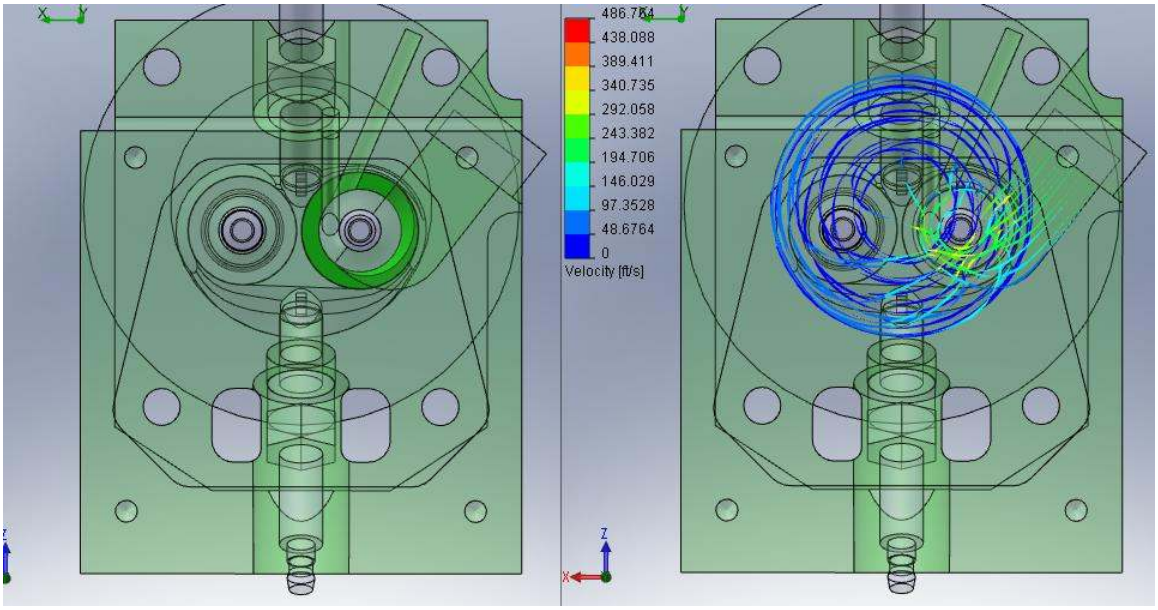

Figure 98 – Iteration 27 – Top View

For iteration 28, all three swirl reducing orifices were activated. The flow rate remained constant and the swirl was removed in the upper portion of the cylinder. There is still a slight motion of swirl over the entire length of the cylinder, but this is much longer than the actual stroke. The measured swirl for the 28th iteration was .80. The results can be seen in figures 99, 100, 101, and 102.

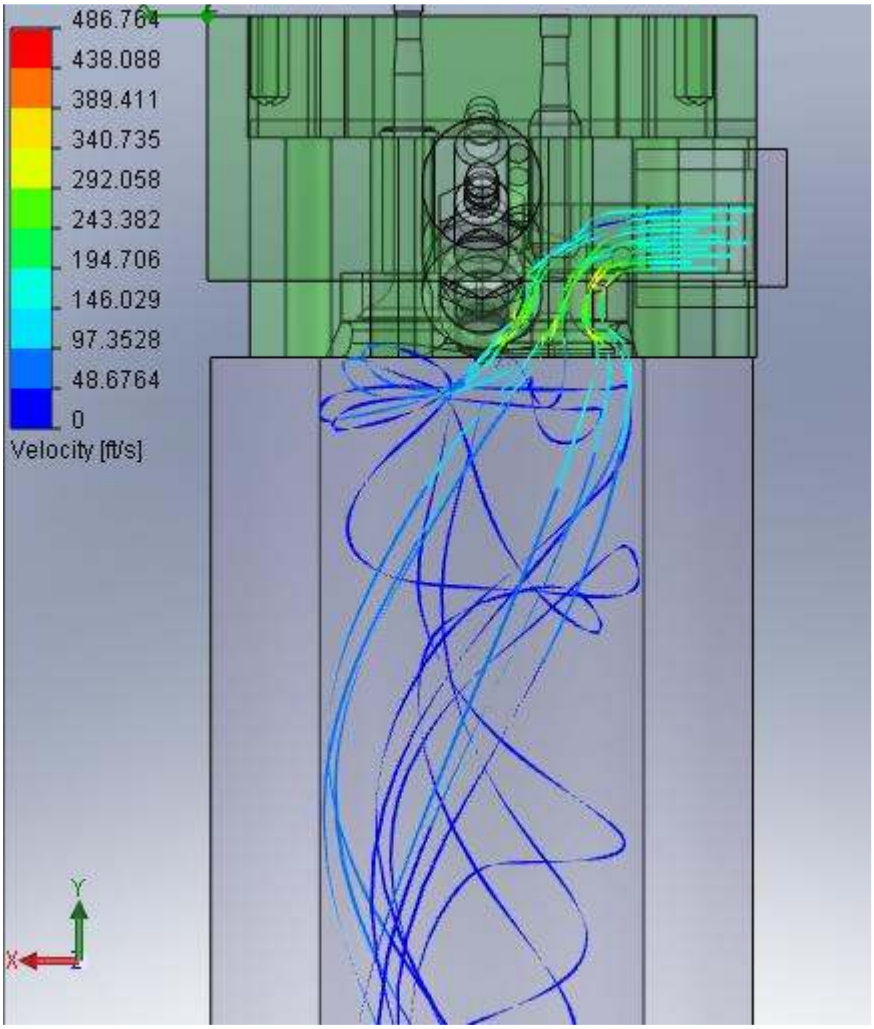

Figure 99 – Iteration 28 –Front View

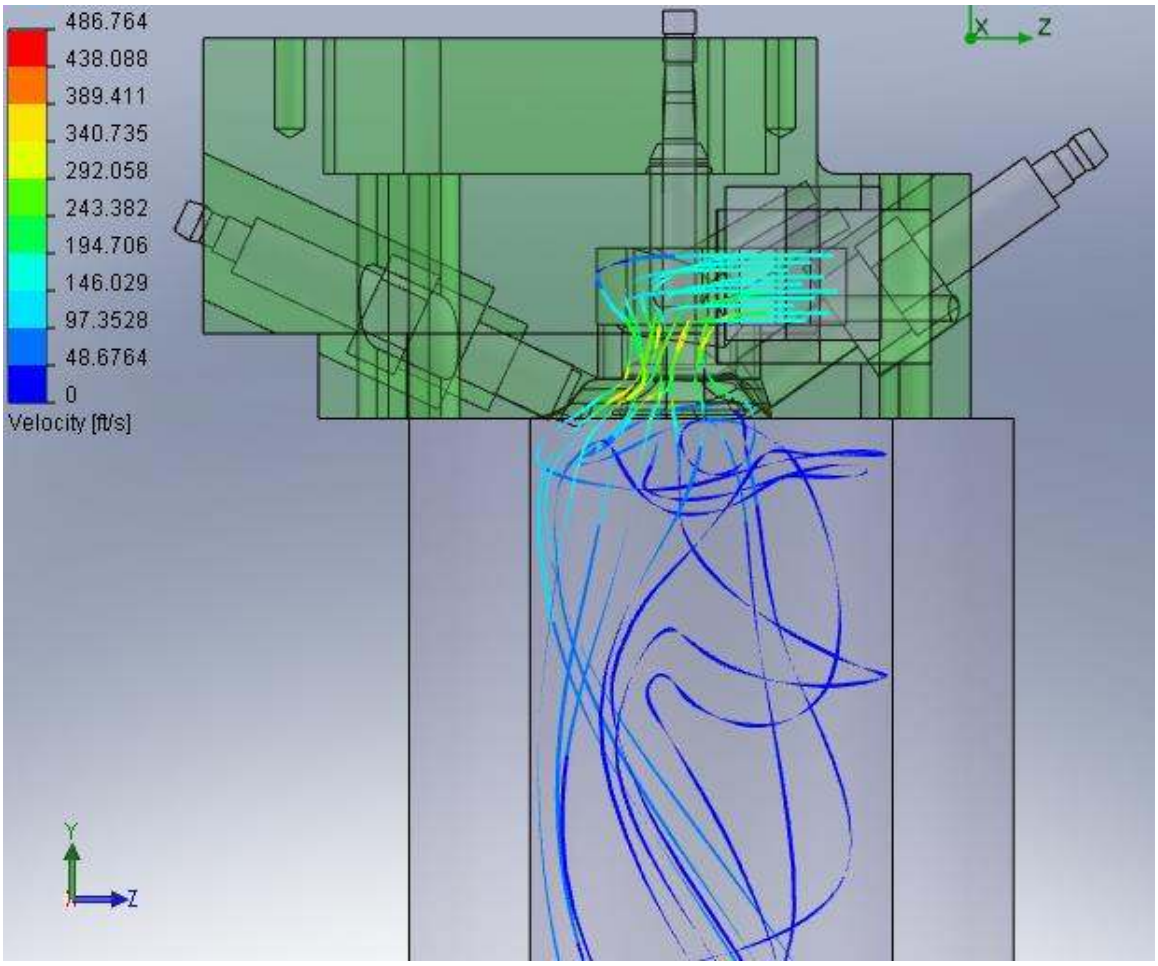

Figure 100 – Iteration 28 – Side View

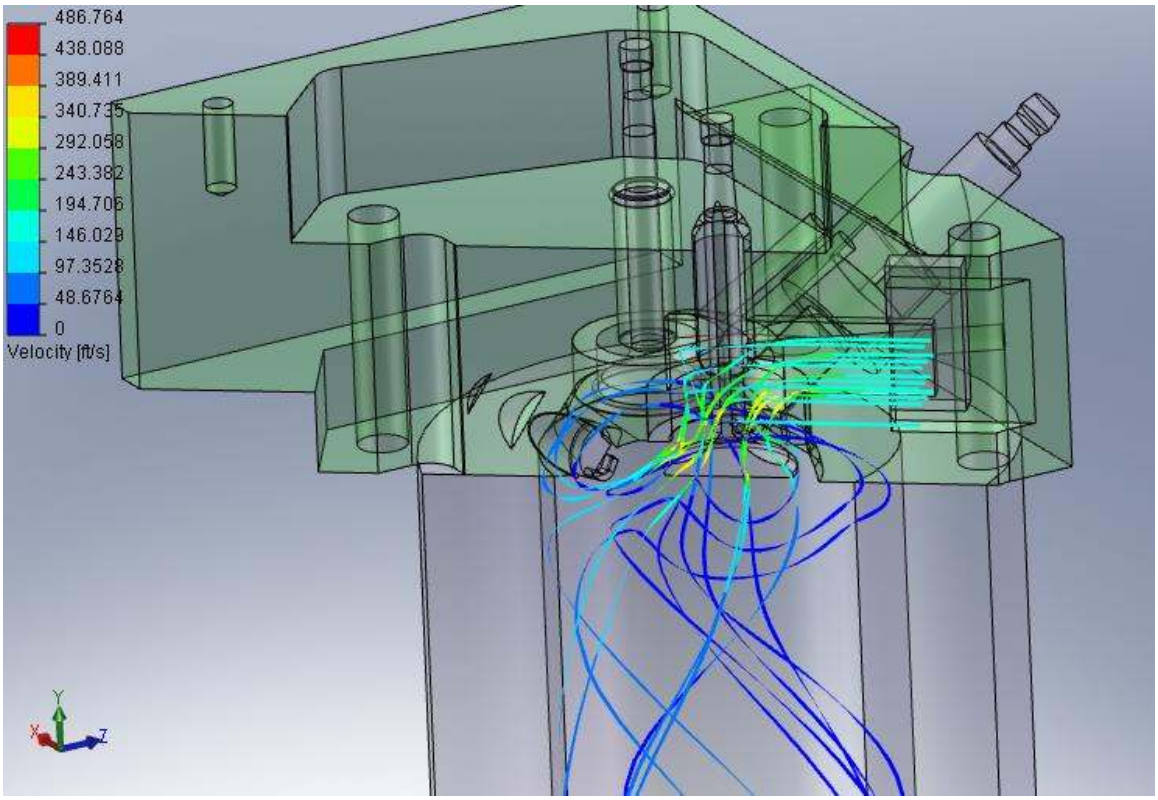

Figure 101 – Iteration 28 – Side View Cutaway

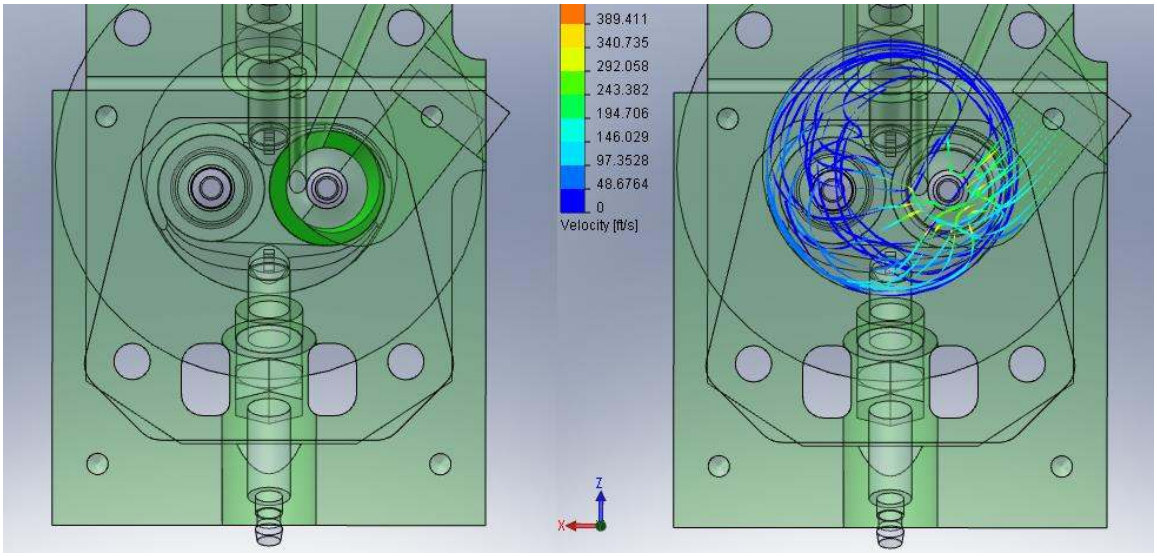

Figure 102 – Iteration 28 – Top View

In the 29th and final iteration, a new swirl generating inlet was attempted. This inlet entered from the top directly above the intake runner. The flow rate was 28.2 CFM, but was unable to produce the desired swirl ratio since it was calculated as 2.35. The results can be seen in figures 103, 104, 105, and 106.

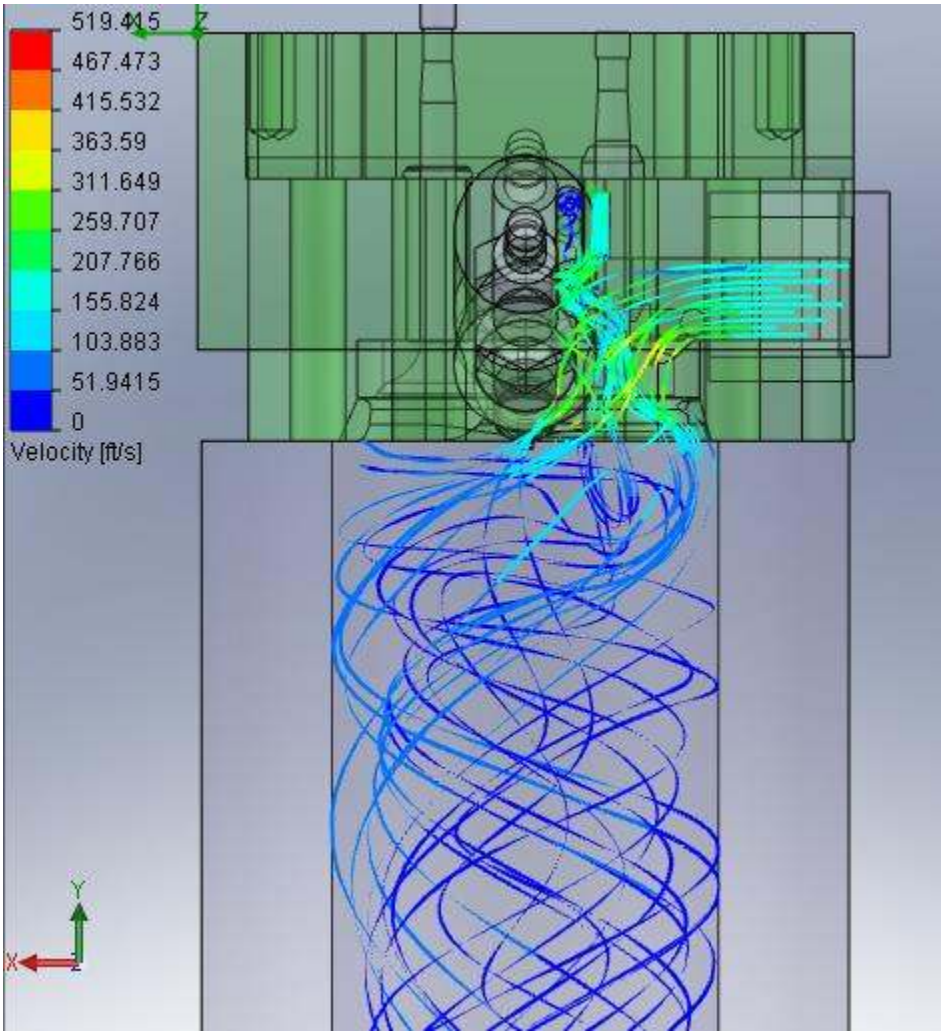

Figure 103 – Iteration 29 – Front View

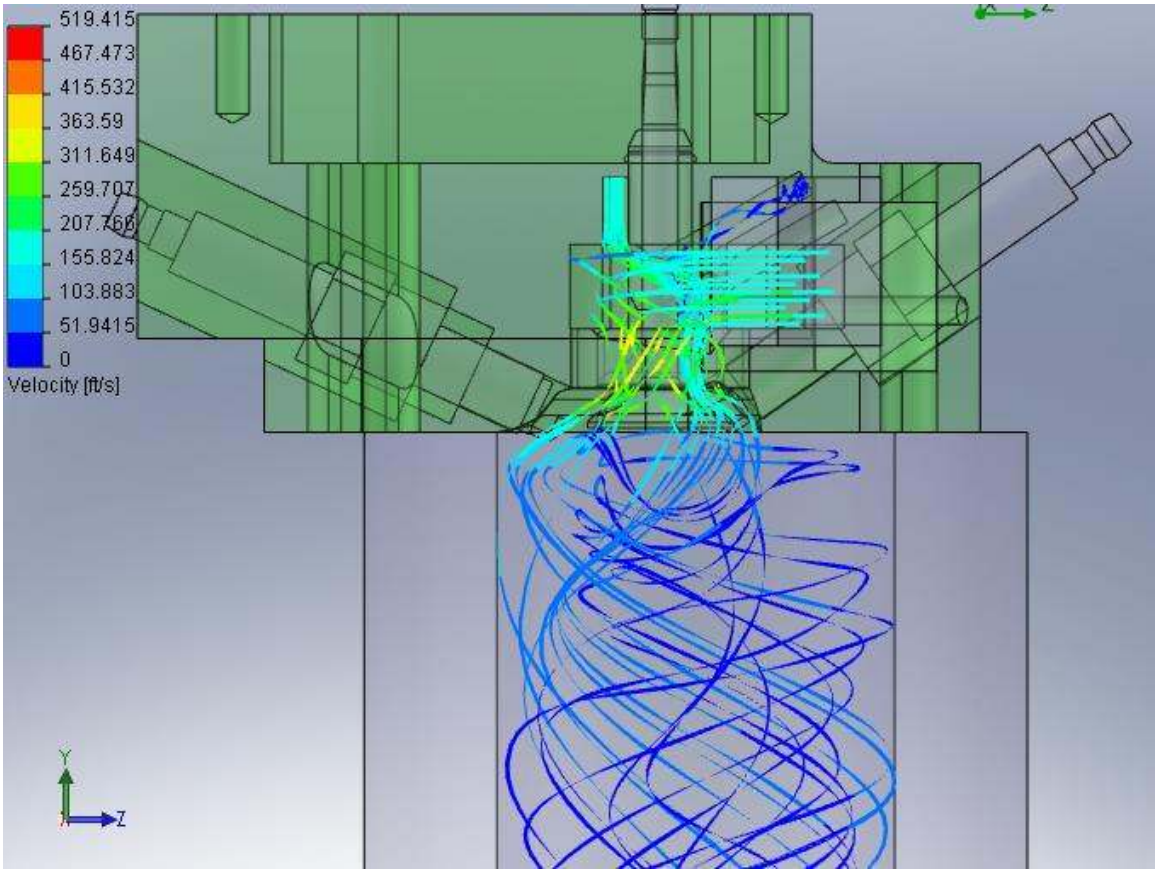

Figure 104 – Iteration 29 – Side View

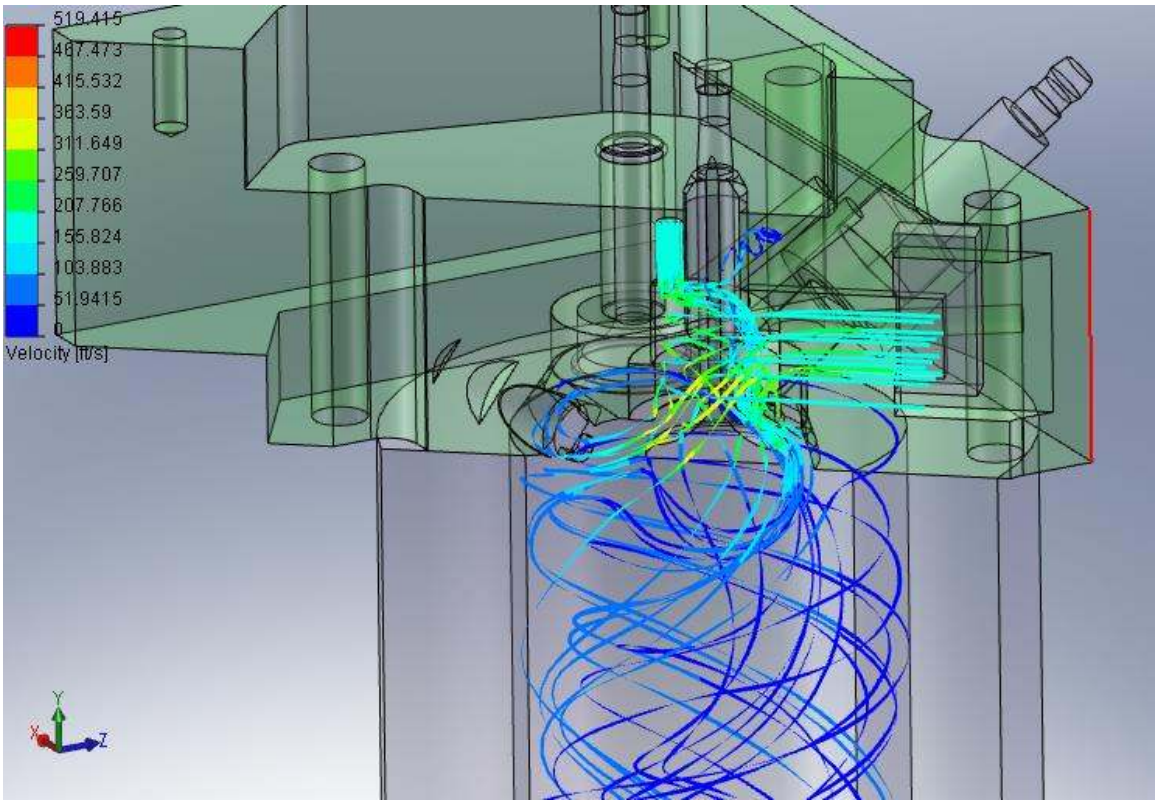

Figure 105 – Iteration 29 – Side View Cutaway

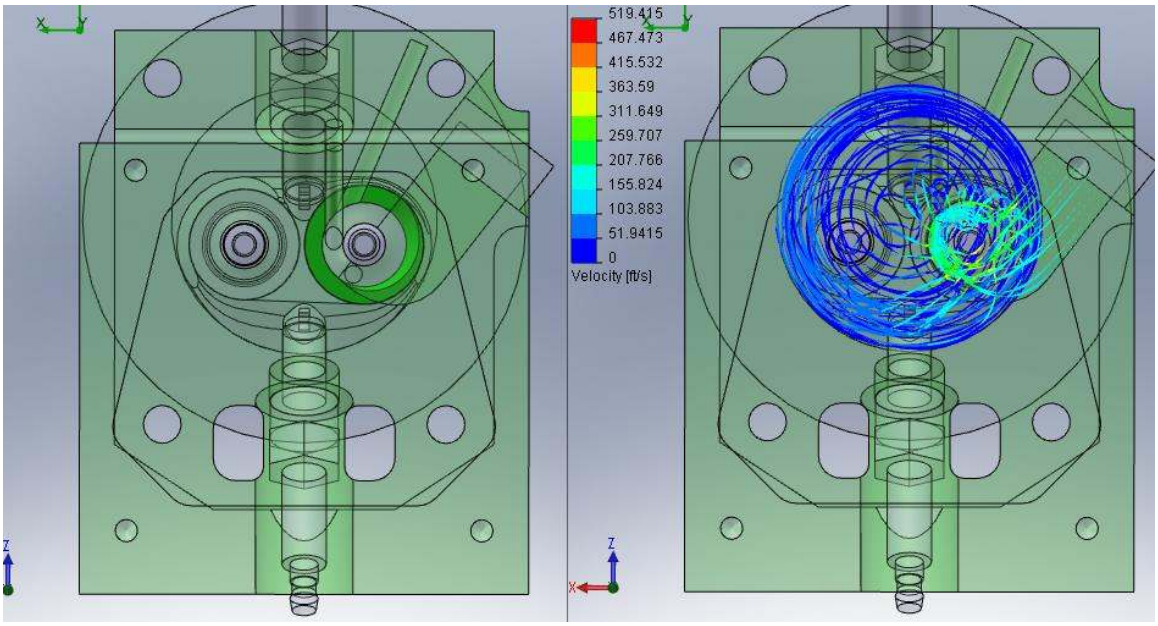

Figure 106 – Iteration 29 – Top View

Chapter 3

Experimental Setup:

Prototyping Methods

Since most of the design work was done in SolidWorks, this design did not require many mechanical iterations. The first prototype was build from SLA (stereo lithography). The goal of this first prototype was to verify the fit of the cylinder head. It also was important in that it allowed for easier visualization of possible iterations that are difficult when trying to view a 2D computer screen.

A UV curing laser is used to harden light sensitive liquid polymer. This is the basic technology behind SLA. A stationary laser is redirected via mirrors to harden the surface of the liquid polymer. The initial surface is close enough to a platform that is parallel to the liquid surface, so that the hardened polymer bonds to the surface and build the initial layer. Then, the platform is lowered and another layer is formed by the laser and is bonded to the previous layer. This is repeated until a series of layers form a 3D part. Since there is no support by liquid underneath, cantilevered pieces of parts support structure is required. It is built by the model maker in a post-processing program and is created with the same resin and at the same time as the model. The consistency is similar to window screen and is designed to be broken away from the model after completion. After being removed from the SLA machine, the part is required to be rinsed and then post cured in a UV oven. Parts can be created in the matter of hours to days depending on complexity. Setting up the part to be made and operating the machine takes significant skill and attention unlike some other methods.

The accuracy of SLA is one of the highest of rapid prototyping methods. The model can only be made out of one type of material and are limited to photosensitive polymers. Parts are often brittle and affected negatively by high humidity. Materials can be made clear, but are usually opaque. For added strength, parts can be nickel coated, making them stronger. The initial model can be seen in figure 107. The resin used creates models that are amber in color. The model has an intake valve seat and guide installed.

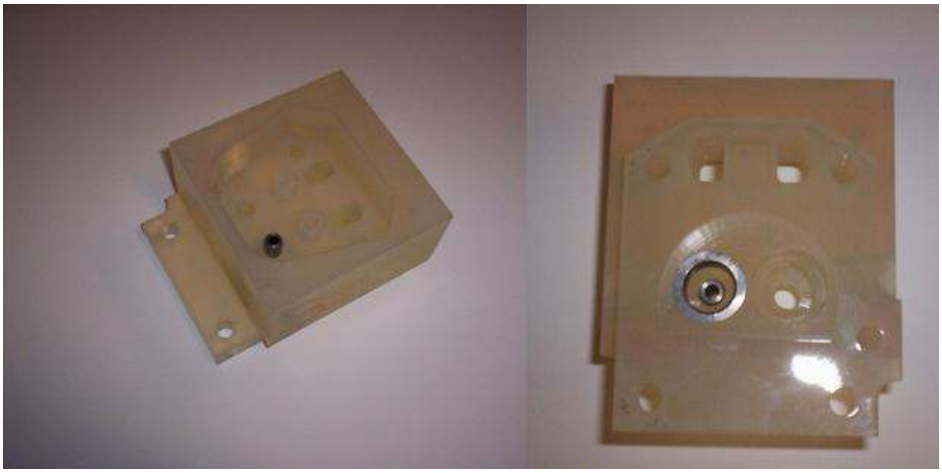

Figure 107 – SLA Prototype

The second model made was made using a 3D printing process. This is otherwise known as fused deposition modeling. The process uses a cartridge filled with a long strand of thermoplastic that is heated and squeezed out of a nozzle onto a platform. Another cartridge with a special support material is applied to support the model in places that would otherwise be left vacant. The platform lowers and another layer is created. After all the layers are completed, the model can be removed and can be placed in a special solution that dissolves the supports and leaves the model intact.

The 3D printing process can use most types of thermoplastics, but most common is ABS because of its durability. Machines can be made to support an array of colors or different types of materials. Since support structures are washed away, entire assemblies

can be created in one step. One of the downsides to this technology is that often times layers do not bond well and may shear or break off on the planes between layers. Models can not be extremely thin and must have adequate layers. SLA models can be made extremely thin since layers bond together extremely well. 3D printing offers a low price and is much easier to use than other prototyping technologies, however, is not as accurate and the models may not be as durable in certain cases.

Flow Bench:

The flow bench is a testing device used to measure the quantity of air that will pass through the intake or exhaust port of a cylinder head. It can also be used for intake manifolds, air filters and even entire systems. For this experiment, we flowed the intake port of our prototype cylinder head. The cylinder head was clamped to a piece of acrylic plate with a 60.325mm hole cut in it. The hole lead into an acrylic tube with the same inside diameter. The actual bore diameter is 60 mm but 2.375in (60.325mm) was the closest available tubing size. This tube enters into a large plenum where a pressure difference from atmospheric of 28in of water is drawn. From this plenum, air is sucked out using a large centrifugal pump and enters another plenum. The air pressure in the second plenum is measured using an inclined manometer to get the most accurate reading. The flowing out of this plenum flows across a square edge orifice. The volumetric flow rate passing through the system can be calculated by:

$$\dot{V} = 200 * \sqrt{\frac{\Delta P}{6}} (CFM)$$

$$\Delta P = inches\ of\ water$$

Due to the flow bench being setup to run larger ports, a calibrated inlet was used. The inlet had an orifice that was previously calibrated. This orifice flowed 41.0SCFM at 6.775" of H_2O. The head was flowed at 28" of H_2O plus the amount read on the inclined manometer reading the pressure difference of the orifice at 28". The equation used for our volumetric flow rate can be seen bellow:

$$\dot{V} = 41.0 * \sqrt{\frac{\Delta P}{6.775}}(CFM)$$
$$\Delta P = inches\ of\ \ water$$

The swirl ratio was found using a pin wheel mounted ½ of a bore diameter bellow the head. The rotational velocity was found using a mark on the pin wheel and a stroboscope. The stroboscope used is manufactured by Ametek and is a Digistrobe III model 1965. From the rotational velocity of the paddle wheel and the diameter of the tube an accurate wall velocity may be calculated. From this, the swirl ratio was calculated. The equation for calculating the angular velocity at the wall can be seen bellow.

$$V_{Wall} = \pi * D * RPM$$
$$RPM = rotational\ rate\ of\ \ pinwheel$$
$$D = Bore\ Diameter$$
$$V_{Normal} = \frac{\dot{V} * 1728 \frac{in^3}{ft^3}}{(D/2)^2 * \pi}$$
$$Swirl\ Ratio = \frac{V_{Wall}}{V_{Normal}}$$

Similar Previous Work:

Previous work involving swirl ports from the University of Miami ICEs lab include a stock 2.5L Pontiac head in the stock form the head flowed a maximum of 131.9 CFM with a swirl ratio of 4.63. This engine has bore equal to 4 inches and intake valves 1.715 inches in diameter. The stock valve to bore ratio for this engine is .43 and with a larger 1.84" valve the ratio increases to .46. The Honda GX120 head has a much smaller valve to bore ratio of only .36. The swirl values will be smaller because the relatively smaller intake valve increases difficulty of swirl generation. This effect was shown in previous experimentation with the Pontiac 2.5L head. The swirl ratio in the stock engine at a lift of .400" was 4.62 with the stock size intake valve. The head designed in this effort had a swirl ratio of 2.87. The use of a 1.84 inch diameter intake valve increases swirl ratio to 4.82. It is possible to generate more swirl by decreasing the flow rate, but adequate swirl was generated to allow the study of swirl. Earlier it was stated based on the results by Pozniak that a swirl ratio above 1.5 gives a noticeable increase in burn rate. The head engineered by Pontiac was created to optimized swirl together with flow rate. By increasing the valve from the stock 1.715" valve to a 1.84" valve, the valve to bore ratio changed from .43 to .46. This 7% change in valve to bore ratio lead to over 14% increase in flow rate at lower lifts and over 10% increase in swirl at the same lift. Flow rate did not increase at higher lifts, but at all lifts swirl was increased for the larger valve size. At .400" of lift the Pontiac has a lift to valve diameter ratio (L/D) of .22 while the Honda GX120 head has a L/D ratio of .24 at .200" of lift, the swirl for the large valve Pontiac head was 4.82 while the Honda was 2.87. Larger valves increase flow rate and ability to generate high swirl. High swirl to bore ratios are important in generating max swirl. The

Honda project was constrained to use the same valves as stock since enlarging them would significantly change intake geometry and this was not the intent of this project. The results for the stock Pontiac 2.5L head can be seen below. The swirl ratio is relatively consistent across all four intake ports of the 4 cylinder engine.

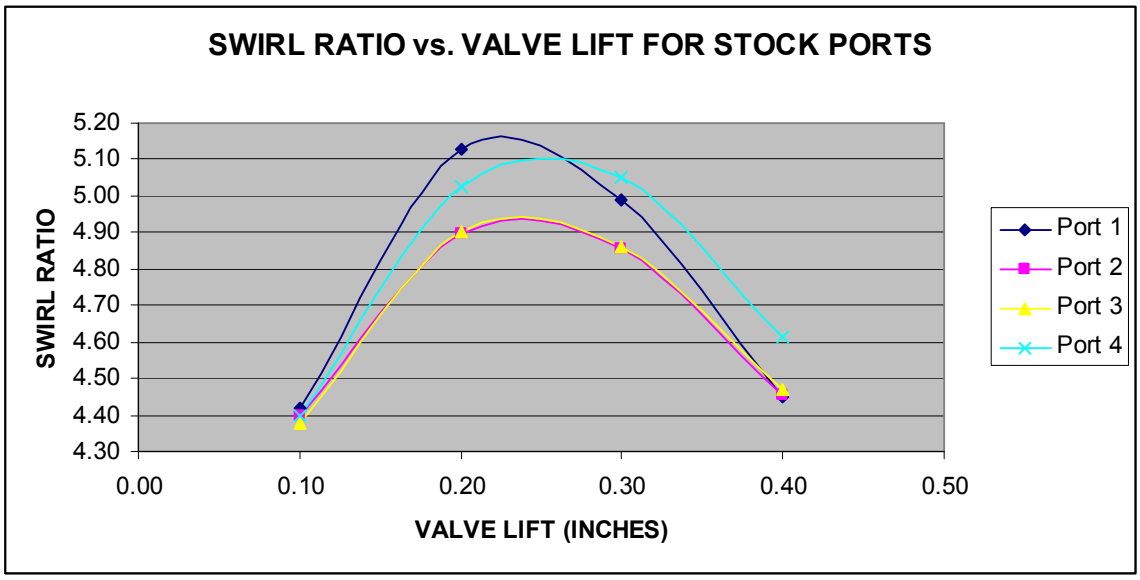

Figure 108 - Stock 2.5L Pontiac

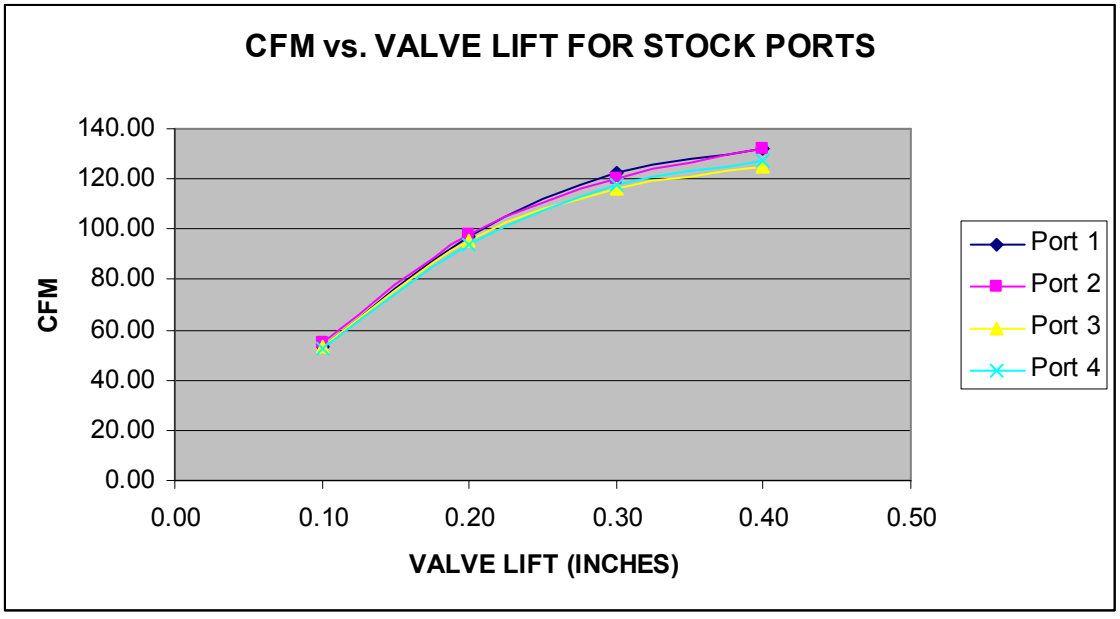

Figure 109 - Stock 2.5L Pontiac

Experimental Setup

The pressure difference was set to 28in plus 3.36in due to the pressure drop in the flow measuring device. The lift was .200". The rotational velocity of the pin wheel was found using a stroboscope. In order for the head to attach to the orifice, a small adapter was created from SLA. It was glued into the head and a series of PVC pipe adapters were used to match the 4" orifice. A picture of the head can be seen in Figure 110.

Figure 110-Experimental Setup

After the adapter was glued into the head, everything was assembled. A hose was connected from the orifice to an incline manometer, while the vertical manometer read the vacuum on the other side of the head. This setup can be seen in figure 111. Clamps were used to secure the head to the bench during testing.

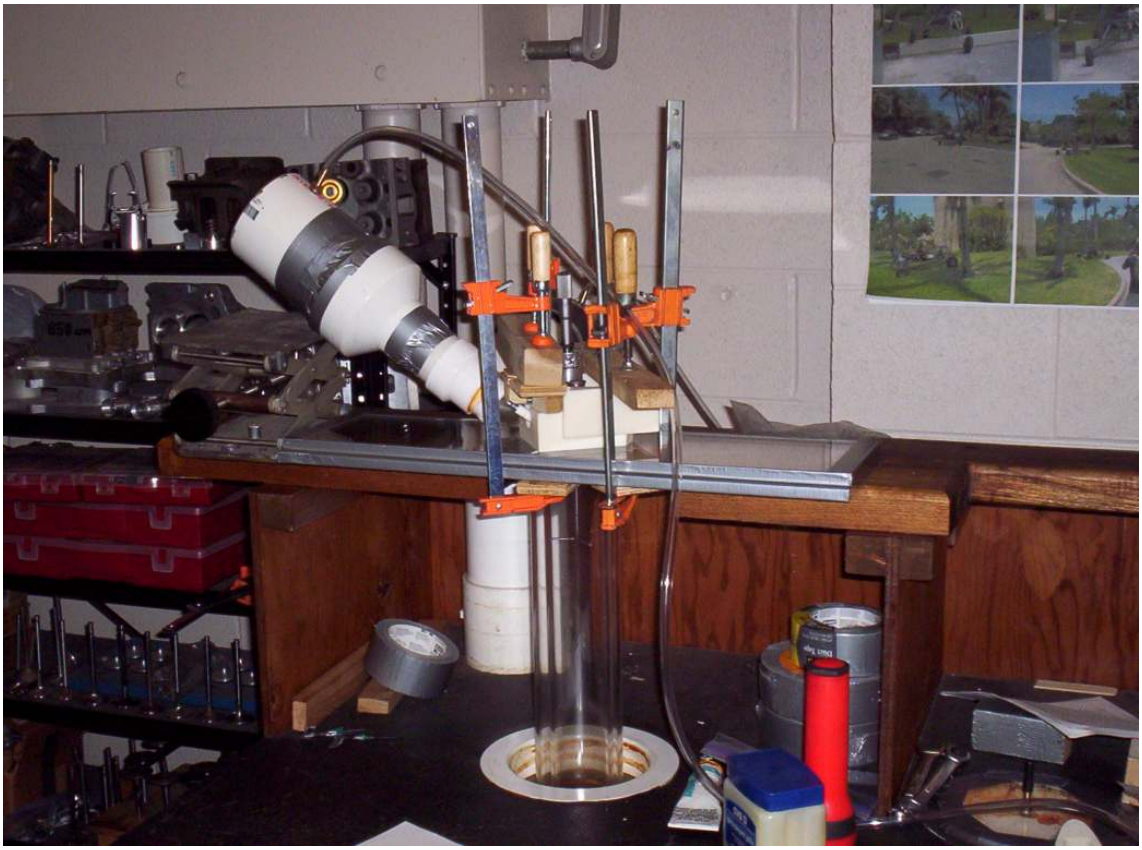

Figure 111-Experimental Setup 2

Chapter 4

Results

The modeling used in the 28th iteration was used in the manufacture of the prototype since it gave the best results. Only slight modifications were done to match the experimental setup. The pressure difference was considered to be a vacuum inside the flow bench, 28 inches of water pressure drop across the cylinder head. During modeling the swirl reducing orifices were capped off near their exit into the port. These results can be seen below in figures 112, 113, 114, and 115. The swirl flow develops close to the head and propagates down without losing intensity throughout the figure.

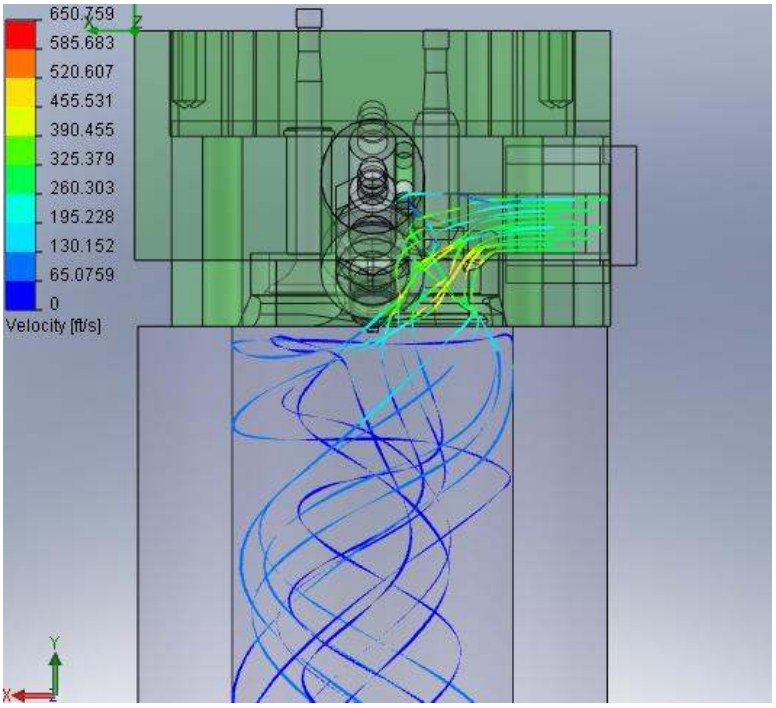

Figure 112-Front Max Swirl

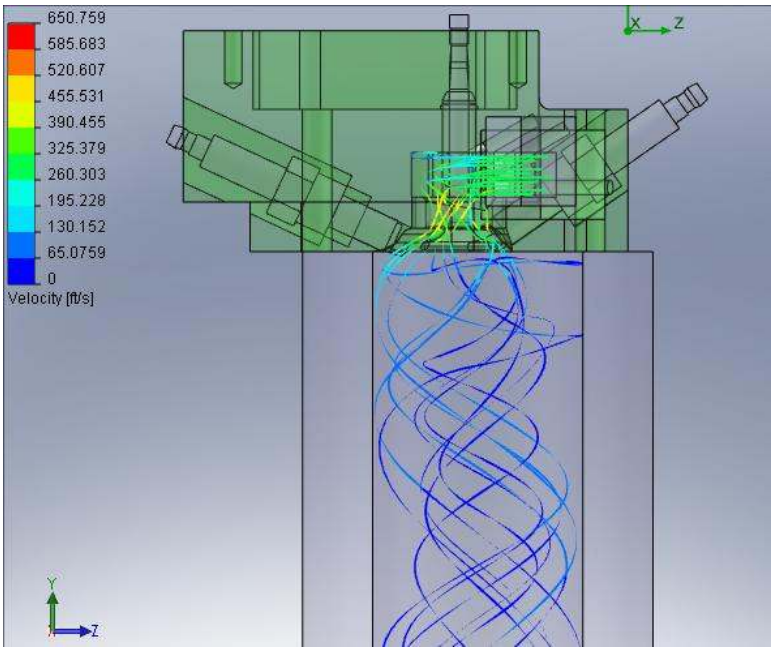

Figure 113-Side Max Swirl

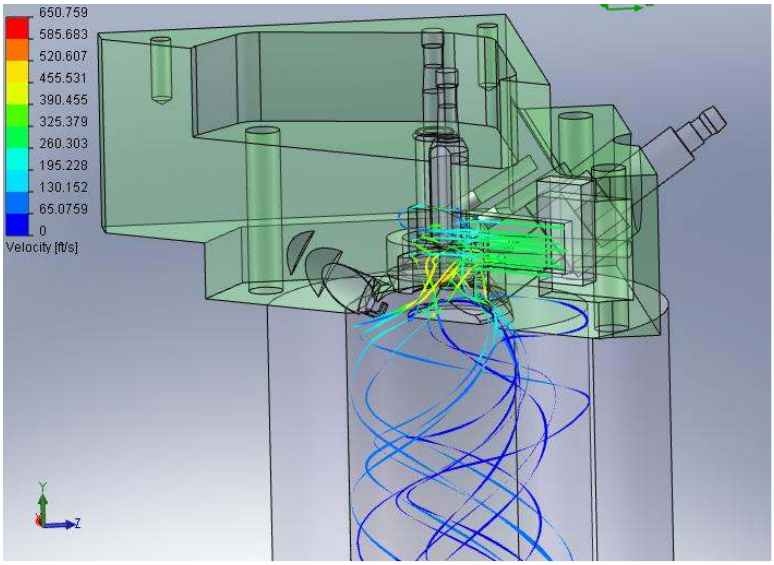

Figure 114- Cutaway Max Swirl

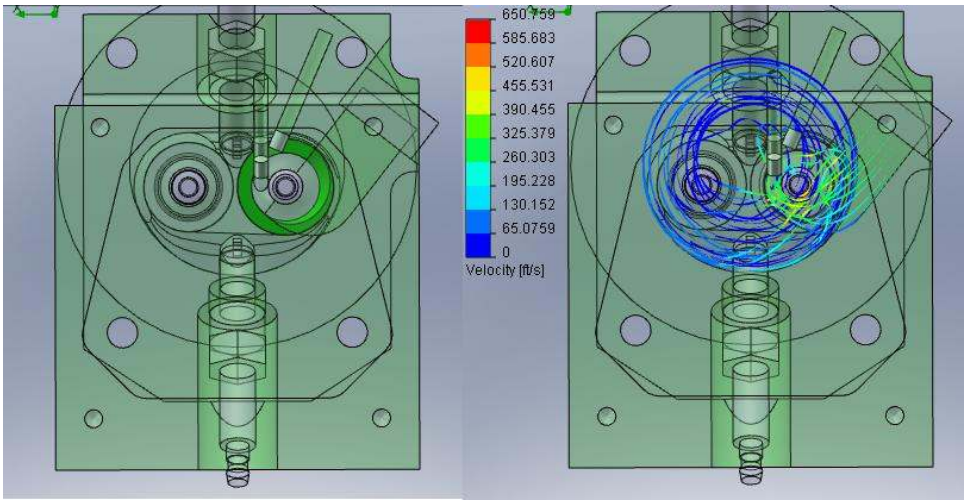

Figure 115-Top Max Swirl

The results for the head with all swirl-reducing orifices open can be seen below in figures 116, 117, 118, and 119. The swirl is much less organized, when the orifices are open. The streamlines exit the valve and do not rotate, but travel generally down into the cylinder. In figure 119, the top view reveals that there is still slight bulk rotation of the gasses.

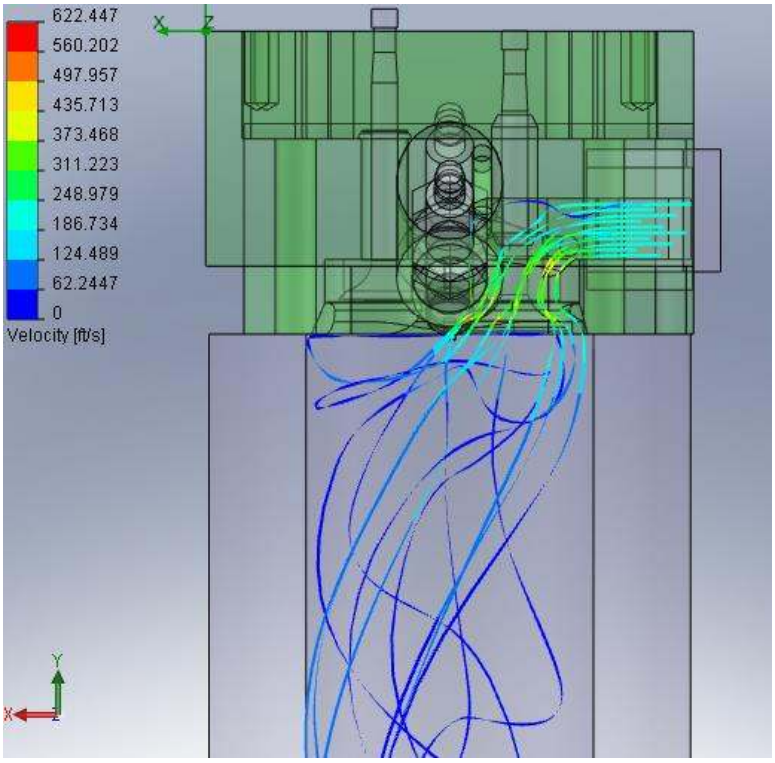

Figure 116-Front Low Swirl

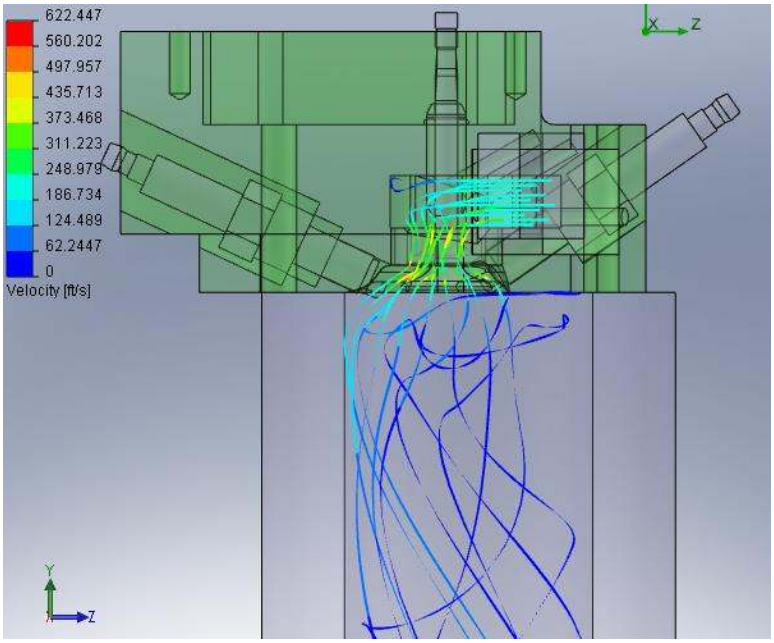

Figure 117- Side Low Swirl

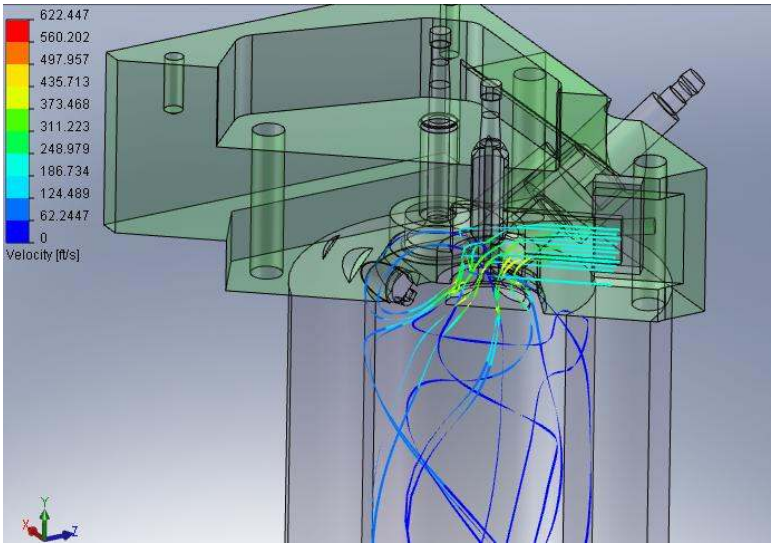

Figure 118-Cutaway Low Swirl

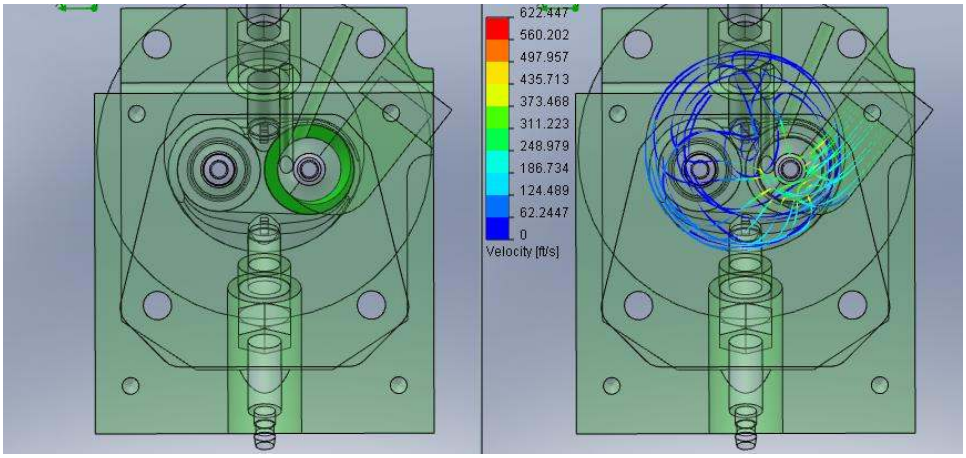

Figure 119-Top Low Swirl

A comparison of the results can be seen in table 1. The flow rate for the experimental and the theoretical results matched closely and the high swirl ratio results were also similar. However, the results for the low swirl ratio did not match as well.

Table 1 – Comparison of Results

	Flowrate(CFM)	High Swirl Ratio	Low Swirl Ratio
Experimental	28.87	2.87	0.80
Theoretical	29.71	2.59	0.56
Percent Error	2.90	9.79	29.41

The experimental results were taken in two sets, they were found not to vary. Based on previous experimentation from the flow bench in the University of Miami ICEs Lab, multiple sets of data were not acquired. Due to the inherent accuracy of a flow bench (flow rate linearly proportional to the square root of the measured pressure drop across the orifice), accuracies of ±0.2% are typical. The flow bench has been calibrated and over the many years of use has proven to be accurate with little variation.

Chapter 5

Conclusions

The results of the high swirl scenario were extremely close. The swirl was measured at ½ a cylinder bore from the head surface. Other experiments usually measure the swirl at 1.0 to 1.5 bore diameters below the head gasket surface, however half the cylinder bore was chosen for computer model variation. Since this head used a helical port swirl developed immediately after exiting the valve and does not rely on valve shrouding or combustion chamber design, swirl developed extremely close to the head and would only decrease as it moved farther down the cylinder

Despite the inaccuracy of the low swirl case, the high swirl experimental flow rate was 28.87 CFM while the theoretical results were 29.71 CFM. The swirl ratio for the experimental was 2.87 as compared to 2.59 for the theoretical. These results are all within 10% or less, which shows good correlation. Since these comparisons are for helical ports, we can conclude that SolidWorks Floworks can be used to help design helical ports and combustion chambers. Future work should investigate the surface roughness of the swirl reducing orifices in the prototype cylinder head as this may affect the experimentally determined swirl reduction rate. Further work will be needed to prove the accuracy of the software with more complex designs, such as shrouded valves and complex combustion chambers.

Bibliography

Heywood, John B. Internal Combustion Engine Fundamentals. NYC, McGraw-Hill: 1988.

Lilly, L.R.C. Diesel Engine Reference Book. London, Butterworths: 1984.

Pozniak, D. , Rydzewski, J. "A Study of In-Cylinder Air Motion in the General Motors Vortec 4.3L, V-6 Engine" Detroit, SAE: 1985.

Pulkrabek, W. Engineering Fundamentals of the Internal Combustion Engine. Upper Saddle River, N.J: Prentice Hall, 1997.

Stone, R. Introduction to Internal Combustion Engines. Warrendale, Pa, SAE: 1999.

Appendices

Table 2- Iterative Results

Iteration	Flow (CFM)	Swirl Ratio
1	25.1	0.31
2	23.2	0.57
3	10.5	0.88
4	9.7	0.98
5	9.6	1.10
6	9.9	0.58
7	9.8	1.19
8	10.1	1.89
9	10.3	1.91
10	23.1	1.51
11	27.2	1.21
12	29.5	1.62
13	33.1	1.43
14	31.7	2.46
15	25.1	2.99
16	24.9	2.75
17	24.7	2.80
18	23.1	2.49
19	25.7	2.99
20	25.7	2.20
21	29.5	2.60
22	29.5	1.02
23	29.5	0.90
24	27.3	2.59
25	27.3	0.87
26	27.3	0.96
27	29.5	0.97
28	29.5	0.80
29	28.2	2.35